



ScuDo

Scuola di Dottorato ~ Doctoral School
WHAT YOU ARE, TAKES YOU FAR



Doctoral Dissertation
Doctoral Program in Mechanical Engineering (33rd Cycle)

Nondestructive, quantitative and local assessment of residual elastic properties in laminated composites

Carlo Boursier Niutta

Supervisors

Prof. G. Belingardi, Supervisor
Prof. D. S. Paolino, Co-Supervisor

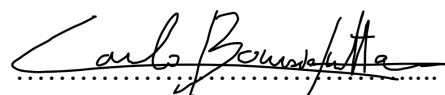
Doctoral Examination Committee:

Prof. S. Abrate, Referee, Southern Illinois University
Prof. F. Aymerich, Referee, Università di Cagliari
Prof. E. G. Koricho, Referee, Georgia Southern University
Prof. J. Montesano, Referee, University of Waterloo

Politecnico di Torino
June 15, 2021

This thesis is licensed under a Creative Commons License, Attribution - Noncommercial - NoDerivative Works 4.0 International: see www.creativecommons.org. The text may be reproduced for non-commercial purposes, provided that credit is given to the original author.

I hereby declare that, the contents and organisation of this dissertation constitute my own original work and does not compromise in any way the rights of third parties, including those relating to the security of personal data.

A handwritten signature in black ink, reading "Carlo Boursier Niutta". The signature is written in a cursive style and is positioned above a horizontal dotted line.

Carlo Boursier Niutta
Turin, June 15, 2021

Summary

Composite materials show several interacting failure modes whose description and evolution prediction constitute a very complex task. The lack of a proper combination of progressive damage models and nondestructive evaluation techniques results in inefficient designs of composite structures from both cost and safety point of view. In this work, an innovative experimental methodology is proposed and validated for the nondestructive assessment of local elastic properties in composites. The methodology aims at isolating the vibrational response of a planar region of the component by clamping its contour. The mechanical vibrations induced through impulse are thus function of only the elastic characteristics of the inspected region. As a demonstrator of the methodology developed here, a preliminary clamping system, which invokes the use of testing machine equipped with compression blocks, is tested on a unidirectional composite plate. After showing the capability of the setup in isolating the vibrational response, local elastic properties are assessed through an optimization problem based on Finite Element analysis. Robustness of the optimization problem is also addressed. Numerical investigations based on a Rayleigh-Ritz formulation developed here show that the robustness can be increased by retaining information related to the modal shape. The effect of an additional concentrated mass is exploited and only two mass positions, i.e., two measures of the first resonant frequency are sufficient to assess the modal shape. Finally, the assessment of the residual elastic properties in damaged composites is also shown. As observations of any nondestructive evaluation techniques are constrained to the exposed surface, an innovative clamping system was designed which exploited the vacuum technique to clamp the boundaries of the inspected region. Complementarily, a new analytical approach is derived and validated for the assessment of the residual elastic properties of the damaged area.

Acknowledgment

The present dissertation and the research within were conducted during my time as PhD student in the research group of Structures and Vehicles Safety of Politecnico di Torino, from April 2017 to the present days.

First, I would like to acknowledge Prof. Giovanni Belingardi and Prof. Davide S. Paolino for the opportunity and the patience in supporting my research. They both guided my activity and allowed me to explore new directions. I also would like to thank the members of my examination committee: Prof. Serge Abrate, Prof. Francesco Aymerich, Prof. Ermas G. Koricho and Prof. John Montesano. In particular, my sincere acknowledgments go to Prof. Serge Abrate, Prof. Francesco Aymerich and Prof. Ermas G. Koricho, whose questions and comments have allowed me to improve and value this dissertation.

I would like to express my gratitude to all my colleagues of the Structures and Vehicles Safety group. Through the daily discussions and support, I was able to further my knowledge greatly. Above all, my appreciation goes to PhD Andrea Tridello for his cooperation and insights in the development of the technique; PhD Raffaele Ciardiello for his assistance in the experimental activity as well as cooperation in teaching; PhD Pier Giuseppe Anselma for the profitable collaborations; Dr. Dario Fiumarella and Dr. Alberto Ciampaglia for the fruitful arguments on composite materials and design. We worked hard, we played harder.

I also would like to sincerely thank Dr.-Ing. Erich J. Wehrle for his recommendations and advisement during my Master's thesis in Munich, which encouraged me to continue the research activity.

To my friends, my partner and my all family, I would like to show my sincere gratitude. In particular, I would like to thank my parents for having taught me that results do not come without education.

To Anna and Antonio

Contents

1. Introduction.....	1
1.1 Assessment of damage	2
1.2 Damage in composites.....	3
1.2.1 Manufacturing defects	3
1.2.2 In-service damage.....	4
1.2.3 Failure modes and effects of damage and defects.....	5
1.3 Nondestructive damage detection	6
1.4 Limitations of current practices and research motivation	9
1.5 Organization	13
2. Detecting Damage Index	14
2.1 From <i>DD</i> to <i>DI</i>	15
2.2 Correlation between elastic properties and impact response	18
2.3 Combination of Finite Element Method and <i>DI_d</i> for the assessment of residual elastic properties.....	20
2.3.1 Materials and methods.....	21
<i>Materials</i>	21
<i>Experimental tests</i>	21
<i>Numerical model</i>	23
2.3.2 Results	26
<i>Four-point bending test: experimental results and numerical model tuning</i>	26
<i>Progressive damaging and assessment of residual elastic properties through the <i>DI_d</i> technique</i>	28
<i>Validation: comparison of experimental and numerical results</i>	31
2.4 Advantages and criticalities of the methodology	32
3. Local Vibrational Analysis	34
3.1 Unidirectional plate	36
3.2 Clamping as isolating: experimental setup	39

3.3 Accounting for material anisotropy.....	44
3.4 Numerical calculations	47
3.5 Results.....	48
3.5.1 First fundamental frequencies.....	49
3.5.2 Estimation of material constants	50
3.6 Sensitivity Analysis	53
3.6.1 Effect of the thickness variation.....	53
3.6.2 Effect of the design domain limits	54
3.6.3 Effect of the clamped boundaries extension	55
3.7 Limitations and possible criticalities of the methodology.....	58
4. Enhancement of the methodology for increasing the optimization robustness	61
4.1 Methods.....	63
4.1.1 Rayleigh-Ritz formulation	63
4.1.2 Mode shape information through a concentrated mass	66
4.2 Results.....	69
4.2.1 Validation of the Rayleigh-Ritz formulation.....	69
4.2.2 Calculation of the reference frequencies	72
4.2.3 Optimization results	75
4.3 Conclusions and possible limitations of the approach.....	77
5. Determination of damage severity through local IET	79
5.1 Materials	80
5.2 Methods.....	82
5.2.1 Experimental setup.....	82
5.2.2 Damage characterization	84
5.3 Results.....	92
5.4 Conclusions and possible limitations	100
6. Conclusions	103
6.1 Damage tolerance approaches.....	103
6.2 Summary of findings	105
6.3 Outlook	106
7. References	111

List of Tables

Table 2.1 Material properties.....	21
Table 2.2 Residual Young's moduli and corresponding DId values at specific locations.....	29
Table 3.1 Thickness variation (highlighted in red the maximum and minimum thicknesses in the plate).....	37
Table 3.2 Material properties.....	38
Table 3.3 Comparison of local and nominal elastic properties.....	50
Table 3.4 Comparison of experimental and numerical resonant frequency.	51
Table 3.5 Effect of thickness scatter on local material properties.	54
Table 3.6 Effect of the design domain limits on local material properties.....	54
Table 3.7 Effect of the design domain limits on local material properties.....	58
Table 3.8 Effect of the design domain limits on the first resonant frequency for 90° orientation.....	58
Table 4.1 Material properties at ply level of the unidirectional layers.....	70
Table 4.2 Convergence results of frequency parameter λ and comparison to the experimental data presented in the literature - $\lambda = \left(\frac{\rho h \omega^2 a^4}{D_{11}}\right)^{\frac{1}{2}}$, $D_{11} = \frac{E_{11} h^3}{12(1-\nu_{12}\nu_{21})}$; ..	70
Table 4.3 Material properties at ply level of the woven fabric.....	73
Table 4.4 First resonant frequency values with and without the 1 g mass load of the unidirectional plate ([0°, 0°, 0°, 0°]) for different material orientations.	73
Table 4.5 First resonant frequency values with and without the 1 g mass load of the symmetric plate ([30°, -30°, -30°, 30°]) for different material orientations.	73

Table 4.6 First resonant frequency values with and without the 1 g mass load of the anti-symmetric plate ($[30^\circ, -30^\circ, 30^\circ, -30^\circ]$) for different material orientations.	74
Table 4.7 First resonant frequency values with and without the 1 g mass load of the woven fabric plate ($[0^\circ, 0^\circ, 0^\circ, 0^\circ]$) for different material orientations.	74
Table 4.8 Optimized material properties at ply level for each material.	75
Table 4.9 Optimized material properties at ply level and relative errors for the symmetric and anti-symmetric laminates without considering the modal shape information.....	76
Table 5.1 Material properties of the 6- and 8-layer plates.....	81
Table 5.2 Comparison of the residual elastic properties for the 6- and 8-layers plate.	96
Table 5.3 Comparison of the equivalent Young moduli for the 6- and 8-layer plates.....	96

List of Figures

Figure 2.1 Scheme of the experimental fixture for impact testing.....	15
Figure 2.2 Example of quasi-static perforation test and impact test to perforation [53].	17
Figure 2.3 Comparison between <i>DD</i> and <i>DI</i> trends for impact tests on a carbon/epoxy laminate with stacking sequence $[0/90]_8$ [53].....	17
Figure 2.4 Specimen cut from impacted plates and used for assessing the residual elastic properties [49].	19
Figure 2.5 Flow-chart of the <i>Did</i> technique.....	20
Figure 2.6 Four-point bending test: (a) experimental setup; (b) numerical model.	22
Figure 2.7 Location of impacts for <i>Did</i> analysis.....	23
Figure 2.8 Qualitative representation of the difference quotients retained for the calculation of the derivative at the <i>k</i> -th location: (a) negative sign; (b) positive sign of the product $\frac{\Delta E_k}{\Delta x_k} \cdot \frac{\Delta E_{k+1}}{\Delta x_{k+1}}$	25
Figure 2.9 Flowchart of the adopted procedure.	26
Figure 2.10 Magnification of intralaminar cracks: failure of the upper four layers.	27
Figure 2.11 Experimental and numerical results of the four-point bending tests. .	27
Figure 2.12 Progressive damaging of composite plate through four-point bending tests.	28
Figure 2.13 Residual Young's modulus evaluation with <i>Did</i>	29

Figure 2.14 Variation of residual Young's modulus with respect to the x-coordinate.....	30
Figure 2.15 Top view of the finite element model of the composite laminate: longitudinal division of layers.	31
Figure 2.16 Comparison of experimental and numerical results of damaged specimen.	32
Figure 3.1 Unidirectional composite plate.....	37
Figure 3.2 Acquired signal with IET frequency spectra and corresponding modal shape: (a) torsional mode shape; (b) flexural mode shape in transverse direction; (c) first flexural mode shape in longitudinal direction.	39
Figure 3.3 Comparison of simply supported and clamped boundaries: (a) finite element model of a plate with the highlighted boundary nodes; (b) modal analysis with simply supported boundaries; (c) modal analysis with fully clamped boundaries.....	41
Figure 3.4 Testing setup: (a) experimental setup; (b) scheme.....	43
Figure 3.5 Experimental procedure: measures at different orientations. (a) 0°; (b) 30°; (c) 60°; (d) 90°.....	46
Figure 3.6 Numerical model.	48
Figure 3.7 Acquired signal and frequency spectra at different orientations: a) 0°; b) 30°; c) 60°; d) 90°.....	49
Figure 3.8 Mode shape with contour lines at different orientations: (a) 0°; (b) 30°; (c) 60°; (d) 90°.....	53
Figure 3.9 Different sizes of the clamped boundaries: (a) 140x90; (b) 108x168; (c) 144x244; (d) 280x180; blue region indicates a local material variation.	57
Figure 4.1 Scheme of the clamped plates made of laminated composites.	63
Figure 4.2 Mode shape with contour lines at different orientations of the unidirectional reinforcement with respect to the x axis: (a) 0°; (b) 30°; (c) 60°; (d) 90°.....	68
Figure 4.3 Example of mass spots symmetric with respect to one of the axes of the rectangular plate.....	68
Figure 4.4 Comparison between experimental data obtained by Low et al. [80] and the presented Rayleigh-Ritz formulation: variation of the frequency for the mass	

positioned (a) along the x direction ($y = \frac{b}{2} = 150$ mm) and (b) along the y direction ($x = \frac{a}{2} = 300$ mm); (c) 3D view.....	72
Figure 5.1 Vacuum bag infusion process.	81
Figure 5.2 Experimental setup of the tensile tests.....	82
Figure 5.3 Experimental setup.	83
Figure 5.4 Clamping device: dimensions and details of the vacuum system.	83
Figure 5.5 Numerical model with local material variation: a) damage in proximity of the boundary; b) damage in the centre.	85
Figure 5.6 Frequency mapping procedure.	85
Figure 5.7 Damage parameter k_E as function of k_v	87
Figure 5.8 Modal contribution of the damaged and intact zones.	90
Figure 5.9 Integral parameter as function of the device domain and defect size...	91
Figure 5.10 Tensile test of specimens equipped with optic fibre.....	92
Figure 5.11 Frequency trend as function of the damage position with respect to the device: (a) 6-layers plate; (b) 8-layers plate.	93
Figure 5.12 Young's modulus variation along the specimen axis as measured through the fibre optic: (a) 6-layers composite; (b) 8-layers composite.	95
Figure 6.1 Damage evolution in cross-ply laminates: (a) strength and stiffness degradation [46]; (b) corresponding failure modes [97].	107

I

Introduction

In recent years, we have witnessed a consistent increase of composite materials application in structural components of aerospace and automotive industries. The main advantage of composite materials lies in the optimal specific mechanical properties. Their application particularly offers mechanical performances comparable to those of standard metals, while the structure weight is consistently reduced. As a major consequence, the environmental impact of transportation systems can be tackled through the lightweight design of their components. In this regard, the increasing restrictions on CO₂ emissions of vehicles have further pushed the automotive and aerospace industries to the use of composite materials.

The widespread diffusion of composite materials is however limited by many factors, both of economical and mechanical nature. Among the economical limitations, the need for conversion of production lines from metals to composites is of particular concern. Apart from the required consistent investments for the production lines, manufacturing processes based on composite materials still require research and improvements. Currently, the use of composite materials for critical structural components is affordable only for low-volumes production [1].

Among the mechanical factors, the complexity of their damage mechanism, which usually consists in a rich collection of cracks of different sizes, geometries and orientations, plays a key role in their limitation. Several interacting failure modes are typical of composite materials and the uncertain evolution of these failure modes still poses doubts about the use of composites in structural applications, where high standard safety requirements are to be met. Indeed, the presence of damage can cause consistent discrepancies between the expected and the actual performances. In order to increase the reliability of composite structures, damage tolerance design approaches are increasingly invoked. Design approaches based on damage tolerance particularly intend to address the question: how much damage can be tolerated before the structural integrity is endangered?

The concept of damage tolerance is not new in the realm of design strategies. Fracture mechanics, which investigates the stress fields in the crack front and adopts energy-based criteria for the crack growth, has particularly provided tools for addressing such design problems in metallic structures. For metals, damage tolerance was established in terms of sufficient strength in the presence of cracks. In particular, this strength, also known as residual strength, was function of the most critical crack. Similar approaches based on the assessment of a residual strength have been proposed for composites. However, due to the complexity of failure mechanisms, where the damage is represented by a highly rich variation of cracks and its evolution depends case by case on the interaction of these cracks, residual strength approaches are not straightforwardly enforceable in composite materials. Indeed, given the complex cracks scenario of composites, it is not a priori known which mechanism will dominate. The design of composite material structures based on damage tolerance still has open questions, some of which will be answered in the present dissertation. In particular, here the focus is posed on the damage assessment in composite structures. In contrast with the current techniques, a new approach for the nondestructive evaluation of defects is here proposed. The possible implications of the proposed methodology on the design strategy in presence of damage is discussed later.

In this chapter, the concept of damage will be firstly defined and detailed. Current techniques for damage assessment, as result of the use of metal structures, will then be discussed and their limitations, as a particular concern for composite applications, will be highlighted. Finally, the approach here proposed will be introduced and organization of the dissertation is presented.

1.1 Assessment of damage

A general definition of damage is given by Sohn et al. [2]. According to the authors, damage can be defined as

“... changes introduced into a system that adversely affect its current or future performance. Implicit in this definition is the concept that damage is not meaningful without a comparison between two different states of the system, one of which is assumed to represent the initial, and often undamaged, state.”

Therefore, examples of damage are cracks in the material, which induce a change of the stiffness, a loss of balancing counterweight, which is the result of a mass change, and the untightening of bolts, which causes a change in the joining.

Further, as reported by Sohn et al., the damage state can be described by answering the following questions:

1. Is there damage in the system (existence)?
2. Where is the damage in the system (location)?
3. What kind of damage is present (type)?
4. How severe is the damage (severity)?
5. How much useful life remains (prognosis)?

The damage state description is a five-step process where, in the order of the presented questions, the knowledge about the damage is increasingly acquired. While the first four questions are specifically related to the damage, the latter involves other aspects of the component application, such as loading and support. Therefore, the nondestructive inspection of structures has focused on the development of techniques able to define existence, location, typology and extent of damage, while the prognosis is defined through proper modelling techniques.

Composite materials are inherently nonhomogeneous and material state damage, i.e., cracks, irregularities, voids etc., is likely to occur. Consequences on the mechanical behaviour must be properly accounted, as their presence can particularly endanger the structural integrity.

1.2 Damage in composites

There are many forms of fibre reinforced plastics composites. The essential feature of all of them is that reinforcing fibres are embedded in a matrix. The fibres, usually glass, carbon or aramid, confer stiffness and strength to the composite. The matrix, which is typically a thermosetting polymer, such as epoxy resin, or less commonly thermoplastic, has three main tasks: protecting the fibres, holding them in predetermined orientations and transferring the load to the fibres. Fibres can be continuous or discontinuous, long or short, in parallel arrays or woven. Fibres are usually put down in layers, also called plies or laminae, whose orientation is dictated by the design requirements. Thermoset matrices undergo a curing process for building chemical cross links. The curing process can be carried out at room or elevated temperature, in vacuum or pressurized atmosphere in order to extract volatiles. Fibres can be impregnated with resin before curing occurs, such as in hand layup, resin transfer moulding or pultrusion processes. As an alternative, fibres impregnated with partially-cured resin, also called pre-preg, are typically used in aerospace industry.

In composites, anomalies in the material state can be categorized as follows: matrix defects, fibre defects and interface defects. Matrix defects particularly concern voids, resin rich areas and uncured matrix. Misalignment, waviness, unimpregnated fibres, irregularly distributed and broken fibres are instead examples of fibre defects. Interface defects finally concern the fibre/matrix debonding, i.e., unbonded regions on fibre surfaces, or the lamina/lamina debonding in laminated composites, i.e., delamination. These anomalies in the material state can occur both in the manufacturing process and during the service life.

1.2.1 Manufacturing defects

In fibre reinforced plastics, the material is produced concurrently with the component, which can affect the overall quality. Complexity of manufacturing processes, combined with the rather limited know-how, can result in several

anomalies, such as misalignment and nonuniform distribution of fibres, voids etc. When fibres are mixed with the resin at the point of manufacture, such as in injection moulding and pultrusion, moisture on fibres leads to poor fibre-matrix bonding. In laminates made from pre-pregs, contaminations due to dirt instead cause poor bonding between laminae and so local delamination. Fibres misalignment, typical of hand layup, consistently affects material stiffness and strength. Voids due to air trapped or incorrect curing process are the most typical defects. They can particularly act as crack initiators, causing premature failure. A further source of anomalies is represented by the curing process. Over-cure and incomplete cure cause brittleness and softness, respectively. Further, mistakes in the curing process can result in nonuniform properties of the matrix through the component. Several studies have also reported the transverse matrix cracks at the end of the curing process, when the laminates cool down [3]. Indeed, the directional dependency of the thermal coefficient results in residual tensile stresses which can induce matrix cracking. Schulte et al. [4] have shown that, by mechanically pre-stressing the 0° plies during the curing process, a residual compressive state in the 90° plies can be induced, which delayed and shifted to higher strains and loads the development of transverse matrix cracks.

1.2.2 In-service damage

During the service life, the component can experience overloads, fatigue and impacts, which result in local damaging. Other sources of in-service damage are creep and environmental conditions. Fatigue loading particularly results in a progressive damaging mechanism. Damage starts with matrix cracking in “off-axis” laminae, i.e., the laminae not aligned with load, thus particularly initiating in plies at 90° . Cracks lengthen as cycles proceed and then interact with each other, causing delamination, i.e., debonding between laminae. Eventually, fibre breakage leads to the final failure.

Impacts on composite structures determine various kinds of damage. Impacts can arise both during handling and assembling, e.g., by dropping the part or hitting with a dropped tool, and in-service with foreign objects as stones, birds etc. Also the collisions with hailstones can severely damage the material. Impacts generally cause matrix cracking and fibre fracture. Fibres particularly fail in the compression side, as compression strength is usually weaker than tensile strength in composites. However, when impact energy is absorbed through high flexural deformation, fibres on the tensile side may fail. Further, under lateral loading, as the case of impact, delamination can occur as caused either by interlaminar stresses due to bending or by matrix cracks in proximity of plies interfaces. Damage due to impact clearly depends on the impact energy. There is a threshold energy for damage to occur, which mainly depends on stacking sequence, thickness and support [5,6]. Only internal damaging mechanisms, such as delamination, occur just above the threshold energy. Higher energy leads to delamination and fibre failure. At very high energy levels, the composite

experiences severe damaging with penetration and perforation. A level of damage, known as barely visible impact damage (BVID), is often used to characterise impact. In this case a slight indentation will be only visible on the impacted side [7].

1.2.3 Failure modes and effects of damage and defects

The complete understanding of consequences of damaged regions on the mechanical behaviour of composites still represents a challenging task. As result of their heterogeneous nature, composites present several failure modes and flaw types which differently affect the mechanical performances. As discussed, anomalies are likely to arise during the manufacturing process as well as during the service life. Such defects can act as crack initiators, causing premature failure, or can consistently affect the material stiffness. Indeed, defects in the material can drive the failure mechanism.

In this regard, the case of the unidirectional plies, which can be considered as a building block of many composite structures, can be exemplary. When tensiled along the fibre direction, unidirectional plies show a linear behaviour until complete cracking occurs. As observed in early studies on composites [8], fibres firstly break singly or in clusters of two neighbouring fibres, while in proximity of the final failure, clusters of four or more broken fibres can be observed. The tensile strength is thus strongly affected by the fibre integrity. Compression along fibres direction is instead governed by the formation of kink bands, i.e., local instability of fibres [9]. Misalignment of fibres consistently affects the failure stress in compression, which thus results usually smaller than that in tension. Also, as reported by Hsiao and Daniel [10,11], the major Young modulus is seriously degraded with increasing fibre waviness and the dominant failure mechanism is the interlaminar shear failure. Tensile loads in transverse direction, i.e., normal to the fibre direction, lead to fibre-matrix debonding. This mechanism is governed by a critical value of dilatational energy for the matrix, which is generally reached in correspondence of the fibre-matrix interfaces as result of the local triaxial stress state [12]. The presence of defects, such as moisture, weakens the fibre-matrix interface, thus reducing the critical value of the dilatational energy. Compression loads in the transverse direction induce failure in an inclined plane in the matrix, indicating the involvement of the shear stress in the process. The application of in-plane shear stress in a unidirectional composite shows significant nonlinear behaviour with inelastic deformation, which can be attributed to both the matrix nonlinearities and to the formation of cracks. Analogous considerations on the influence of the micro-structural material state on the mechanical response of the component can be argued for other composite typologies, e.g., woven based laminates.

The combination of different loading conditions introduces further uncertainties in the driving failure mechanism, as it does not follow a unique scheme. For example, the application of transverse loading (tension or

compression) to a unidirectional ply tensioned in the fibre direction does not affect the tensile strength. Instead, the application of in-plane shear stress contributes to the fibre failure and a quadratic combination of these loading condition can be considered as proposed by Hashin [13].

When unidirectional plies are stacked to produce laminates, other failures can arise. For example, the application of loads transverse to the laminate plane may induce delamination, i.e., crack between two adjacent layers. Delamination particularly affects the compressive strength of composites, while its effect on the tensile properties, i.e., tensile strength and in-plane stiffness, is limited if not null. Damage induced by impact involves delamination and usually a multiple-cracks scenario, whose evolution under external load is not strictly depending on the most critical crack, i.e. the most extended crack normal to the loading direction, as in metals [14]. The identification of such most critical crack is particularly critical, as cracks can combine and interact with a priori unknown schemes. This raises doubts also on the current practice of adopting the residual compressive strength of impacted laminates as a design factor. The definition of a residual strength is indeed not unambiguous in composites, given the directional dependency of their mechanical properties [14].

Further, it is also worth highlighting that, as a ply placed within the laminate, the unidirectional composite experiences combined loading conditions which govern the failure at the ply level. Crack growth is constrained by the presence of the other layers, which further complicates the failure prediction. For example, as a single layer, a unidirectional composite tensioned in transverse direction presumably fails from the largest matrix defect. Within a laminate, the failure process in the same composite shows progression in terms of multiplication of ply cracks. Each ply can indeed sustain the presence of multiple cracks, thanks to the presence of other layers. As cracks approach laminae interface, delamination occurs. For increasing delamination, the load bearing capacity decreases until final failure [15].

Previous observations highlight that the prediction of damage consequences still has open questions. The rather complex and highly varying failure modes demand for increasing information on the actual health state. In particular, the multitude of damage mechanisms combined with the limited knowledge of their evolution and interaction suggests the need of assessing the damage severity on the basis of the material response in presence of damage or flaws. Its proper assessment, in terms of existence, location, typology and severity of the damage, is particularly crucial for the application of composite materials.

1.3 Nondestructive damage detection

In order to detect defects, many nondestructive techniques have been developed over the years. Two categories can be recognized: the first involves local investigation methods, whereas in the second category the global behaviour is analysed. The local methods are particularly able to assess the existence, the

location and the typology of defects. The severity of the damage condition is only assessed in terms of extension of the damaged region, but not in terms of residual properties. The global methods instead investigate the behaviour of the component and, through comparison with the undamaged condition, are able to assess the severity of the damage as residual properties. Usually, these refer to residual stiffness. Nondestructive methods are briefly discussed below. For further details, the reader can refer to [16].

Among the local techniques, the most used approaches are ultrasonics, with the variants acousto-ultrasonics and laser ultrasonics, radiography, thermography and shearography. Low frequency vibration methods can adopt both global and local investigation schemes, even though the local ones are confined to the subjective ability of the operator.

Ultrasonics inspection particularly investigates the material condition through ultrasonics waves, also called stress waves. Waves are induced by means of piezoelectric transducers, which convert the input signal from electrical to mechanical and conversely for the output signal. Material quality is investigated by measuring the attenuation of the ultrasonics wave. To this aim, transmitted waves can be considered by adopting two transducers. In alternative, waves reflected by the back surface can be retained through only one transducer. By combining normal and oblique pulse echoes, a highly detailed volumetric image of complex damage states can be produced, as shown by Aymerich et al. [17] for impacted composite laminates. Ultrasonics inspections are characterized by three investigating modes: A-scan, where punctual measurements are realized to assess damage depth, B-scan, where several A-scan measures allow to obtain information as function of the position and C-scan, which is the most adopted scheme. C-scan consists of several B-scan style paths, which allow to map the component. Ultrasonics testing is currently the only nondestructive technique leading to certification [18].

Acousto-ultrasonics is a recent technique, where ultrasonics waves are pulsed in the material through transducers and the transmitted signal is sensed through acoustic emission techniques [19]. In particular, the transmitted acoustic signal, also called stress wave factor, is function of the damage content of the material. Acousto-ultrasonics is adopted in composites by measuring the so-called Lamb waves propagating through the material. Differently from standard ultrasonics, a line rather than a point is interrogated. This allows for inspection of large areas. The existence of multiple propagating modes however complicates the extraction of results. By limiting specimen thickness and frequency range, only two modes are observed: the flexural mode, called a_0 and the longitudinal mode, called s_0 . Sending and receiving transducers are employed for measuring the signal. In particular, the receiving transducer monitors both transmitted waves and reflected waves to the sending transducer. Reflections occur in correspondence of boundaries, i.e., component borders and damage. The analysis of the reflected waves through acoustic emission techniques then provides information on the defect position and size. Recently, it has been suggested that s_0 waves can be

adopted for the nondestructive assessment of local elastic properties [20]. Talreja [21] firstly pointed out the correlation between stress wave factors and material properties, by observing that the stress wave factors depend on the relative orientation between the transducers and the material.

In laser ultrasonics method, the mechanical impulse is not provided through contact between the surface and the transducers, but through a laser signal. As a non-contact technique, the signal is not dependent on the transducer orientation with respect to the surface. Laser based ultrasound thus has the great potential for inspecting components with significant curvatures. However, apart from the costly equipment, the low signal levels represent the major disadvantage.

Radiography is based on the attenuation of electromagnetic radiations after crossing the tested sample. In particular the transmitted radiation I is related to the incident radiation I_0 through the linear absorption coefficient μ as follows

$$I = I_0 e^{-\mu \cdot x} \quad (1.1)$$

where x is the thickness of the sample. The absorption coefficient μ and, in particular, its ratio with the density ρ called mass absorption coefficient, is the discriminating factor. Composites are characterized by low values of the $\frac{\mu}{\rho}$ ratio and therefore require low incident radiations. In composites with carbon fibre reinforcements, fibres and matrix usually present similar mass absorption coefficients. Consequently, radiography cannot be adopted for detecting fibres alignment. Differently, glass fibres have larger values of mass absorption coefficient than carbon and polymers and radiography is increasingly used with glass fibre composites. Radiography is generally better for detecting volume defects than planar damage, as cracks. This significantly limits its application to composites which are generally in sheet form, with cracks lying in the plane of the sheet. In this regard, Arhamnamazi et al. [22] have compared the accuracy of X-Ray radiography and C-Scan methods in damage detection in glass fibre laminates. Results show that C-Scan technique is more accurate for inspection of damage.

The thermography technique measures the response of the structure, in terms of temperature gradients, to a rapid thermic impulse. The gradients are measured through an infra-red camera. With the heat impulse, the surface temperature rises. The heating transfer to the rest of the component depends on the local thermal properties. A defect, such as a delamination, slows the heat diffusion. At the infra-red camera, defects thus appear as hot-spots. Thermography is a very expensive technique, but is able to investigate rather quickly large regions [18]. Further, it provides little information about the volumetric distribution of damage [23]. Montesano et al. [24,25] have shown the ability of the infrared thermography technique in monitoring the damage states in textile composite laminates under fatigue. Temperature profiles captured during cycling testing directly well correlated with corresponding stiffness degradation profiles, thus proving the accuracy of thermography as fatigue damage metric. In a following work [26],

infrared thermography was adopted in stepwise fatigue tests to investigate the existence of a high cycle fatigue limit. One single stepwise test was sufficient to determine the fatigue limit, which resulted in very good agreement with standard fatigue characterization.

Shearography is an optical method which adopts speckle shearing interferometry to measure displacement gradients at the structure surface. Speckles are generated through a laser and a speckle pattern is firstly assumed in the unstressed state. Then, the component is deformed, the speckle pattern is modified, and the gradients are established by subtraction with the reference state. Generally, in correspondence of defects, displacement gradients are more rapid. The structure is usually loaded through vacuum systems, even though thermal loads or vibrations can be also adopted [27]. Garnier et al. [18] have successfully applied this technique to specimen with variable geometry.

Low frequency vibration methods can be global or local. The local method is the so called ‘coin-tap’ test where an operator locally impacts the component through a coin and listen to the resulting sound. The pure subjectivity of the test does not allow extensive use. In global methods, resonant frequencies as well as modal shapes and damping are measured through proper recording equipment. These methods are very attractive for interrogating the whole component rather quickly, eventually through a single measure. As modal characteristics are retained, the structural health monitoring arises from the observation that changes in the structural properties have consequences on the natural frequencies [28]. These techniques are particularly able to quantify material variations caused by defects. However, as the global behaviour is retained, only high-level damage or large defects, such as errors in the stacking sequence or incorrect fibre volume fraction can be detected. The capacity to locate local damage is significantly limited. Low frequency vibration methods can be successfully applied for quality control [29–31].

1.4 Limitations of current practices and research motivation

Nondestructive evaluation techniques have focused on the damage assessment by particularly determining existence, location, and typology. The damage severity is instead characterized in terms of extension of the damaged region. The characterization of damage severity as extension, i.e., crack length, has historical reasons. In metal structures, the evolution of the most critical crack, i.e., the crack among possibly multiple cracks that would grow unstably to fracture, well correlates with the degradation of the strength. Therefore, expressions of the residual strength as function of the crack length can provide good measures of the damage tolerance. For complex crack plane geometries or loading cases, a comprehensive collection of the relevant expressions can be found in the handbook [32]. For the simple case of brittle fracture from the unstable growth of

a crack lying normal to the applied stress, the expression of the maximum applicable stress, i.e., the residual strength, is given as

$$\sigma = \frac{K_{Ic}}{\lambda \cdot \sqrt{a}} \quad (1.2)$$

where K_{Ic} is the fracture toughness of the material, a is the crack length and λ is the geometry parameter. In metals, once the crack extension is known, the damage tolerance can thus be established in terms of sufficient strength in presence of cracks.

Techniques described in Section 1.3 are currently adopted in aerospace and automotive industries for determining the damage condition in composite components [33–35]. Garnier et al. [18] have compared the application of ultrasonics, thermography, and shearography methods on impacted components typical of the aerospace industry. Three specimens of different geometries have been particularly retained. The three techniques have well established location and extension of the damage in the three specimens.

As current nondestructive techniques characterize the damage severity in terms of extension of the damaged region, following the approach pursued for metals, the concept of residual strength in presence of cracks as measure of damage tolerance has been carried to composite structures [36]. The similar trend of the residual strength as a function of the damage evolution further justifies this approach. However, the definition of a residual strength in composites is ambiguous if the complex collection of failure mechanisms is accounted. As the damage is represented by a highly rich variation of cracks, its evolution depends on the interaction of these cracks. Given the complex crack scenario of composites, it is not a priori known which failure mechanism will dominate. Even though location, typology and extension of the damage state can be well characterized, the prediction of the failure mechanism still depends on the boundary conditions, whose complete description is unfeasible to address. As a major consequence, residual strength approaches are not straightforwardly enforceable in composite materials for establishing the damage tolerance. As a further implication, location, typology and extension of the damaged region are not sufficient for characterizing the damage state in composites.

A new metric of the damage severity is required, which is not limited to the extension of the damaged zone. At microscopic level, material properties are the result of the interaction between atoms. The elastic properties, i.e., the Young moduli and the Poisson's ratio, are the result of the repulsive and attractive forces interchanged between atoms. The presence of defects, such as cracks, voids etc., locally affect atomic interactions and, at the macroscopic material level, can be highlighted as local variation of the elastic properties. Reduction of local elastic properties can be thus adopted as metric of the damage severity. Such metric is only function of the actual multiple crack scenario, while it is not influenced by

the dimensions of the damaged zone or by boundaries conditions, such as supports and attachments.

Currently, few techniques are able to assess the damage severity in terms of residual elastic properties. As discussed in Section 1.3, methods based on low frequency vibration are able to quantify material variations due to defects. Lifshitz and Rotem [37] firstly proposed the use of vibration measurements for damage detection. They particularly searched for changes in the dynamic moduli, which are related to shifts in the natural frequencies, to detect damage in elastomer specimens. However, vibration methods analyse the global behaviour, thus resulting sensitive only to high level damage or large defects. Zak et al. [38] performed experimental and numerical analyses of composite beams and plates. These structures were clamped at one side and delaminated at the other. Different ratios of delamination length with respect to the total structure length were considered. Results showed that for delaminations of length up to 30% of the total structure length, the reduction of the first resonant frequency was smaller than 5%. Similar values were obtained for higher modes. Further, they also showed that when the delamination moves from the neutral plane, the drop of the natural frequencies was even smaller. Vibration methods are inherently unable to localize the damage. Cawley and Adams [39] proposed a frequency based approach for damage localization. They showed that the ratio between the frequency shifts of modes i and j , $\frac{\Delta\omega_i}{\Delta\omega_j}$, is only function of the damage position. Even though attractive, the method lacks robustness, as the small reductions of natural frequencies consistently affect the detection. Analogous considerations can be done for the approach proposed by Hu and Wang [40]. The authors retained the modal deformation energy, which depends on the modal shape, to localize the damage on an impacted plate. In particular, the plate is divided into subregions and, according to the modal shape, the modal deformation energy is calculated for each subregion. For a given modal shape, a damage index can be defined in each subregion as the ratio between the modal deformation energy before and after the impact. High values of the damage index for a given subregion indicates the location of the damage. Apart from the tedious repetitions of the frequency measurement necessary to assess the modal shape, the small variations of the natural frequencies compromise the robustness of the methodology. When global vibration behaviour is analysed, the in situ anomaly is concealed by the surrounding intact material [41].

Acousto-ultrasonics is a well-established technique whose capability of assessing damage state in composite structures has been widely addressed. Measurements of the signal are expressed through the so-called Stress Wave Factor (SWF), which usually refers to the s_0 Lamb waves, i.e., flexural waves, in composites. In its earliest definition, the SWF essentially consisted in counting the peaks in the received signal [42]. The peak counting was indeed found to be related to the material strength [43]. As an alternative, Talreja proposed the definition of five SWFs in the frequency domain of the received signal [21]. The

author showed that the proposed SWFs were particularly sensitive to the relative orientation of the transducers with respect to the material, as a result of the material anisotropy. Therefore, a correlation between the SWFs and the local elastic properties was suggested, even though not explicitly articulated. Recently, Pillarisetti and Talreja [20] have shown that the same SWFs definition well correlates with the crack density in damaged composites. However, as stated by the authors, a correlation between local elastic properties and measured SWFs still needs to be established. In this regard, the nonphysical meaning of the SWFs does not help. Further, as acousto-ultrasonic measurements are comparative, repeatability is particularly critical to provide adequate sensitivity of SWFs for the detection of damage. As shown by Russel-Floyd and Phillips [44], when statistical methods are applied to account for the scatter of SWF readings, even impact damage of 15 mm diameter becomes undetectable.

As an alternative to the methods described in Section 1.3, Seo and Lee [45] investigated the electrical resistance change as damage parameter in fatigue tests of carbon fibre reinforced plastics. They showed that the measured stiffness and electrical resistance presented a very similar trend of change. In particular, as the damage proceeds, the electrical resistance increases due to the rise of microcracks, which reduce the material conductivity. They thus proposed a damage parameter based on the electrical resistance measurements, given by the ratio of the initial and the actual value. However, it is worth noting that the proposed damage parameter correlates well with global stiffness of the specimen, while damage cannot be localized. This compromises the applicability of the method to real structures. Further, another limitation arises from the need of conductive materials as carbon fibre reinforced plastics.

Similar considerations can be done for the multi-physics approach based on the measurement of the dielectric response in composite laminates, as recently proposed by Vadlamudi et al. [46]. By measuring the dielectric response, the methodology is not limited to conductive materials. The technique intends to observe and model the variation in the dielectric response as a function of the damage development and evolution in order to characterize the current material state. This interesting idea is based on the observation that the presence of cracks, voids etc., increases the presence of internal surfaces thus altering the capacitive properties of the material [47,48]. The technique thus intends to characterize the current material state. Even though the methodology has been shown to be able to well identify the different phases of damage progression, it is worth noticing that the global stiffness is again considered, which limits the localization of the damage.

The goal of this dissertation is to present a new methodology for the nondestructive inspection of composite structures. The methodology aims at the nondestructive, local and quantitative assessment of the residual elastic properties. In particular, the technique intends to characterize the damage severity condition through the quantitative evaluation of the elastic constants of the damaged zone. The methodology is particularly based on a local vibrational analysis, where a

proper equipment is adopted to localize the vibrational response. After showing the sensitivity of the technique to the local material properties, the assessment of damage severity is addressed. This also introduces a new metric of the damage severity, which is not limited to the extension of the damaged zone.

1.5 Organization

This dissertation is focused on the characterization of damage severity in terms of residual elastic properties in composite materials. The Detecting Damage Index technique is firstly investigated for the nondestructive assessment of local material properties. This methodology was recently brought into the realm of nondestructive characterization tests of composite material components [49]. In Ch. 2, the application of the Detecting Damage Index to a progressively damaged composite plate is shown and limitations are discussed. Thereafter, the work introduces the new methodology based on local vibration analysis (see Ch. 3). The methodology is firstly shown to be sensitive to the local material properties and its enhancements, as well as its limitations, are analysed in Ch. 4. In Ch. 5, the local vibrational technique is adopted to characterize the damage severity of impacted composite plates. Conclusions and possible implications of the proposed approach, with particular reference to the damage tolerance design strategies, are finally given in Ch. 6.

II

Detecting Damage Index

Technical literature has widely investigated the tolerance of composite materials to impact damage. Pursuing metal approaches, the residual load-bearing capability has been the first concern. However, the prediction of the post-impact load-bearing capability of a damaged composite structure is more difficult than in metals, as the damage zone is generally complex in nature. Great efforts have been also made to improve the impact resistance of fibre composites, by focusing on the governing parameters related to the constituents [50]. Another approach looks at the energy absorption aptitude of the composite structures, as result of the energy balance between the incident energy, the energy absorbed by the material and the energy returned to the impactor. Energy balance approaches in impact testing of laminates can be also adopted to orient preliminary design choices, as proposed by Quaresimin et al. [51].

Energy balances approaches particularly allow to evaluate the level of damage accumulation of composites during impact events. The manner in which composite materials respond to impact loading and dissipate the incident kinetic energy, E_i , is very different to that of metals. For low and intermediate impact energy, metals absorb energy through elastic and plastic deformation, whose consequences on the load-carrying capability are usually limited. At high energy, perforation may occur and its effects can be predicted through fracture mechanics principles. In composites, whose plastic deformation is very limited if not null, the impacting energy E_i is dissipated both through elastic deformation and by fracturing. Net of the elastic energy E_{el} , whereby the impactor rebounds, the residual part of the incident energy is absorbed in creating large areas of fracture. Impact damage is thus strictly correlated to the absorbed energy E_{abs} , which can be in turn interpreted as a measure of the material damage.

In this chapter, a recently proposed nondestructive technique will be investigated which is based on energy absorption aptitude. The methodology, called Detecting Damage Index (DI_d), is particularly able to quantify local elastic

properties. After detailing the historical background, the technique will be presented. Its accuracy in assessing local elastic properties will then be shown in combination with the finite element method. Finally, possible limitations and drawbacks will be discussed.

2.1 From *DD* to *DI*

In 1998, Belingardi and Vadori proposed a new damage variable, called Damage Degree (*DD*), to assess damage accumulation caused by low velocity impacts [52]. The damage variable is defined as the ratio between the absorbed energy and the impact energy, i.e.,

$$DD = \frac{E_{abs}}{E_i} \quad (2.1)$$

In impact testing, the incident energy can be calculated from the measurement of the impactor velocity right before the impact, once its mass is known. Instead, the absorbed energy is calculated as the area surrounded by the load-displacement curve. In particular, the displacement of the dart can be computed through a double numerical integration of the acceleration, calculated from the force-in-time signal acquired during the impact test. As discussed, the absorbed energy can be interpreted as a measure of the material damage.

A scheme of the testing fixture for impact testing adopted in [52] is depicted in Fig. 2.1.

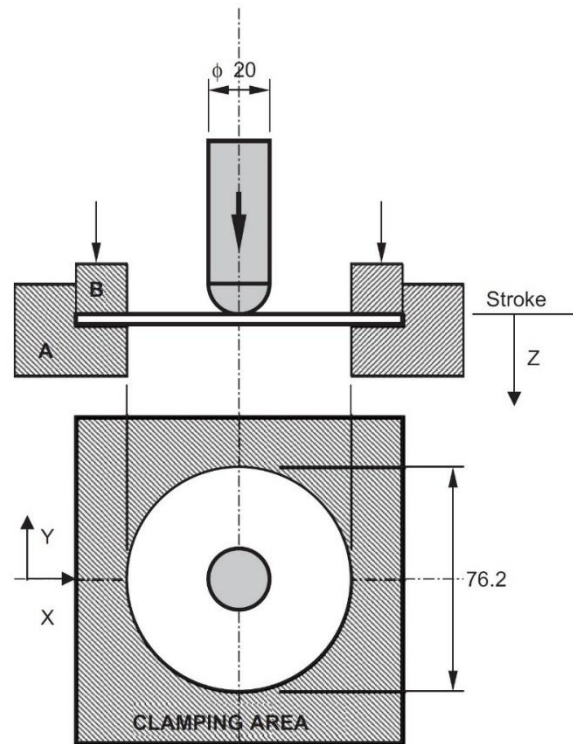


Figure 2.1 Scheme of the experimental fixture for impact testing.

The specimen panels are fixed through a proper clamping system which provides uniform pressure on the clamping area. The testing frame also allows to prevent slippage of the specimen. From the measurement of the impactor velocity, right before the impact, and of the impact force, the DD parameter can be determined. Therefore, the DD parameter is not specifically defined for this experimental fixture. It is also worth noting that, in the case of the experimental fixture of Fig. 2.1, the impact response concerns only the circumferential region whose diameter is 76.2 mm. Indeed, due to the clamping system, only the material comprised in the circular region will be involved in the impact event.

As the impact energy increases, the material is further damaged, which results in increased energy absorption. At the limit case of penetration, whereas the impactor is arrested within the material with no rebound, the absorbed energy equals the incident energy and the DD reaches the value of one. In particular, in correspondence of the first occurrence of penetration, i.e., the first time the absorbed energy reaches the level of the incident energy, a saturation energy can be identified. This threshold energy indeed represents the maximum energy level the laminate can dissipate through only internal damage mechanisms.

In thick laminates, for impact energy above the penetration threshold, the impactor moves increasingly deeper into the laminate, until perforation takes place, and the impactor passes through the laminate. At this stage, the impact data force becomes constant with respect to the displacement. As the impactor moves through the laminate, only the friction between the perforated walls and the lateral surface of the impactor slows its fall.

A range between penetration and perforation can be identified for thick laminates. While for thin laminates the penetration and the perforation energies are comparable or even equal, for thick laminates, the energy required by the dart to go through the laminate cannot be neglected. As a consequence, for thick laminates, two threshold energies, i.e., the penetration energy and the perforation energy are to be discerned.

The damage variable DD of Eq. (2.1) is not able to catch the range between penetration and perforation, as it assumes the value of one after penetration. In order to overcome this issue, a new damage parameter was thus introduced by Belingardi et al. [53], called Damage Index (DI). The DI is defined as

$$DI = \frac{E_{abs}}{E_i} \cdot \frac{s_{MAX}}{s_{QS}} \quad (2.2)$$

where the DD is multiplied by the ratio between the maximum displacement recorded during the test and the displacement value recorded in quasi-static perforation test at the instant when the force becomes constant. In case of perforation during the impact test, the maximum displacement is again recorded in correspondence of the force constancy. An example of quasi-static perforation test and impact test to perforation is reported in Fig. 2.2 taken from [53].

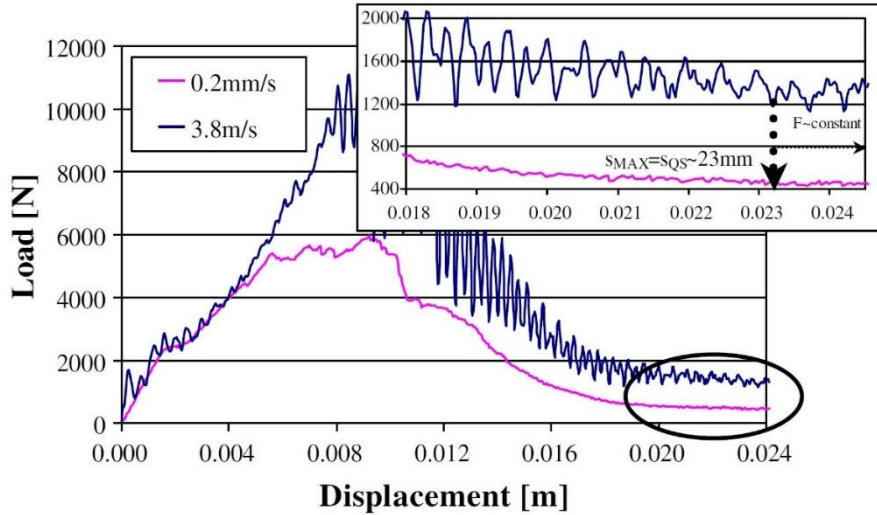


Figure 2.2 Example of quasi-static perforation test and impact test to perforation [53].

The normalization of the maximum displacement with respect to the corresponding value measured in quasi-static perforation tests allows to account for strain-rate effects on the s_{MAX} , as it can vary with the impact velocity. The quasi-static displacement for normalization suggests the choice of an absolute reference value.

An example of DD and DI trends is reported in Fig. 2.3, taken from [53]. Impact tests on carbon/epoxy laminates with stacking sequence $[0/90]_8$ are compared. Both DD and DI increase linearly with the impact energy. In correspondence of the penetration threshold, the DD variable saturates to the value of one, while DI shows a sudden but finite growth which proceeds until perforation occurs.

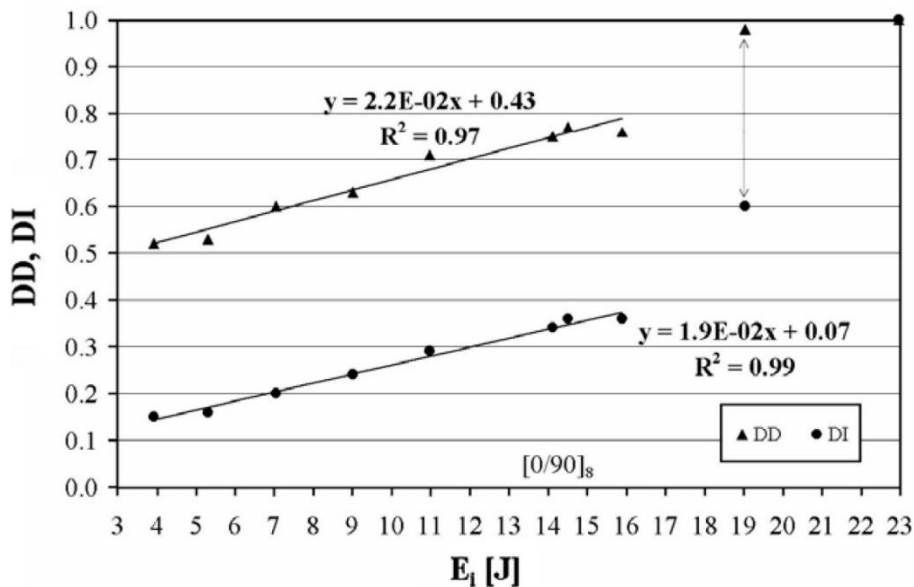


Figure 2.3 Comparison between DD and DI trends for impact tests on a carbon/epoxy laminate with stacking sequence $[0/90]_8$ [53].

In Fig. 2.3, it is worthwhile noticing that both the fitting curves of DD and of DI do not intersect the origin. However, while the DD shows an abrupt rise, the initial step of the DI is rather small and the extrapolated DI values for very low energy levels are very close to zero. This suggests another positive aspect of the new damage parameter: differently from the DD variable, the DI is able to represent the damage induced by impacts at almost null energies.

The damage accumulation in repeated impact tests was also investigated through the DI , in order to highlight the rate of accumulation and the onset of severe damage modes. In [54], the authors compared the vacuum infusion and hand lay-up manufacturing techniques on the basis of the response to repeated impact loading. Results showed that the DI computed after repeated low energy impacts was constant and the force-displacement curve did not change with the impact number. In other words, low energy impacts did not affect the material state and the elastic properties of the laminate remained constant impact after impact.

Low energy impacts can be thus adopted to non-destructively investigate changes previously introduced into the system by damaging events. In addition, by properly correlating the elastic properties to the impact response, the nondestructive methodology can establish residual elastic properties. It is worthwhile noticing that, as the impact response concerns a local region of the component, as shown in Fig. 2.1, local elastic properties are assessed.

2.2 Correlation between elastic properties and impact response

The Detecting Damage Index (DI_d) technique was brought in the realm of the nondestructive characterization for components made of composite material by Tridello et al. [49]. A nondestructive impact is exploited to quantify the residual elastic properties in damaged composites. As the residual energy absorption aptitude is evaluated for a circumscribed region of the component, as shown in the fixture setup of Fig. 2.1, local elastic constants are assessed. The DI_d technique requires a preliminary characterization activity to identify the correlation between residual elastic properties of the material and the DI_d parameter, which is defined as

$$DI_d = \frac{E_{abs}}{E_{th}} \cdot \frac{S_{MAX}}{S_{QS}} \quad (2.3)$$

where E_{th} is the so-called threshold energy, which is defined as the impact energy at which the reduction of local elastic properties is less than 5%. An impact at the threshold energy can be considered as nondestructive for the material. This value is a material property which has to be identified with a preliminary characterization.

The preliminary experimental campaign particularly consists of two sets of impact tests: the so-called “*single impact set*” and “*double impact set*”. In the

“single impact set”, several material plates are subjected to an impact test. Increasing impact energy is considered for each plate in order to increasingly damage the composite. Tensile tests are then performed on specimens cut from the impacted plates around the damaged area, as shown in Fig. 2.4 taken from [49].

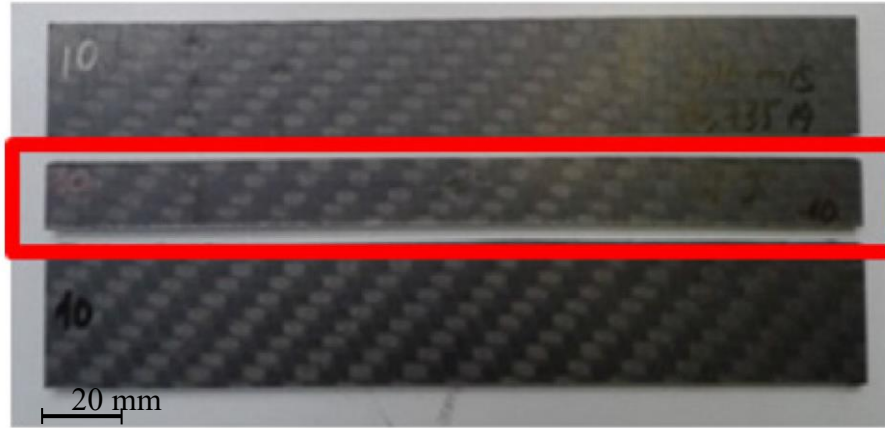


Figure 2.4 Specimen cut from impacted plates and used for assessing the residual elastic properties [49].

In order to determine the residual elastic properties, longitudinal strains are measured through an extensometer mounted near the damaged zone. The tensile tests allow to correlate the residual elastic properties to the impact energy. Further, from this correlation, the threshold energy E_{th} , i.e., the impact energy at which the reduction of local elastic properties is less than 5%, is evaluated.

The “double impact set” involves two impact tests. A new set of composite plates is initially impacted at increasing energy levels and then impacted again on the damaged area at the threshold impact energy E_{th} . The DI computed after the second non-damaging impact is namely the Detecting Damage Index DI_d , in accordance with Eq. 2.3. The “double impact set” allows to correlate the DI_d parameter to the impact energy. Combining this information with the results of the single impact set, where the residual elastic properties are correlated to the incident energy, the residual elastic properties can be expressed as a function of the DI_d parameter. The proper nondestructive test to estimate the residual elastic properties of the investigated component is thus performed at the threshold energy E_{th} .

Finally, it is worth reminding that the preliminary campaign is preceded by the quasi-static perforation test to compute the displacement value s_{QS} at the instant when the force becomes constant, as already defined in Eq. 2.2.

The flow-chart of Fig. 2.5 summarizes the procedures involved in the DI_d technique and previously described. From the “single impact set”, the correlation between the residual elastic properties (E_{res}) and the impact energy (E_i) is determined, as well as the threshold energy E_{th} . The “double impact set” instead allows to correlate the DI_d parameter to the impact energy (E_i). Finally, by combining the results of the two impact sets, the residual elastic properties are

related to the DI_d parameter. This correlation is exploited in the proper nondestructive test for the assessment of the residual elastic properties on the damaged component.

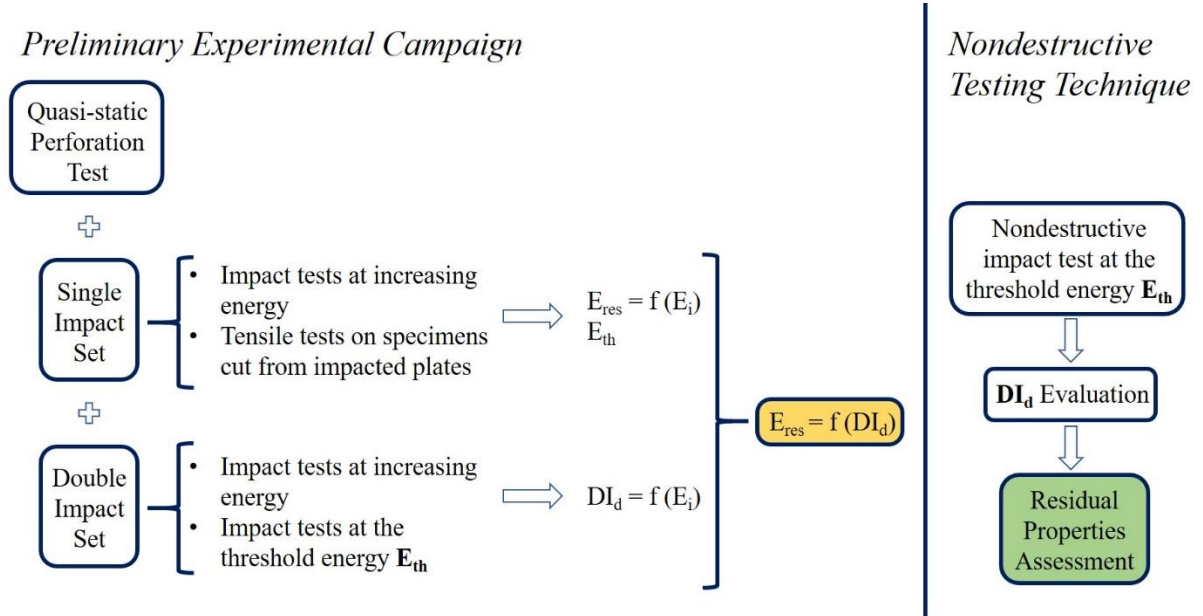


Figure 2.5 Flow-chart of the DI_d technique.

2.3 Combination of Finite Element Method and DI_d for the assessment of residual elastic properties

In this section, the effectiveness of the DI_d technique is shown on a carbon/epoxy laminate in combination with the finite element method. Results refers to the experimental and numerical activity published in [55].

A composite laminate plate is firstly damaged through repeated four-point bending tests. Then, the DI_d technique is adopted to map the residual elastic properties on the damaged plate. The mapping procedure consists of 8 nondestructive impacts in different locations along the longitudinal direction of the plate. The threshold energy E_{th} and the correlation between the DI_d parameter and the residual elastic properties were determined in the previous work by Tridello et al. [49], where the same material was adopted. Indeed, the nondestructive technique involves nondestructive impacts at the threshold energy, which, as discussed, can be seen as a material property. The variation of the Young modulus along the plate is then accounted in the finite element model of the laminate subjected to bending test through continuous polynomial curves.

Finally, the resulting experimental and numerical force-displacement curves are compared to establish the accuracy of the technique. The combination of the experimental activity and the numerical finite element analysis points out that the DI_d methodology is effectively able to predict the local residual elastic properties of damaged composite components. In particular, the combination of finite element and DI_d methods will be firstly presented in detail. Experimental and numerical results are then shown and commented.

2.3.1 Materials and methods

Materials

A structural composite laminate specifically developed for automotive applications is retained for the tests. The composite material is the same adopted by Tridello et al. [49] in their investigations and previously in [41]. It consists of a matrix made of epoxy resin reinforced by eight layers of twill woven carbon fabric. The first layer is a 380 gsm fabric with 0.45 mm thickness and an 800 gsm fabric with 0.88 mm thickness is used in the remaining seven layers. The stacking sequence is $[0/90]_4$.

In the numerical analysis, the laminate is modelled with seven layers of thickness 0.88 mm and one layer of thickness 0.45 mm, oriented according to the stacking sequence. A total thickness of 6.61 mm is thus obtained. Even though the first layer is different from the other seven, this difference can be neglected when considering the global mechanical behaviour of the laminate. The measured elastic properties (Young's modulus, shear modulus and Poisson's ratio) are reported in Table 2.1, as assessed in [49].

Property	Value
Density	$1.45 \cdot 10^3 \text{ kg/m}^3$
Young's modulus in longitudinal and transverse direction ($E_{11} = E_{22}$)	54 GPa
Shear modulus (G_{12})	3.5 GPa
Poisson's ratio ($\nu_{12} = \nu_{21}$)	0.08

Table 2.1 Material properties.

Given the symmetry of the woven fabric, the mechanical properties and the Poisson's ratios in the in-plane directions 1 and 2 are the same (i.e., $E_{11} = E_{22}$, $\nu_{12} = \nu_{21}$).

Experimental tests

In order to clearly identify the elastic field of the composite material, two different plates are tested in four-point bending tests until complete failure occurs. The tests are performed on a servo-hydraulic testing machine (Instron 8801). In agreement with the recommendations of the ASTM standard D6272 [56] for four-point bending test of reinforced plastics, the load span is one third of the support span. As shown in Fig. 2.5, the loading noses are 50 mm distant. The support noses are consequently placed at a distance of 150 mm. Fig. 2.5a shows the experimental setup. The resulting experimental curves of force with respect to displacement are exploited to tune a finite element model of the laminate subjected to four-point bending test, which is shown in Fig. 2.5b.

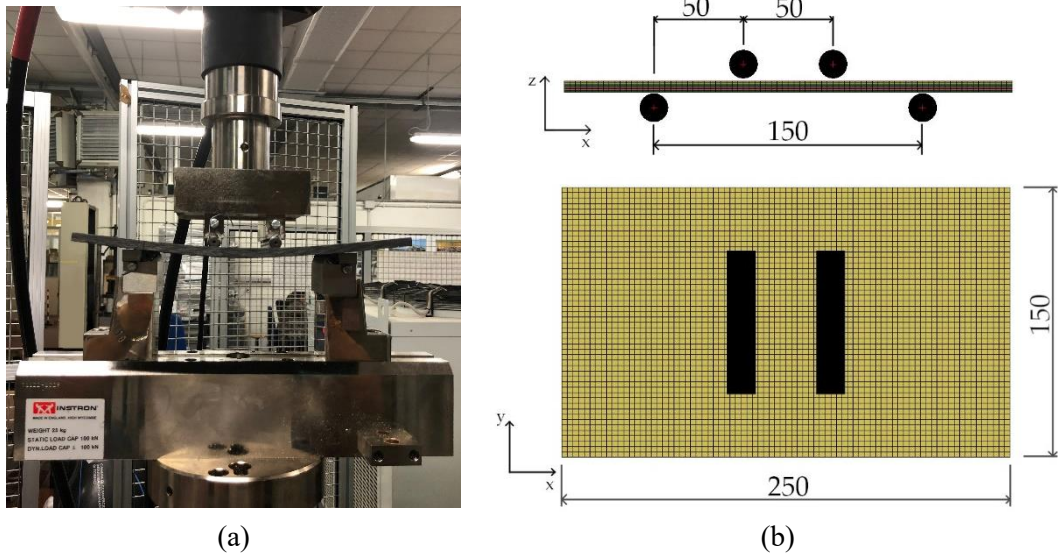


Figure 2.6 Four-point bending test: (a) experimental setup; (b) numerical model.

The same experimental setup is adopted to progressively damage an undamaged composite plate. The plate is loaded until incipient failure occurs and then unloaded. Achieved failure is not complete, as the load-carrying capacity of the composite laminate is still significant. The repeated four-point bending tests reduces progressively the plate stiffness. A significant damage level is thus induced.

The residual Young modulus of the damaged plate is then assessed through the Detecting Damage Index (DI_d) technique. The preliminary characterization activity is firstly necessary to identify the correlation between residual elastic properties and the DI_d parameter. Results of the preliminary characterization campaign are reported in [49]. Indeed, the series of impact tests was performed on a set of plates made of the same composite fabric. In particular, the impact tests were carried out using a free-fall drop dart testing machine (CEAST 9350 FRACTOVIS PLUS), in agreement with the recommendations of the ASTM standard D5628 [57]. The mechanical clamping system, shown in Fig. 2.1, was adopted to clamp the plates. The circular unclamped region has a diameter of 76 mm. The preliminary experimental activity is characterized by several impact tests at increasing energy levels. The impact energy was defined by varying the impactor mass for a given impact velocity. The impact velocity, which is controlled by the drop height of the dart, was measured in each test with an optoelectronic device. A piezoelectric load cell, mounted in proximity of the tip of the impact dart, acquired the force signal at a sample rate of 1 MHz.

Through the preliminary activity, the threshold energy E_{th} is evaluated. The plate previously damaged with the repeated four-point bending tests can be thus inspected through a series of impacts at the threshold energy. In particular, the damaged plate is impacted along the middle line. Moving along the longitudinal direction of the plate (x direction of Fig. 2.6), the impacts are located in correspondence of the external noses, in the regions where bending moment is linearly increasing, in correspondence of the internal noses and finally in the

middle of the load span. Seven impacts are applied in total to the plate, as shown in Fig. 2.7.

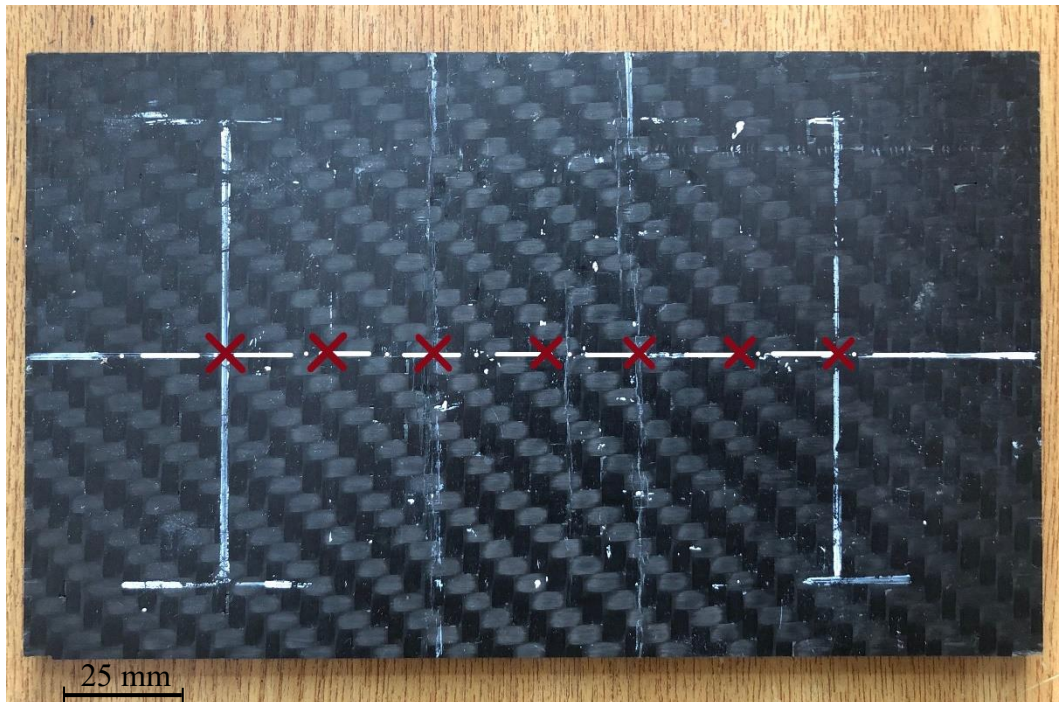


Figure 2.7 Location of impacts for DI_d analysis.

The corresponding residual Young modulus is calculated from the DI_d parameter, as defined in Eq. 2.3.

Numerical model

The four-point bending test is simulated using the commercial software LS-Dyna. The 8 layers of the woven fabric composite are modelled with Belytschko-Tsai 4-node shell elements, with one integration point through the thickness. For each layer of the composite, a layer of shell elements is considered, thus resulting in 8 integration point through the thickness. Solid elements of cohesive material are placed between the shell layers, in order to represent the resin among layers. Solid elements of cohesive consider a specific formulation of LS-Dyna, which allows to transfer moments between the shells. In particular, nodes of solid elements coincide with those of the shells. The material card `*MAT_LAMINATED_COMPOSITE_FABRIC`, which is specific for fabric composite, is adopted for the composite layers. This material model assumes a slightly modified version of Hashin criteria for failure [58]. However, the attention is here focused on the elastic field and parameters related to the post-failure behaviour of the material are not addressed. The cohesive material model `*MAT_COHESIVE_TH`, with properties of the resin, is assigned to the cohesive elements. Finally, the span noses are modelled as rigid cylinder walls. The upper cylinders, shown in Fig. 2.6b, move downwards with a prescribed motion law. In order to avoid penetrations and numerical instabilities, the upper and lower

cylinders are placed at the initial distance of 1 mm from the laminate. Contact between laminate and cylinders is based on a penalty formulation with a penalty factor which adaptively guarantees the numerical stability [59]. This formulation accounts for thickness offsets of shells.

The accuracy of the numerical model is firstly verified with respect to the experimental results of the two composite plates, tested until complete failure occurred. This allowed to clearly identify the elastic field of the material. Indeed, the main objective is to validate the numerical model with respect to the elastic behaviour, as the interest of this activity is the quantification of the residual elastic properties of the damaged composite. Then, the same numerical model is used in comparison with the experimental results of the progressively damaged plate. In this case, the mechanical model has to account for the variation of Young's modulus on the plate, as inspected through the DI_d technique.

The residual elastic properties of the damaged plate are mapped through the DI_d technique. As will be shown later, the Young modulus varies along the x -direction according to the location of measurement, with the damage mostly located in correspondence of internal rolls. It seems reasonable to assume that the Young modulus varies continuously along the longitudinal x -direction. Here, a polynomial curve is considered for each region included between two consecutive measure locations, x_k and x_{k+1} .

For each polynomial curve, the two Young moduli at the extremities, E_k and E_{k+1} , with k the considered location, are known from the DI_d measurements. In addition, the two derivatives at the extremities can be estimated. In order to evaluate the derivatives, the difference quotient for each region is calculated as

$$\frac{\Delta E_k}{\Delta x_k} = \frac{E_k - E_{k-1}}{x_k - x_{k-1}} \quad (2.4)$$

in accordance with its definition.

The difference quotient is a measure of the average rate of change of the function, here the Young modulus, over the interval Δx_k . By considering two consecutive difference quotients, $\frac{\Delta E_k}{\Delta x_k}$ and $\frac{\Delta E_{k+1}}{\Delta x_{k+1}}$, the derivative at the k -th location has been estimated as follows:

1. when the product $\frac{\Delta E_k}{\Delta x_k} \cdot \frac{\Delta E_{k+1}}{\Delta x_{k+1}}$ returns a negative value, the derivate at the k -th location is assumed equal to zero. This can be justified by considering that a change in the sign of the difference quotient implies a change in the derivative of the function, as well;
2. when the sign of the product $\frac{\Delta E_k}{\Delta x_k} \cdot \frac{\Delta E_{k+1}}{\Delta x_{k+1}}$ is positive, the derivate at the k -th location is assumed equal to average value $\frac{\frac{\Delta E_k}{\Delta x_k} + \frac{\Delta E_{k+1}}{\Delta x_{k+1}}}{2}$;
3. the derivatives at the extremities, $k = 1$ and $k = 7$, are assumed equal to zero.

A graphical representation of the difference quotients retained for the calculation of the derivative at the k -th location is represented in Fig. 2.8.

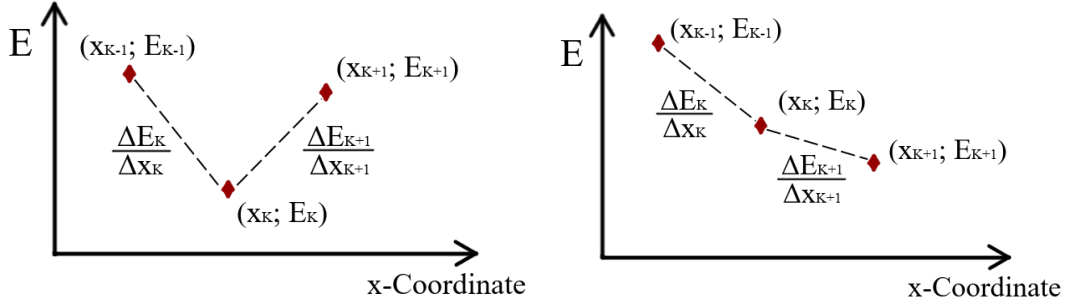


Figure 2.8 Qualitative representation of the difference quotients retained for the calculation of the derivative at the k -th location: (a) negative sign; (b) positive sign of the product $\frac{\Delta E_k}{\Delta x_k} \cdot \frac{\Delta E_{k+1}}{\Delta x_{k+1}}$.

Red points represent the Young modulus, as measured through the DI_d . In particular, Fig. 2.8a refers to the case of negative product $\frac{\Delta E_k}{\Delta x_k} \cdot \frac{\Delta E_{k+1}}{\Delta x_{k+1}}$, while Fig. 2.8b refers to the case of positive sign of the product $\frac{\Delta E_k}{\Delta x_k} \cdot \frac{\Delta E_{k+1}}{\Delta x_{k+1}}$.

As the two Young moduli and the derivatives are known at the extremities, a third-order polynomial curve can be constructed for each interval included between two consecutive impact locations. This approach guarantees the continuity of the Young modulus with respect to the x -coordinate.

In the numerical model, this variation is accounted by longitudinally dividing the layers of shells into parts. Each part consists of one row of shell elements and is identified by its x -coordinate. In particular, each part can be longitudinally localized in correspondence of the middle of the element size. In this work, a mesh of 3 mm has been adopted. According to the location of the part in the x direction, the corresponding third-order polynomial curve can be identified. The Young modulus is consequently calculated. A material card is defined for each part with the corresponding elastic properties.

The described procedure is summarized in the flowchart of Fig. 2.9. The first part concerns the verification of the finite element model of the four-point bending tests. The second part involves the use of the DI_d technique to map the residual Young's modulus on the plate. The verification is performed by comparison of the experimental and numerical force-displacement curves. In particular, the finite element model considers a continuously variable Young's modulus along the longitudinal direction of the plate (x direction of Fig. 2.6), as described.

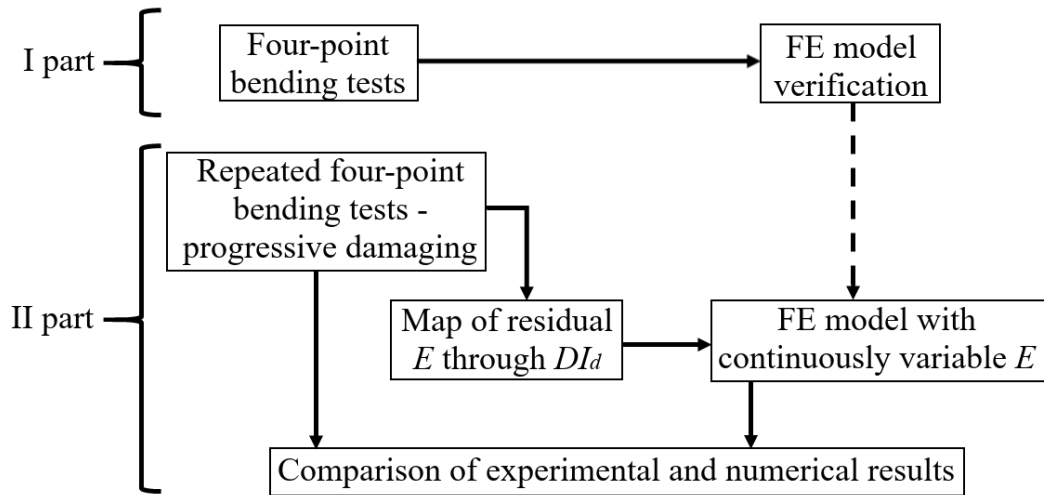


Figure 2.9 Flowchart of the adopted procedure.

2.3.2 Results

In this Subsection, the experimental and numerical results are presented. Firstly, experimental and numerical data related to the completely failed plates are compared. Results of the progressive damaging of the composite plate through the repeated four-point bending tests are then shown, as well as the correlation between the residual elastic properties and the DI_d variable, as obtained in [49]. Residual elastic properties are thus estimated through the DI_d methodology. The Young modulus is mapped with respect to the longitudinal coordinate and the third-order polynomial curves are constructed as previously described. Finally, in order to show the accuracy of the nondestructive technique, the experimental results of the progressively damaged plate are compared to the numerical model which accounts for the residual properties.

Four-point bending test: experimental results and numerical model tuning

In the four-point bending tests, the two undamaged composite plates have undergone almost complete failure. The main objective of this experimental activity is to clearly identify the elastic field of the material. Therefore, tests were performed even after the first failure occurred and the first load drop was measured.

The upper layers, which are subjected to compressive loads, showed the most significant failures. Intralaminar cracks propagate in correspondence of the inner span noses. Fig. 2.10 shows a magnification of the cracks, obtained through an optical microscope. The complete failure can be appreciated for the upper four layers.

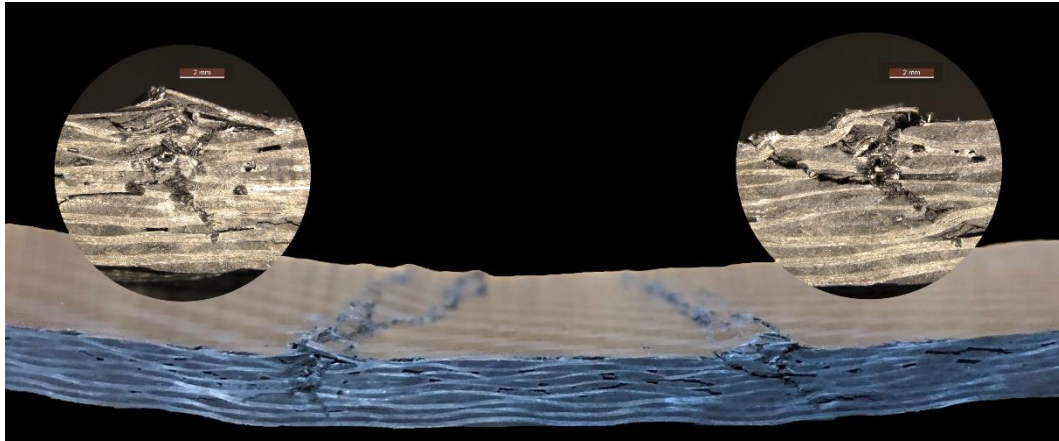


Figure 2.10 Magnification of intralaminar cracks: failure of the upper four layers.

The numerical model is analysed only in the elastic field and it results in good agreement with the experimental data, as shown in Fig. 2.11. Displacement of the numerical analysis has been evaluated on the rigid cylinders.

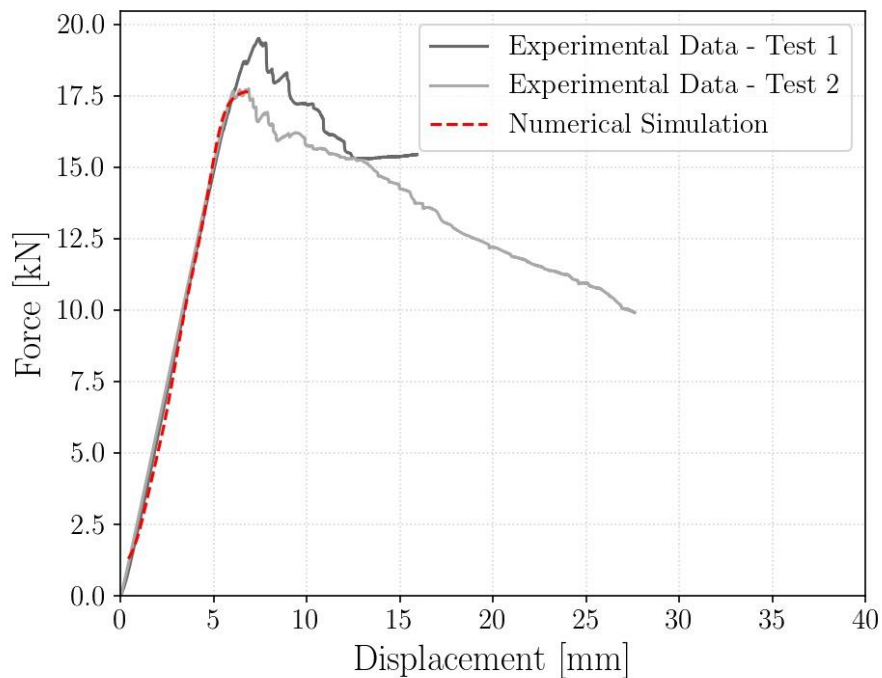


Figure 2.11 Experimental and numerical results of the four-point bending tests.

As discussed, the rigid wall cylinders are initially distanced from the composite laminate. Consequently, the initial path of the force-displacement curve is characterized by the growing contact between laminate and cylinders, which is not significant for the purpose. The numerical force-displacement curve has been thus shifted leftwards and results of the numerical analysis are reported from 1 mm of displacement.

Progressive damaging and assessment of residual elastic properties through the DI_d technique

An undamaged composite is then subjected to repeated four-point bending tests. Load is increased until incipient failure occurs and then decreased. Achieved failure is not complete, as the load-carrying capacity of the composite laminate is still significant. In total, five repetitions are performed, as shown in Fig. 2.12, where the resulting force-displacement curves are numbered as Test n.1, Test n.2, Test n.3, Test n.4 and Test n.5.

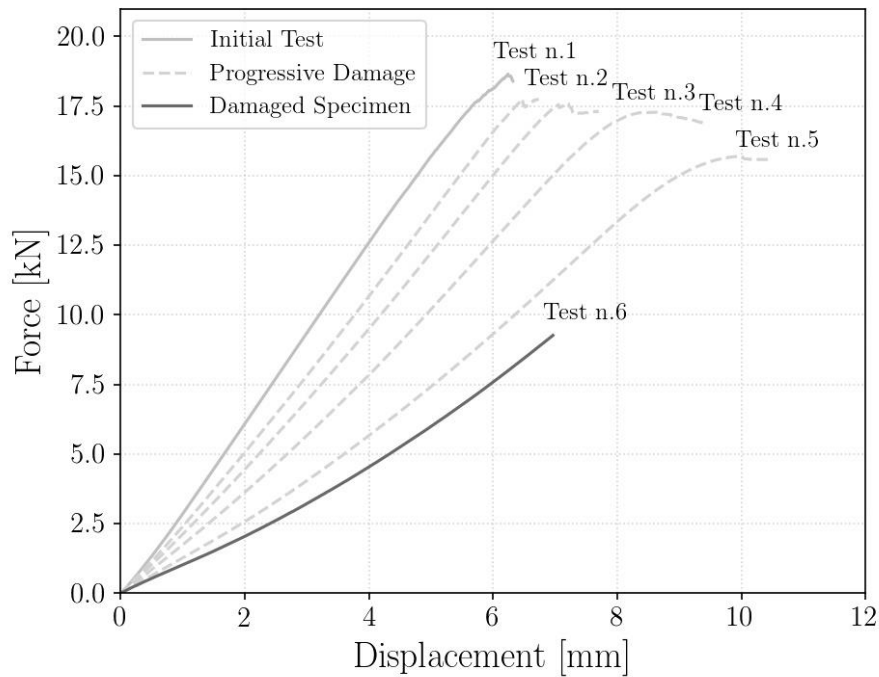


Figure 2.12 Progressive damaging of composite plate through four-point bending tests.

As the damage increases, the plate stiffness progressively decreases. Loading and unloading cycles are performed until the residual stiffness of the composite plate is about 40% of the original value. This is shown with the Test n.6 (damaged specimen curve), which is performed only in the elastic field. A significant damage level is thus induced through the five tests.

The DI_d technique is then adopted to estimate the residual elastic properties. Preliminary characterization tests allowed to evaluate the threshold energy E_{th} , which can be considered a material parameter and in this case was equal to 5 J. Details of the preliminary characterization tests can be found in [49], where the same material was used. Fig. 2.13 shows the resulting correlation between the residual elastic properties of the analysed composite and the DI_d parameter. The dotted line is thus retained to evaluate the residual elastic properties in the progressively damaged plate. Cross markers represent the results of the preliminary characterization tests. The slope of the dotted line particularly suggests that the higher is the DI_d , the lower the residual elastic properties.

According to Eq. 2.3, the DI_d parameter increases with the absorbed energy E_{abs} . Indeed, the absorbed energy is a measure of the material damage.

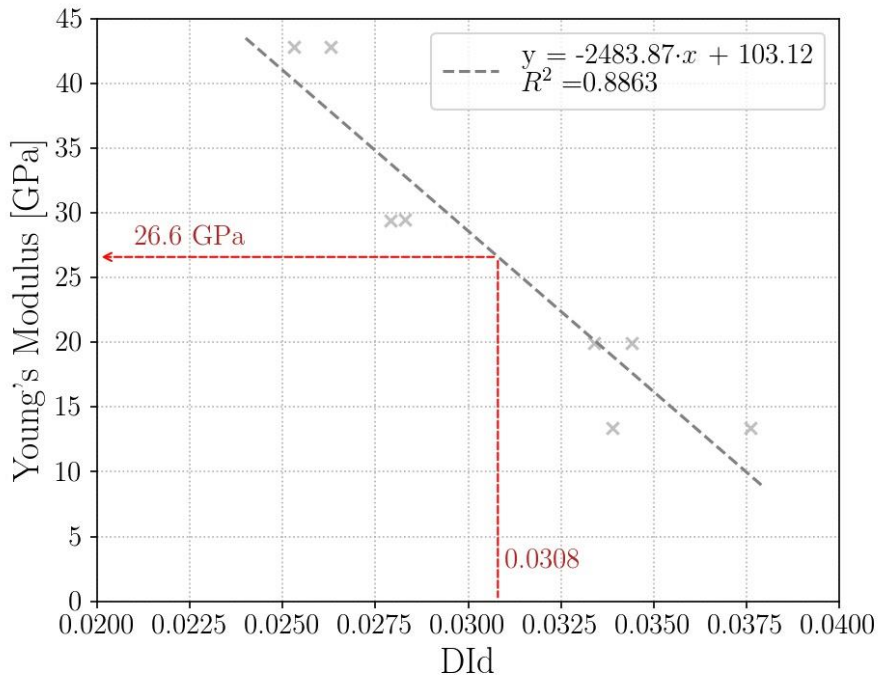


Figure 2.13 Residual Young's modulus evaluation with DI_d .

As reported in Fig. 2.7, the elastic properties have been estimated at seven locations along the middle line of the composite plate. Table 2.2 reports the measured DI_d values and the corresponding Young moduli, as well as the locations in x -direction of the impacts.

x -coordinate [mm]	DI_d	E_{res} [GPa]
50	0.0283	32.8
75	0.0297	29.5
100	0.0360	13.7
125	0.0308	26.6
150	0.0360	13.7
175	0.0297	29.5
200	0.0283	32.8

Table 2.2 Residual Young's moduli and corresponding DI_d values at specific locations.

In correspondence of the external noses, even though the bending moment is null in the four-point bending test and no damage should be present, the elastic modulus is equal to 32.8 GPa, which is significantly different from the original value of 54 GPa. This can be justified by taking into account that the circular unclamped region considered for the DI_d test has a diameter of 76.2 mm. Consequently, elastic properties are assessed as an average of the unclamped region.

Further, as clamping boundary conditions have to be realized all around the laminate, the diameter of 76.2 mm limits the region where the residual properties can be measured through the DI_d . Moving outwards from the external noses, only few measurements of the residual properties can be obtained and results would be affected by the damaged portion of the plate. Based on these considerations, we can assume that, at a distance of 38 mm from the external noses (half of the diameter), the damaged portion of the plate would not affect an ideal measurement through the DI_d . The Young modulus is thus here considered equal to the original value of 54 GPa.

From the seven measurements of the Young modulus and considering the two assumed external values, eight third-order polynomial curves can be constructed, as previously described. As a consequence, a continuous variation of the Young modulus with respect to the x -coordinate is obtained. This result is shown in Fig. 2.14, where measured Young's moduli are marked with red squares and assumed values with black thin diamonds.

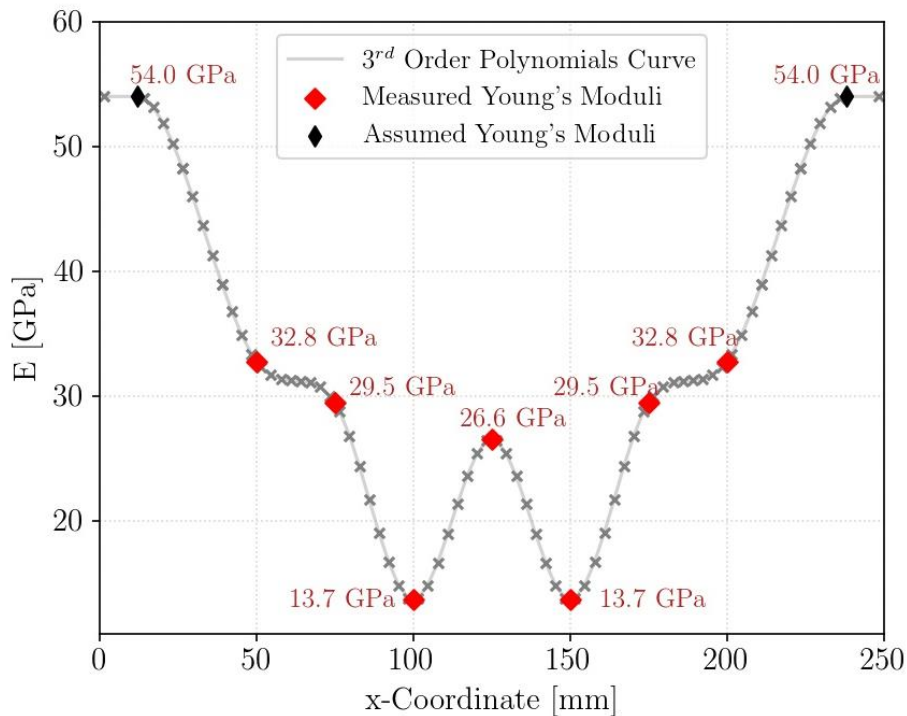


Figure 2.14 Variation of residual Young's modulus with respect to the x -coordinate.

The continuous curve is adopted in the numerical model to account for the variation of the Young modulus. Layers of shells have been longitudinally divided into parts, which are represented with different colours in Fig. 2.15.

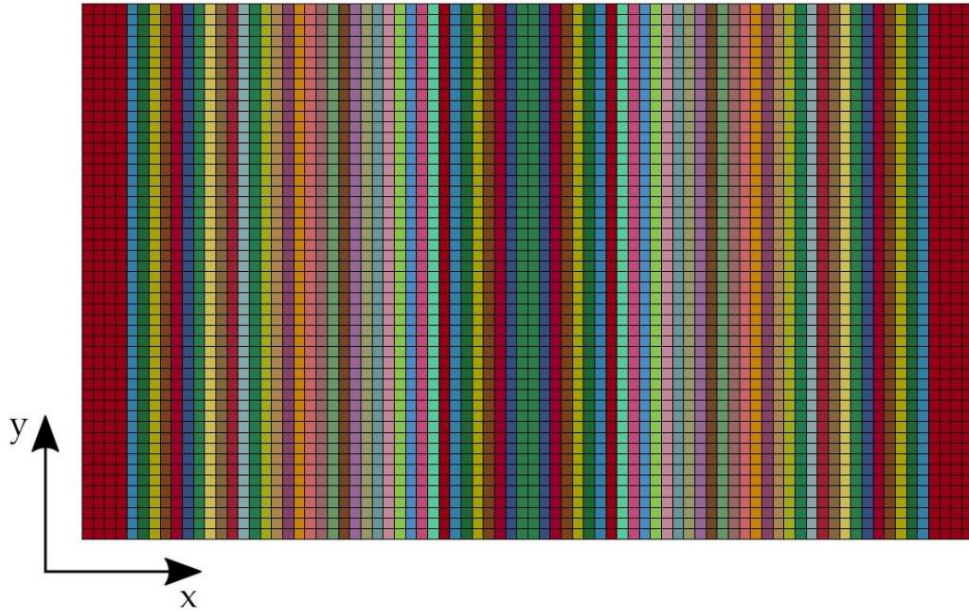


Figure 2.15 Top view of the finite element model of the composite laminate: longitudinal division of layers.

The continuous curve allows to evaluate the Young modulus in correspondence of the x -coordinate of each part. A material card has been defined for each part with the corresponding elastic properties. Cross markers of Fig. 2.14 represent the Young moduli assigned to each material card.

Moving outwards from the external noses, the elastic modulus increases from 32.8 GPa to 54 GPa and then is assumed constant. It should be noted that, as the bending moment is here null, the mechanical behaviour of the numerical model will not be affected by the value of the elastic modulus estimated for this region.

Validation: comparison of experimental and numerical results

The model of the composite plate with variable elastic modulus is adopted for simulating the four-point bending test. Results of the numerical force-displacement curve are then compared to those obtained with the progressively damaged plate. As shown in Fig. 2.16, experimental and numerical results are in very good agreement, with limited discrepancies in slope. Results of numerical analysis are once again reported from 1 mm of displacement. The numerical displacement is measured on the rigid cylinders and these are initially distanced from the composite laminate, in order to avoid penetrations and numerical instabilities. Consequently, the initial path of the numerical force-displacement curve concerns the contact between laminate and cylinders and is not significant for the purpose.

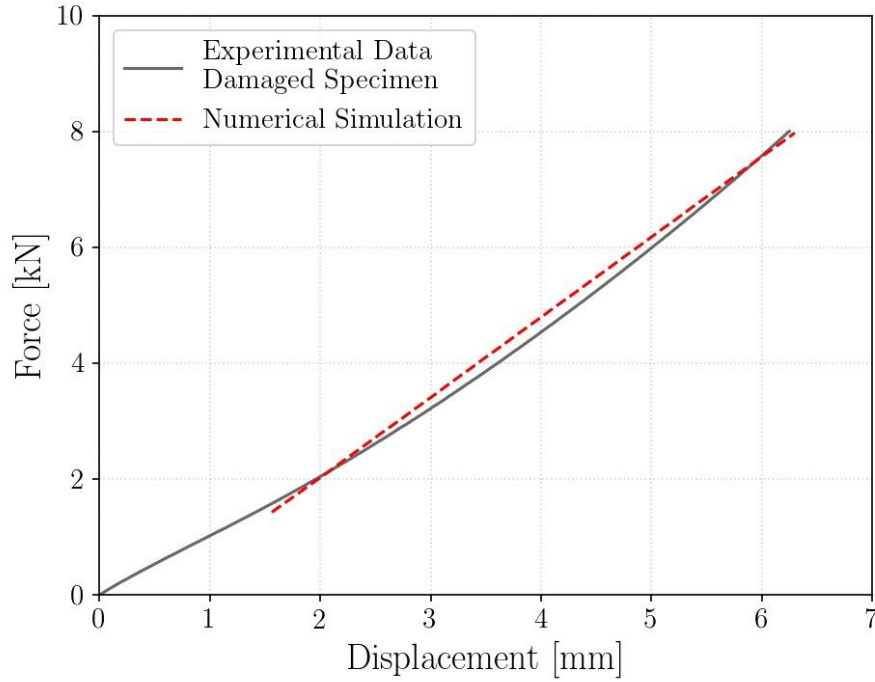


Figure 2.16 Comparison of experimental and numerical results of damaged specimen.

Experimental response shows an increasing stiffness as the plate is bent. This hardening effect can be explained by taking into account that the considered material fails under compressive loads, as shown in Fig. 2.10. The four-point bending tests are repeated until incipient failures occur. Consequently, cracks propagate in the upper layers subjected to compressive loads. When testing the composite plate, these cracks are progressively closed under compression. This allows to sustain loads in the failed layers and an increasing stiffness is thus obtained. The hardening effect can be also appreciated in the force-displacement curves with progressive damage of Fig. 2.12 (dotted lines).

The limited discrepancy between experimental and numerical results highlights the accuracy of the DI_d technique in mapping the residual elastic properties of the damaged plate. Further, this result validates the approach which accounts for the variable elastic modulus with a continuous polynomial curve in the finite element model.

2.4 Advantages and criticalities of the methodology

The DI_d is proved effective in monitoring the structural integrity or manufacturing quality. The DI_d allows the nondestructive, quantitative and local assessment of the health state of composite structures. Indeed, severity of the damage condition is evaluated in terms of residual elastic properties, rather than in extension. Further, through the clamping system, the retained impact response concerns a circumscribed region of the component, thus localizing also the determination of the residual elastic properties. A map of the residual properties

can be achieved. In combination with the finite element method, the mechanical behaviour, at least in the elastic field, can be precisely described.

The main drawback of the methodology is represented by the extensive preliminary experimental campaign necessary to correlate the residual elastic properties to the parameter DI_d . As discussed, the preliminary experimental campaign consists of two sets of impact tests, in addition to the quasi-static perforation tests. As each set of impact tests requires at least five measurements at increasing energy levels, a consistent amount of material has to be employed. Further, in order to perform the tensile tests, specimens around the impact energy must be realized, which further affects costs and time. As shown in [49], each material property must be characterized after the impact, i.e., tensile tests must be performed at 0° , 45° and eventually 90° . In addition, the DI_d adopts costly equipment, such as the load cell for the acquisition of the force signal or the optoelectronic device for the measurement of the velocity of the impactor.

In regard to the damage condition assessment, it is worth to notice that, even though the methodology evaluates the severity in terms of residual elastic properties, the extent of defective region cannot be determined. As a consequence, as discussed in Subsection 2.3.2, residual elastic properties are assessed as an averaged value of the inspected region. As shown in the mapping procedure, even though cracks were localized in correspondence of the inner noses, the impact response, and so the detected properties, varied in accordance with their position in the investigated region. The residual properties are averaged according to the participation of the damage to the impact response.

Finally, a source of uncertainty is represented by the threshold energy, whose value is estimated from the correlation between the residual properties and the impact energy in the “*single impact set*”. When considering a defective zone, an impact at the threshold energy can add further damage to the component, as the presence of severe defects consistently reduces the load carrying capability of the material. This aspect poses questions on the significance of the threshold energy and needs further investigation. On the other, it is worth noticing that the reduction of the threshold energy, i.e., the energy at which the nondestructive impact is performed, is limited by the practical constraint imposed by the noise in the impact data. Indeed, low values of the threshold energy reduce the signal to noise ratio in the computation of the DI_d , thus affecting the accuracy of the methodology.

In the next chapters, a new methodology will be presented, which overcomes some of the limitations discussed for the DI_d .

III

Local Vibrational Analysis

In vibrational methods, the dynamic response of a plate, in terms of vibration modes and frequencies, is exploited to estimate the material elastic constants of composites. To be more precise, as vibrational methods are dynamic tests, the “dynamic” elastic properties are assessed [60]. Vibrational tests generally employ two types of excitations, which consist of impulse excitation and continuous variable excitation. In impulse excitation, an impulser is usually used to mechanically strike the specimen. An initial displacement is thus imposed to the hit point of the structure which starts vibrating around the equilibrium position. Continuous variable excitation commonly involves the use of loudspeakers or shakers fed by a variable frequency oscillator. Transducers, accelerometers, microphones, or laser Doppler vibrometer are used as response detectors.

In order to compute the material constants from the experimental vibrational tests, an inverse method is adopted. In contrast with forward methods, which determine modal parameters, i.e., natural frequencies, modal shapes and damping, from the material properties through a modal analysis, inverse methods are employed to determine the elastic constants from the measured modal characteristics. Inverse methods usually involve an optimization scheme, where the elastic properties are handled as design variables. The optimization problem is aimed at minimizing the discrepancy, in terms of modal characteristics, between the experimental results and the results of a modal analysis based on a numerical model of the component. At each iteration of the optimization problem, according to the set of elastic properties defined by the optimization algorithm, the modal parameters are calculated with the modal numerical analysis and compared with the corresponding experimental result. The modal analysis can be based on analytical formulas, semi-analytical methods, such as the Rayleigh-Ritz method, or finite element models. These approaches can be employed even in combination.

With regard to the layer-wise identification for a multi-layered laminated plate, several vibrational tests are needed depending on the number of materials

used in the multi-layered laminate plate. The larger the number of materials used in a multi-layered plate, the higher the number of required vibration tests. When considering a composite laminate, whose layers are made of the same material, four natural frequencies are at least required to obtain a reasonable set of estimates for the four elastic parameters, independently from the stacking sequence [61]. However, by incrementing the number of information, the accuracy and the robustness of the inverse method process can be increased. In this regard, several studies are present in the literature which combine modes and frequencies [62–64].

With respect to the experimental tests, due to its simplicity and inexpensive procedures, the Impulse Excitation Technique (IET) is widely employed. Currently, an ASTM standard procedure is provided only for testing isotropic materials [65]. Despite this, multiple studies have successfully applied such a procedure to orthotropic and anisotropic laminated materials [66]. Paolino et al. [41] demonstrated the suitability of the IET even for assessing the residual elastic properties of damaged composite laminates. In particular, they impacted composite specimens and adopted the formulations of the ASTM standard [65] for longitudinal vibration test to calculate the residual elastic constants. Results were then compared with those obtained through standard tensile tests, showing the applicability of the technique even for composites. With similar approach, Maciel et al. [67] showed that the IET is able to measure the progressive damaging of composite specimens in fatigue tests.

Vibrational methods are thus suitable for quantifying material variations caused by defects. The structural health monitoring particularly arises from the observation that changes in the structural properties have consequences on the modal characteristics, i.e., resonant frequencies, modal shapes and damping. As discussed, the testing equipment is usually such that interrogates the whole component rather quickly, eventually through a single measure. As the global behaviour is retained, vibrational methods are limited to only the detection of high-level damage or large defects, such as errors in the stacking sequence or incorrect fibre volume fraction. In presence of local damage, e.g., that caused by impact, the shift in the natural frequencies, related to the local change in the elastic properties, is usually very limited. The in-situ anomaly is concealed by the surrounding intact material, thus restricting the application of vibrational methods for nondestructive inspection. Further, even if the shift in the resonances were measurable, the identification of damage location is not straightforward.

However, the DI_d methodology has revealed that local elastic properties can be assessed when the response to the nondestructive impact concerns only a localized region of the component. In particular, in order to circumscribe the impact response, boundaries of the investigated zone were clamped (cf. Ch. 2). Pursuing the approach of isolating the response to only a portion of the component, a new methodology is here introduced. Rather than nondestructive impacts, the vibrational response is investigated. The methodology is based on the IET.

The methodology intends to combine the local investigations performed in the DI_d technique with the advantages of the vibrational methods. The testing rapidness, the limited costs of the experimental setup and, mainly, the direct correlation between modal characteristics and material properties are among the most favourable factors to overcome the issues discussed for the DI_d technique, while benefiting from its positive aspects. The methodology here introduced is thus based on a local vibrational analysis, i.e., the vibrating phenomenon involves only a circumscribed region of the component.

In this chapter, the methodology will be presented which allows to estimate local elastic properties of laminated composites, i.e., the Young moduli in longitudinal and transverse directions E_{11} and E_{22} , the dynamic shear modulus G_{12} and the Poisson's ratio ν_{12} . The approach assumes that the stacking sequence of the laminate is known and the stacked plies are made of the same material. Experimental validation of the technique is performed on a composite plate with unidirectional carbon fibre reinforcement, which is firstly described. The sensitivity of the methodology to the presence of a defect is then analysed, by referring to the dimensions of the isolated region. Finally, limitations and possible criticalities are discussed. Results of the present Chapter have been also published in [68].

3.1 Unidirectional plate

Experimental tests are performed on a laminated composite plate. The composite laminate consists of seven layers of unidirectional carbon fibre reinforcement impregnated with epoxy resin. 300 gsm unidirectional reinforcement is used in each layer, while the epoxy matrix is specifically developed for good surface finishing. Unidirectional prepreg plies are stacked in parallel and vacuum bagged. The prepreg plate is finally cured in autoclave at 130°C for 90 minutes under the pressure of 6 bar. The resulting unidirectional composite plate is shown in Fig. 3.1. The stacking sequence is $[0]_7$.

The dimensions of the unidirectional plate are 300 mm x 300 mm. Regarding the thickness, as its value consistently affects the frequency response and in particular the value of the first fundamental frequency of a clamped plate, twelve measures at different locations on the plate have been considered. These locations are shown in Fig. 3.1. As reported in Table 3.1, the thickness varies from a minimum value of 0.94 mm to a maximum value of 1.13 mm.

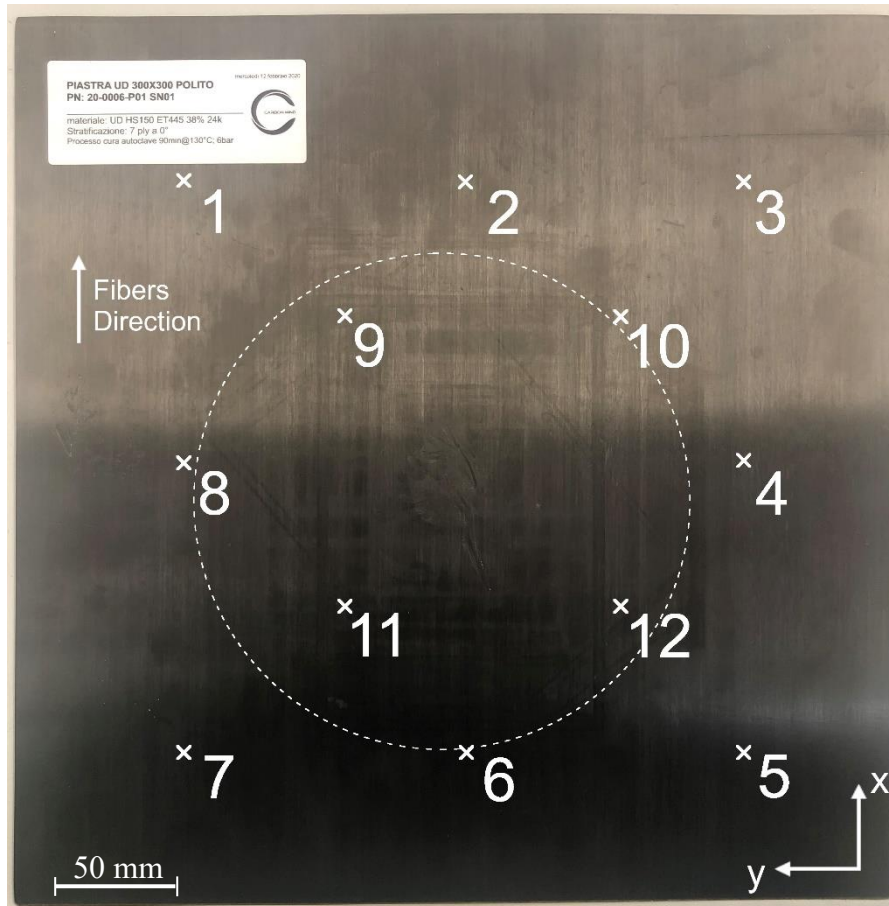


Figure 3.1 Unidirectional composite plate.

Reference Point	Thickness [mm]
1	1.11
2	1.11
3	1.12
4	0.94
5	1.06
6	1.08
7	1.13
8	1.04
9	1.08
10	1.05
11	1.09
12	1.11

Table 3.1 Thickness variation (highlighted in red the maximum and minimum thicknesses in the plate).

Investigations for the assessment of local material properties concerned the region shown in Fig. 3.1 through the dotted line. This includes points 6, 8, 9, 10, 11 and 12, whose average thickness of 1.08 mm has been considered in the numerical calculations.

The nominal material properties of the composite plate (Young's moduli, shear modulus and Poisson's ratio) have been provided by the supplier, according to the orthotropy axes. These values are reported in Table 3.2. The Poisson's ratio

in the transverse direction ν_{21} , calculated from data reported in Table 3.2, results equal to 0.019.

Property	Value
Density	$1.55 \cdot 10^3 \text{ kg/m}^3$
Young's modulus in longitudinal direction (E_{11})	131.1 GPa
Young's modulus in transverse direction (E_{22})	7 GPa
Shear modulus (G_{12})	3.93 GPa
Poisson's ratio (ν_{12})	0.35

Table 3.2 Material properties.

The nominal material properties have been non-destructively verified by analysing the free vibrational response of the plate. In particular, the IET has been adopted to test the freely supported plate and results have been compared to a modal analysis of finite element model of the plate with free boundaries. The mechanical vibrations have been measured through an accelerometer. The first torsional mode, the first flexural mode in the longitudinal direction and the first flexural mode in the transverse direction have been retained. The accelerometer was particularly positioned on the composite plate in correspondence of the maximum modal displacement of the considered mode. The fundamental frequencies are equal to 15 ± 2 Hz, 99 ± 2 Hz and 19 ± 2 Hz, for the torsional mode, for the first flexural mode in the longitudinal direction and for the first flexural mode in the transverse direction, respectively.

In order to verify the material properties provided by the supplier, the measured frequencies have been compared to the corresponding modes, obtained through the modal analysis. In particular, the modal analysis has been performed on a finite element model of the plate with free boundaries, where the elastic constants provided by the supplier are considered. The plate is modelled with Belytschko–Tsay four nodes shell elements whose formulation involves 6 degrees of freedom per node. The mesh size of 1 mm, with 90000 elements and 540000 degrees of freedom, is considered to discretize the structure. A uniform thickness of 1.08 mm is assumed. Further, in accordance with the number of layers of the unidirectional composite, seven integration points are assumed through the thickness, while one integration point in the element plane is used. Finally, the inertial effect of the accelerometer is accounted through a lumped mass, equivalently distributed on the nodes of the plate in accordance with its location. For example, in the case of the torsional mode, the accelerometer was positioned at one of the corners of the plate, where the modal displacement is maximum. Accordingly, its mass is distributed in the corresponding nodes in the finite element model. As result of the modal analysis, the resonant frequencies are extracted through the Lanczos method [59]. The resulting resonances are 16 Hz for the torsional mode, 98 Hz for the first flexural mode in the longitudinal direction and 20 Hz for the first flexural mode in the transverse direction, which are in good agreement with the free vibrational tests. The resulting frequency spectra and the corresponding mode shapes are shown in Fig. 3.2.

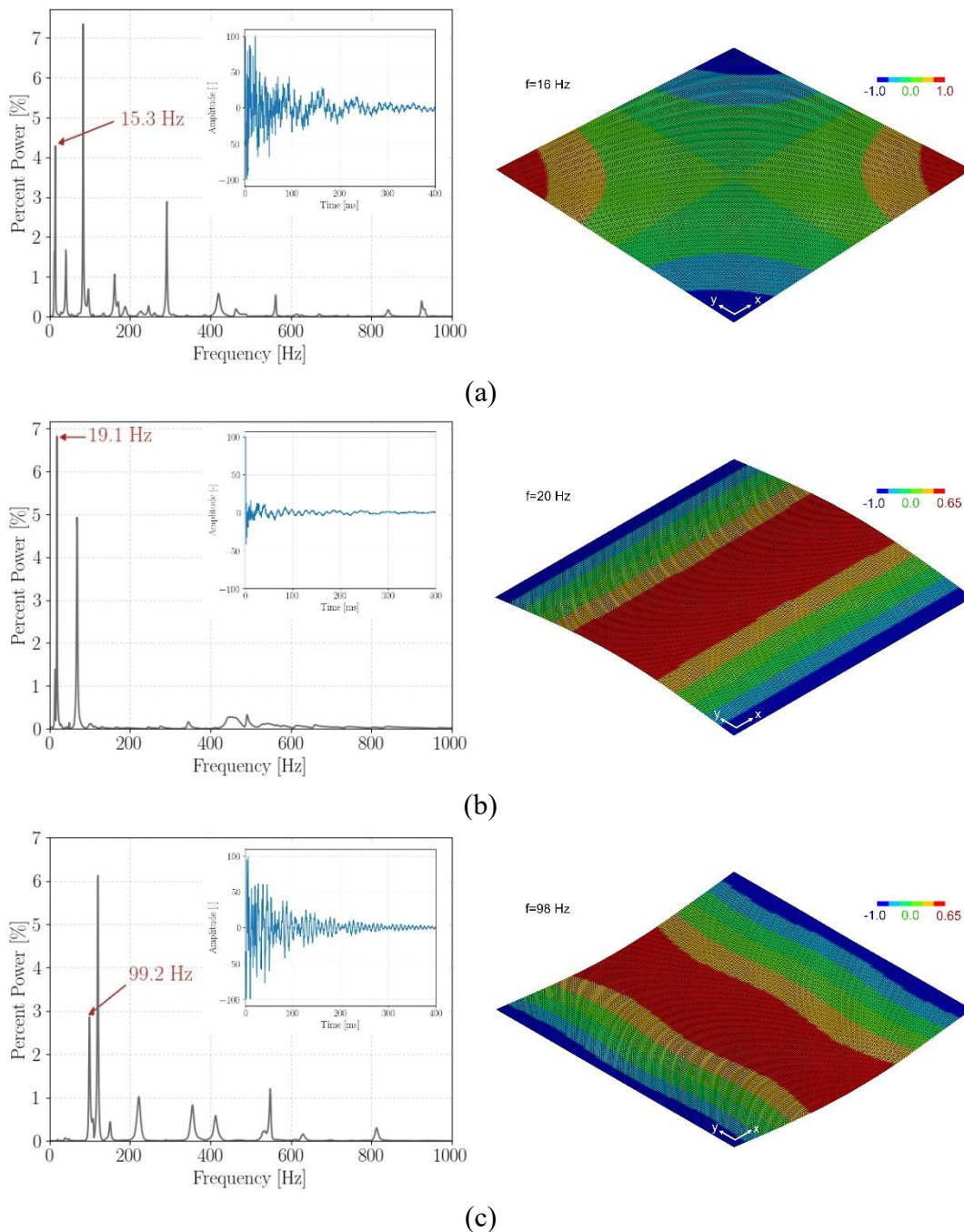


Figure 3.2 Acquired signal with IET frequency spectra and corresponding modal shape: (a) torsional mode shape; (b) flexural mode shape in transverse direction; (c) first flexural mode shape in longitudinal direction.

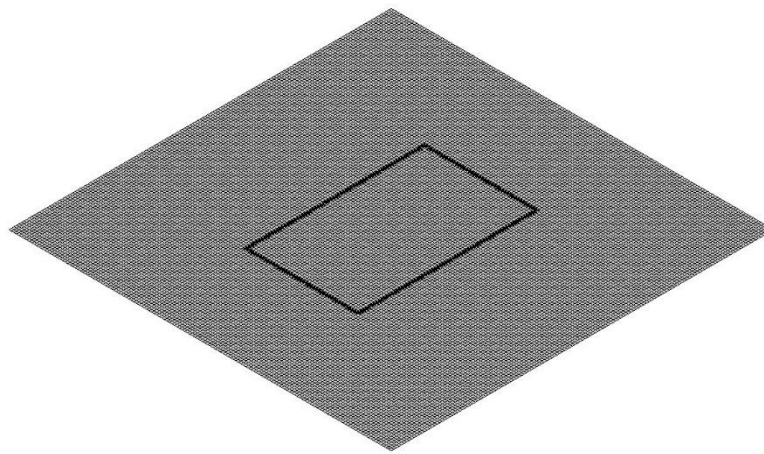
The material properties provided by the supplier can be considered as the global material properties of the plate.

3.2 Clamping as isolating: experimental setup

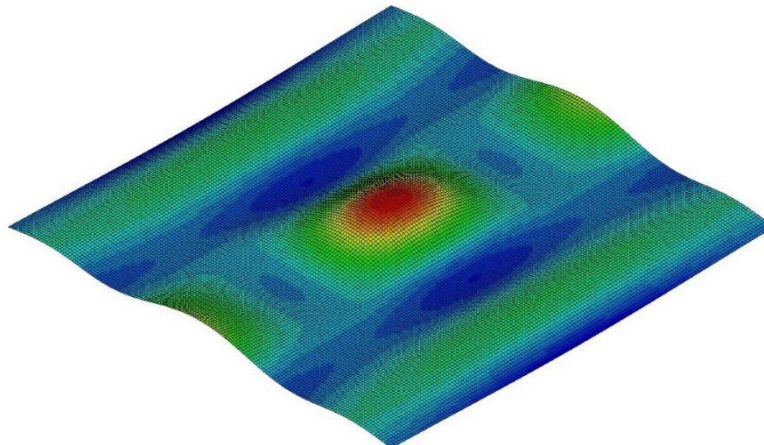
In order to determine the local material properties, the vibrational response must be mostly related to a local region of the component, while the influence of the excluded surrounding material is limited. This can be achieved by clamping

the investigated region at its extremities, as also proposed in the DI_d technique. Differently from the simply supported boundaries, where the modal shapes necessarily involve both the retained region and the outer material, clamped conditions allow to isolate the zone where the vibrational response is of interest, thus resulting in a modal response of the system which is function only of the characteristics for the analysed region, i.e., of its material properties.

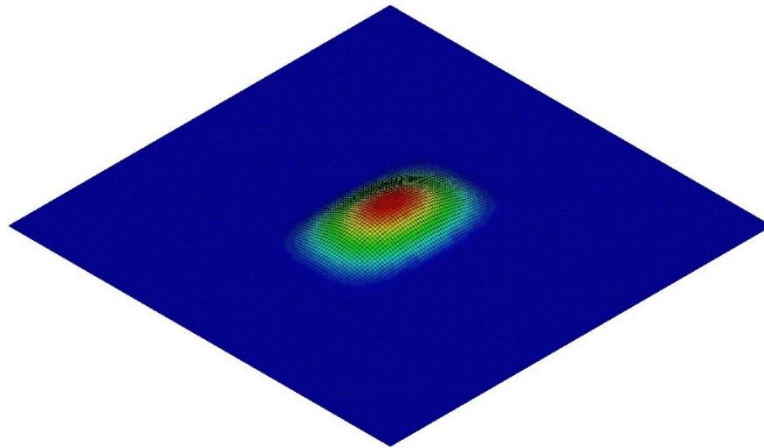
The insulation of the vibrational response obtained through clamped boundaries can be shown through a finite element modal analysis. Fig. 3.3a shows a finite element model of a plate where the highlighted path of nodes circumscribes the region under investigation. Two modal analyses are performed: the first assumes simply supported boundary conditions in the highlighted nodes, while in the second, fully clamped boundaries are considered. As shown in Fig. 3.3b, with simply supported boundary conditions, the plate vibrates both inside and outside of the analysed region. Instead, when fully clamped boundaries are considered, a specific mode which involves only the region to analyse can be appreciated (Fig. 3.3c). This mode is a function of the analysed region properties.



(a)



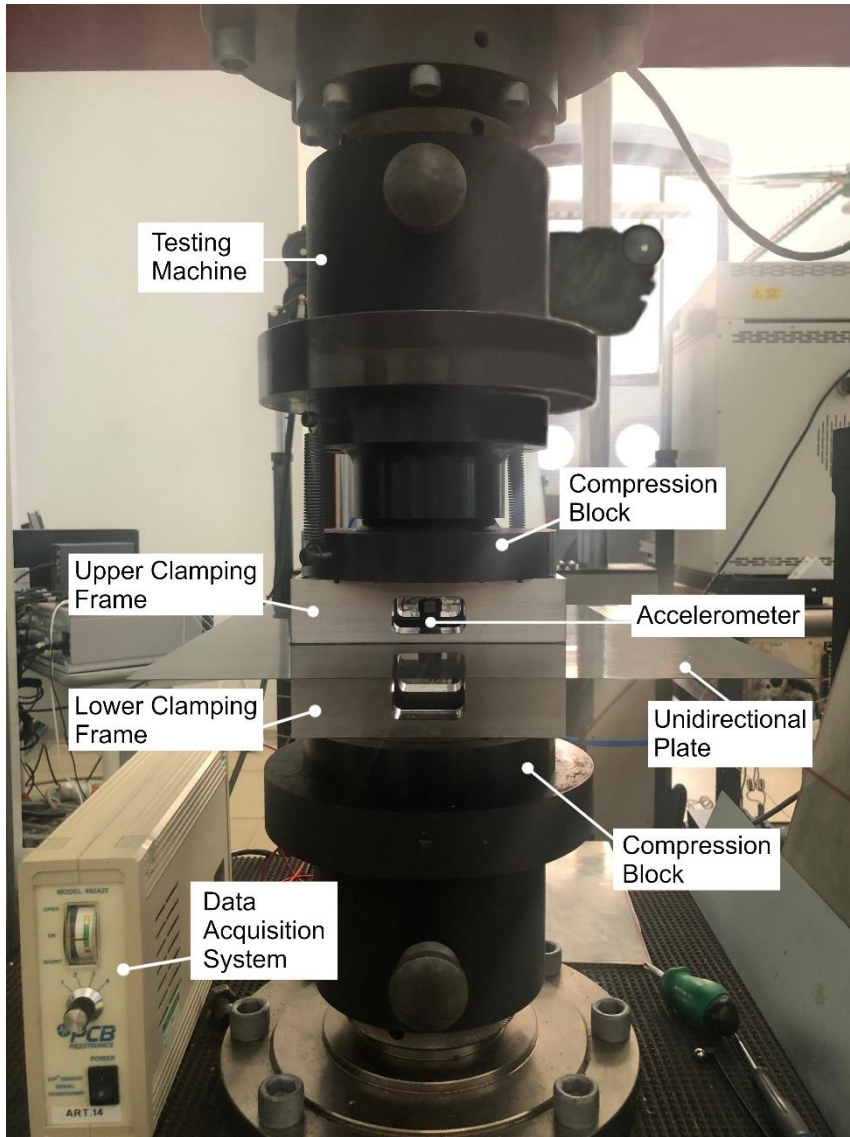
(b)



(c)

Figure 3.3 Comparison of simply supported and clamped boundaries: (a) finite element model of a plate with the highlighted boundary nodes; (b) modal analysis with simply supported boundaries; (c) modal analysis with fully clamped boundaries

Clamped boundaries are usually made by means of frames screwed to the composite plate. This is the typical setup considered in literature studies [69]. However, holes required by the screws cause irreversible damage to the plate. Here clamped boundaries are realized by compressing, one against the other, two rectangular aluminium frames, symmetrically disposed above and below the plate, as shown in Fig. 3.4a. A universal testing machine, Zwick Roell Z100, equipped with compression blocks, is used to compress the frames. The compression provided by the testing machine allows to clamp boundaries of the retained region, without damaging the composite plate. The maximum load of 1 kN is applied for clamping. This allows to recover clearances in the system while limiting in-plane stresses induced in the plate. Indeed, under the applied compressive load, the frames slightly deform. Due to the friction, the deformation of the frames induces spurious in-plane stresses in the investigated region, which can significantly alter the measure of the resonant frequency.



Testing Machine

Compression Block

Upper Clamping Frame

Accelerometer

Lower Clamping Frame

Unidirectional Plate

Compression Block

Data Acquisition System

(a)

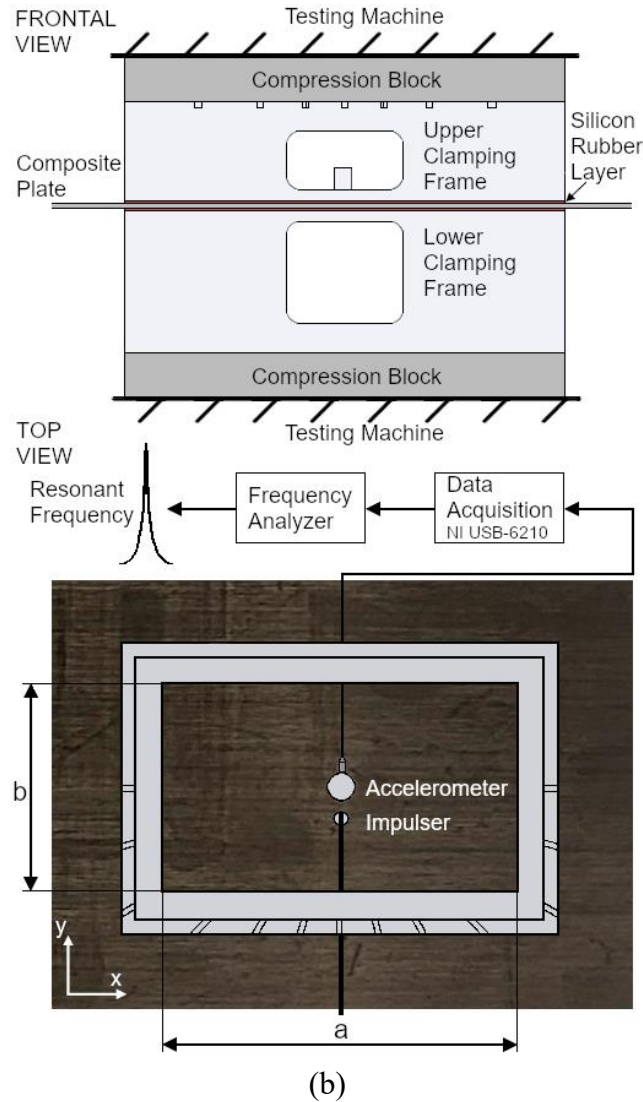


Figure 3.4 Testing setup: (a) experimental setup; (b) scheme.

The proposed experimental equipment thus allows to localize the measure of the resonant frequencies. The investigated region has rectangular shape of sides a equal to 140 mm and b equal to 90 mm, as shown in the scheme of the experimental setup of Fig. 3.4b. As discussed, the proposed methodology is based on the IET. An impulser is used to excite the plate. The impulser was realized by gluing a steel sphere to a plastic rod of length approximately equal to 15 cm, in accordance with the recommendations of the ASTM E1876 [65]. The resulting mechanical vibrations are measured through an accelerometer, positioned at the centre of the considered region, which provides the output signal for the z -axis, i.e., the axis perpendicular to the plate. The accelerometer is attached to the plate by means of beeswax and has a mass of 15 g. The signal is transferred to a data acquisition system (National Instruments NI USB-6210) and to an analyser (Buzz-o-sonic[®]), which provides the fundamental resonant frequency. The data acquisition system has a sample rate of 25 kHz and the signal is analogic-to-digital converted with a resolution of 16 bits. The analyser performs the Fast Fourier Transform of the signal with a resolution smaller than 1 Hz.

Finally, a 0.5 mm layer of silicon rubber is interposed between the frames and the composite plate, as shown in Fig. 3.4b. As it is well known, thickness consistently varies in fibre reinforced plastics. This can be also appreciated for the unidirectional plate here considered for validation, as reported in Table 3.1. Plate flatness is critical for establishing a uniform contact between frames and plate, as previously observed by other authors [70]. The variation of the thickness can result in a local loss of clamped boundaries. Indeed, location of the clamped boundaries is strictly affected by the contact between frames and plate. When loaded, the silicon rubber can deform, thus establishing a uniform contact with the plate. The silicon rubber thus permits to compensate thickness variations typical of composites.

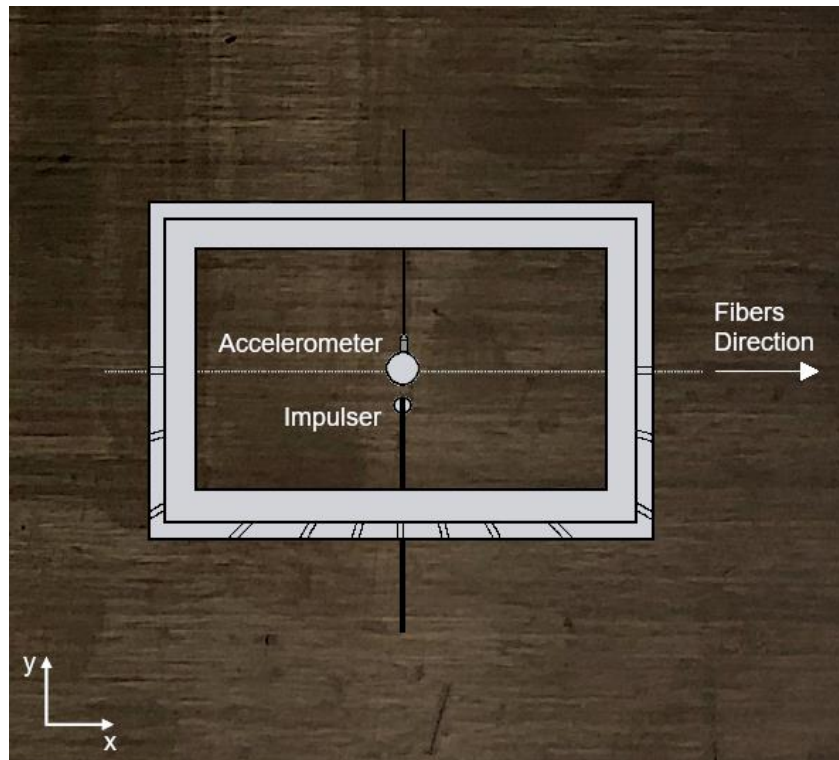
3.3 Accounting for material anisotropy

Standard IET tests are performed with freely-supported boundary conditions, thus involving the overall component in the vibrating phenomenon. Several resonant frequencies are retained in order to assess the unknown elastic properties. In composite laminates with stacked plies made of the same material, the elastic unknowns are four, namely E_{11} , E_{22} , G_{12} and ν_{12} , and at least four resonances are required to extract a reasonable set of estimates. Here, differently from standard IET test, only the first resonant frequency is retained. Indeed, the first mode is predominant, well recognizable and easily measurable in clamped plates. In addition to its predominance, the first resonant frequency well fits with the clamping system described in Section 3.2.

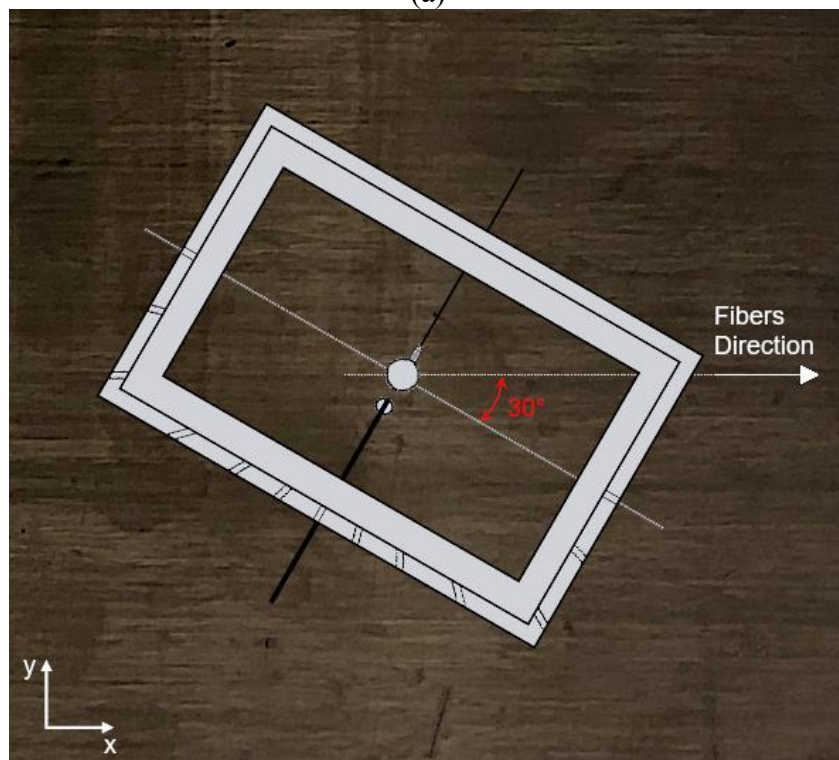
Perfectly clamped boundaries are rather difficult to achieve, given the noninfinite stiffness of the system. In particular, the out-of-plane stiffness is affected by the interposed silicon rubber layer. From an experimental point of view, boundary conditions can be considered fully clamped when the displacement in their correspondence is limited with respect to the displacement of the central portion. While for the higher modes, the material in proximity of the boundaries is increasingly involved in the vibrational response, the first mode shape only involves the displacement of the central portion of the investigated region. In this regard, the use of the accelerometer is also helpful, as the presence of a concentrated mass affects the modal shape, by concentrating the displacement in correspondence of the mass itself. The accelerometer thus contributes to the reproducibility of the tests. This aspect will be further investigated in the next chapter.

In order to obtain different measures of the first resonant frequency, the anisotropy of composite materials is exploited. Due to the material orthotropy, elastic properties are directionally dependent. Therefore, by rotating the clamping frames with respect to the composite plate, the elastic properties of the clamped region vary. Accordingly, the relative orientation between the clamping frames and the plate influences the measured resonant frequencies. Only the first resonant frequency of the rectangular clamped region is thus retained for each orientation.

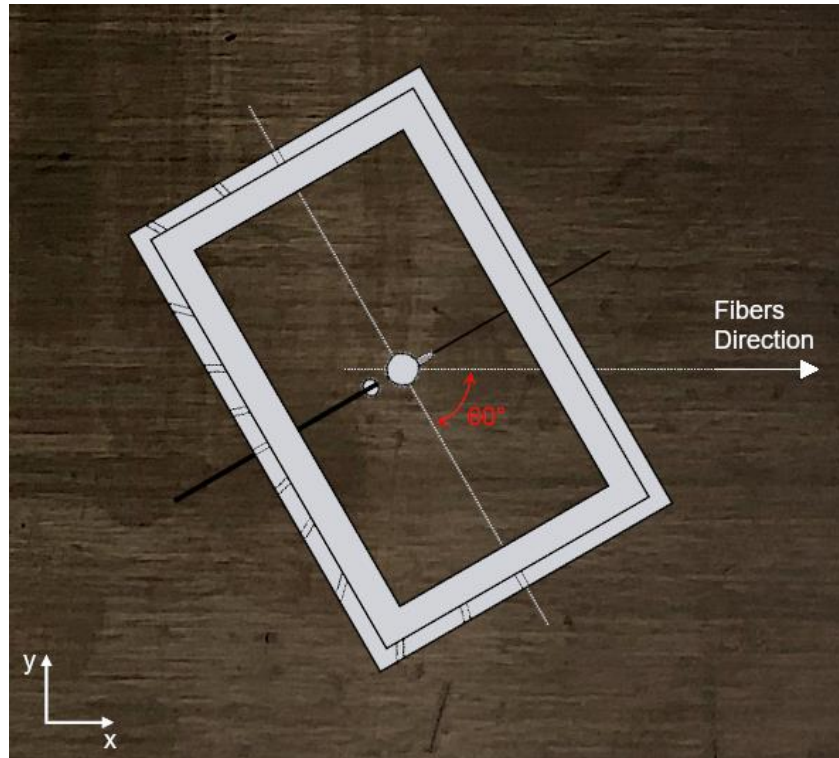
The procedure is validated on a composite plate with unidirectional reinforcement. Four measures of the first resonant frequency are performed in order to assess the local elastic properties. By considering the angle between fibres direction and the main axis of the frames, IET test is performed at 0° , 30° , 60° and 90° , as shown in Fig. 3.5a-d.



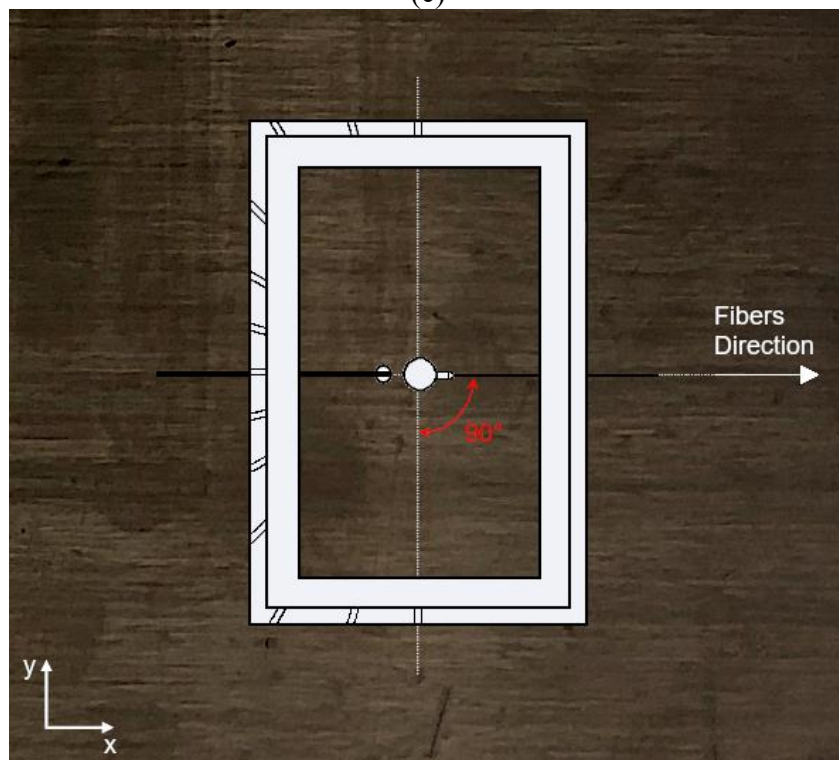
(a)



(b)



(c)



(d)

Figure 3.5 Experimental procedure: measures at different orientations. (a) 0°; (b) 30°; (c) 60°; (d) 90°.

It is worth noting that the dependency of the resonant frequency on the material orientation is emphasized by the asymmetry of the rectangular shape of the examined region. Indeed, as the ratio a/b between the dimensions of the rectangle increases, the variation of the resonant frequency with the material

orientation increases. In contrast, a circular shape suppresses the dependency of the resonant frequency on the relative orientation between the frames and the plate. Therefore, by rotating the upper and lower rectangular frames with respect to the composite plate, different values of the resonant frequency are measured.

3.4 Numerical calculations

Local elastic properties are determined from the measured frequencies. The inverse problem combines a finite element analysis and an optimization process in order to compute the material constants. In particular, finite element modal analysis is performed within an optimization problem, where the elastic parameters, namely E_{11} , E_{22} , G_{12} and ν_{12} , are handled as design variables. The objective function is given by the sum of the relative errors between the measured and the numerical resonant frequencies for each orientation. The zero-order Nelder-Mead algorithm has been adopted for the optimization [71]. In particular, a sub-routine has been coded in Python, which exploits the package PyOpt for the optimization and a proper parametrization of the finite element model.

According to the values assumed by the elastic constants at each iteration of the optimization process, a finite element modal analysis of the rectangular clamped plate is performed for each orientation of the fibres. In particular, the python code modifies a parametrized finite element model and calls the LS-Dyna executable to perform the simulation. The first fundamental frequency is retained from the eigout file and compared with the corresponding experimental frequency. Within the optimization process, the difference between the experimental and the numerical frequencies is thus minimized by varying the elastic properties. Therefore, the material constants are determined as the result of the optimization process. The structural optimization problem is formulated as follows

$$\min_{\underline{x}} \sum_i \left| \frac{f_{exp,i} - f_{num,i}(\underline{x})}{f_{exp,i}} \right| \quad (3.1)$$

where $\underline{x} = [E_{11}, E_{22}, G_{12}, \nu_{12}]^T$

$$100.0 \leq E_{11} \leq 200.0 \text{ GPa}$$

$$5.0 \leq E_{22} \leq 10.0 \text{ GPa}$$

$$2.0 \leq G_{12} \leq 6.0 \text{ GPa}$$

$$0.3 \leq \nu_{12} \leq 0.4$$

where f_{exp} is the measured frequency, f_{num} is the numerical resonance and subscript i refers to the i -th orientation between the clamping frames and the composite plate. In Eq. (3.1), the variation intervals for each design variable are also reported, which are selected for the unidirectional plate. By limiting the design domain with reasonable values, a unique solution can be obtained for the elastic properties, speeding up the optimization process.

The commercial software LS-Dyna is used for the numerical calculations. The resonant frequencies are extracted through the Lanczos method [59]. The finite element model consists in a rectangular plate of dimensions 140 mm and 90 mm, clamped at the extremities, as shown in Fig. 3.6.

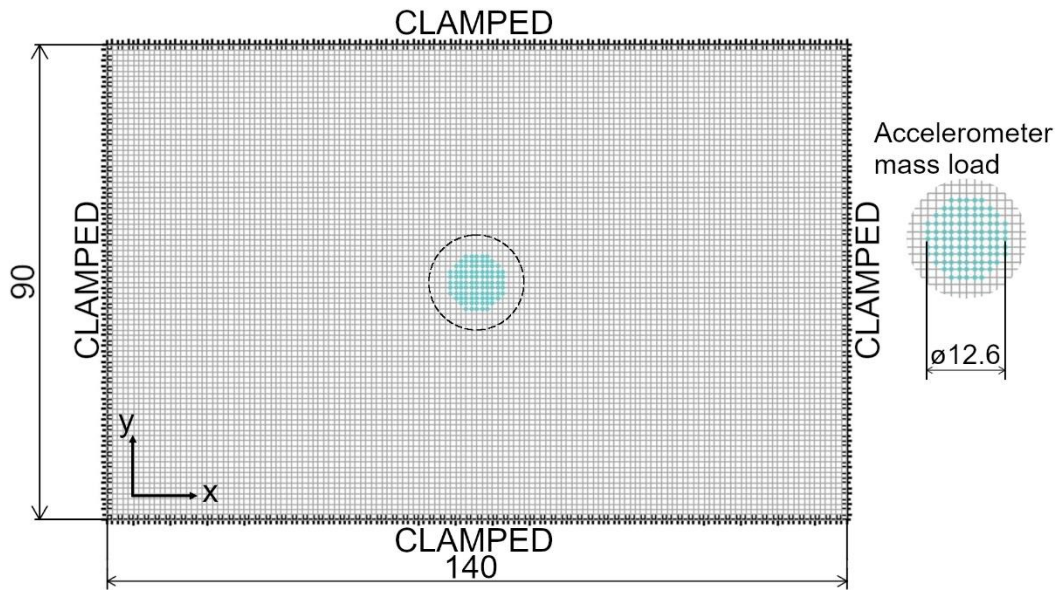


Figure 3.6 Numerical model.

The Belytschko–Tsay four nodes shell elements formulation with 6 degrees of freedom per node are used to model the structure. Through a convergence study, the mesh size is determined at which the numerical frequencies converge. As a result, the mesh size of 1 mm, with 12600 elements and 75600 degrees of freedom, is considered to discretize the structure. The plate has uniform thickness of 1.08 mm. In accordance with the number of layers of the unidirectional composite, seven integration points are assumed through the thickness, while one integration point in the element plane is used.

Fibres direction is set through a user-defined vector in LS-Dyna environment, thus specifying the different material orientations. The inertial effect of the accelerometer is accounted through a lumped mass. Its value has been equivalently distributed on the central nodes of the plate in correspondence of the accelerometer location, as shown in Fig. 3.6.

3.5 Results

In this section, results of the IET tests performed at different orientations are reported. From the measured frequencies, local elastic properties are determined according to the optimization scheme of Eq. (3.1). The calculated values are compared to their reference values as given in the provided datasheet of the unidirectional plate.

3.5.1 First fundamental frequencies

In this Section, the experimental results are analysed. As described in Section 3.3, the first resonant frequency is measured for fibres oriented at 0° , 30° , 60° and 90° with respect to the main axis of the rectangular frame. Five replications for each fibre orientation are performed. Measured scatter is extremely limited with a range equal to ± 2 Hz. The frequency spectra are shown in Fig. 3.7 for each orientation (Fig. 3.7a for 0° , Fig. 3.7b for 30° , Fig. 3.7c for 60° and Fig. 3.7d for 90°). Due to the material anisotropy, the first fundamental frequency varies from 246 Hz to 410 Hz. In anisotropic plates, the elastic properties are directionally dependent. The orientation of the material with respect to the clamped boundaries influences the bending stiffness, thus resulting in a variable resonant frequency. In contrast, the inertial effect of the accelerometer mass reduces the frequency variation with the fibre orientation, as it lowers the resonant frequencies.

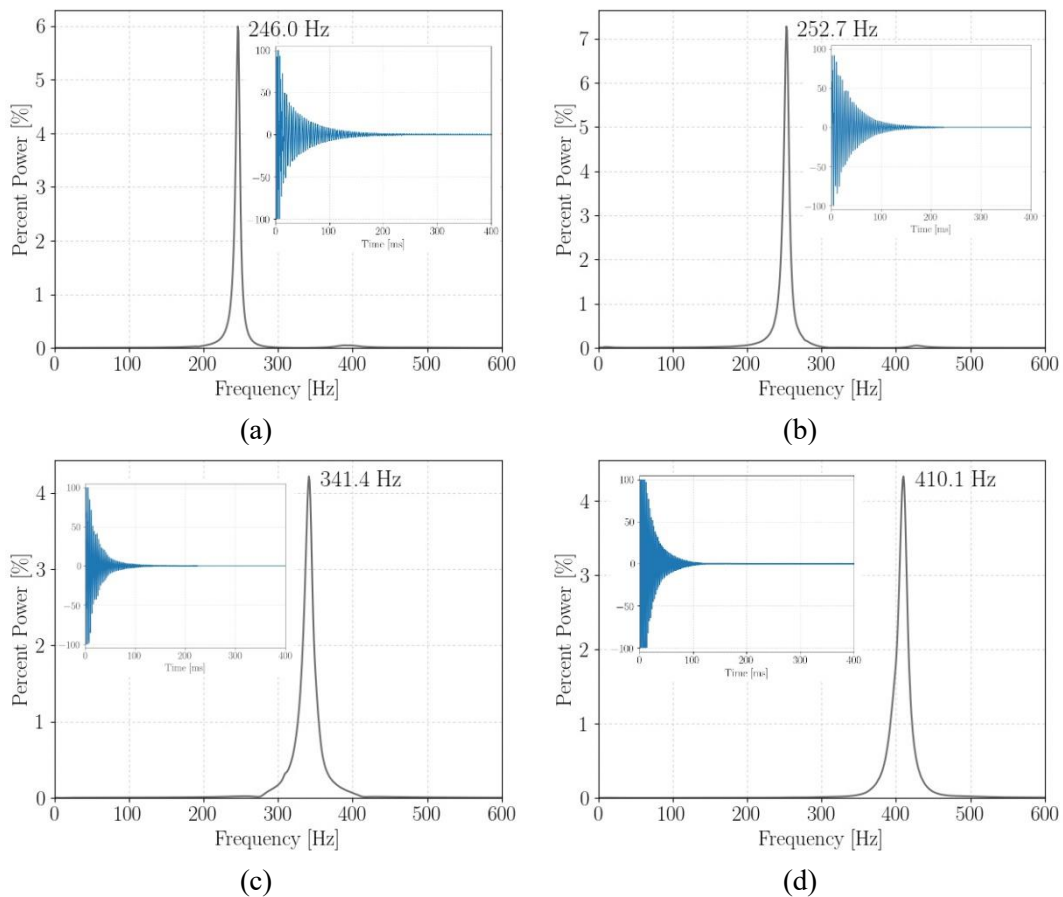


Figure 3.7 Acquired signal and frequency spectra at different orientations: a) 0° ; b) 30° ; c) 60° ; d) 90° .

According to Fig. 3.7, the first resonance peak is clearly visible and well isolated from the other resonance peaks, thus highlighting the effectiveness of the experimental measures. The differences between measured frequencies are emphasized by the rectangular shape of the isolated region. In rectangular plates, the bending stiffness is mostly related to the elastic properties in the direction of

the rectangle short edge, i.e. the transverse direction [72]. Indeed, the different proximity of the constraints enhances the sensitivity of the bending stiffness to the elastic properties in the transverse direction. This sensitivity to the material properties in the transverse direction increases with the ratio between the dimensions, a and b , of the rectangle. Therefore, by rotating the rectangular frames with respect to the unidirectional plate from 0° to 90° , a substantial increment of the bending stiffness and, accordingly, of the resonant frequency, is experimentally found.

In particular, when the fibres are parallel to the long edge a of the frames, i.e., oriented at 0° , the stiffness of the analysed region is mostly related to the Young modulus in the transverse direction E_{22} . The bending behaviour is thus governed by the epoxy matrix. When the fibres are parallel to the short edge b of the frames, i.e., oriented at 90° , the Young modulus in longitudinal direction E_{11} mostly affects the stiffness, thus leading to a higher value of the resonant frequency. At 90° , the bending behaviour is governed by the fibres. Therefore, in very anisotropic materials, as a unidirectional plate, the wide range of elastic properties leads to a measurable variation of the resonant frequencies. The rectangular shape of the frames thus permits to exploit the anisotropy of composite materials, enhancing the dependency of the resonant frequency on the material orientation.

It is worthwhile noticing that the consistent variation of the first resonant frequency with the material orientation confirms the sensitivity of the technique to the local elastic properties.

3.5.2 Estimation of material constants

The assessment of the material constants is carried out according to the Eq. (3.1). For the thickness, an average value of 1.08 mm has been assumed in the numerical calculations. The local elastic properties, as determined through the optimization process, are reported in Table 3.3. The obtained values are compared to the nominal material constants provided by the supplier, resulting in very good agreement.

Property	Nominal value	Local value	Percent Discrepancy
E_{11} [GPa]	131.1	126.0	-3.8%
E_{22} [GPa]	7.0	6.8	-2.9%
G_{12} [GPa]	3.93	3.8	-3.3%
ν_{12} [-]	0.35	0.34	-4%

Table 3.3 Comparison of local and nominal elastic properties.

The difference between local estimates and nominal elastic properties is smaller than 4%. In particular, the actual local properties are smaller than the corresponding reference values provided by the supplier. In regard to this deviation, three main aspects can be highlighted. Firstly, the methodology adopts a dynamic test to assess the material constants. Static and dynamic tests can lead

to different results [60], even though differences are typically limited [65]. Further, in the proposed procedure, flexural behaviour of the plate is tested. In composites, flexural material properties typically differ from the corresponding values assessed through tensile testing [73]. The position of fibres through the thickness affects the flexural rigidity, while the tensile stiffness is not influenced. As a consequence, a discrepancy between tensile and flexural properties can occur. Finally, the variability of the thickness along the plate, which is not accounted in the numerical calculations, affects the measure of the resonant frequency and, consequently, the estimation of the local elastic properties. Plate thickness is mostly influenced by the manufacturing process. In particular, the fabrication causes local variations in the amount of epoxy matrix and in the plate thickness. This affects in turn the local percentage of volume fibres and accordingly the local elastic properties. In regard to the resonant frequency, its value decreases as the plate becomes thinner. However, as the amount of matrix decreases, the local elastic properties increase, thus partially compensating the effect on the resonant frequency. The effect of thickness variation is further discussed in the next section with a dedicated sensitivity analysis.

As a further aspect, the discrepancy between local estimates and nominal material constants can be due to the noninfinite stiffness of the boundaries, as described in Section 3.2. Indeed, perfectly clamped boundary conditions are difficult to achieve [74]. The resonant frequency of a non-perfectly clamped plate is definitely smaller than the resonance obtained with fully clamping. Therefore, as a result of the comparison between the experimental and numerical resonances, as intended in Eq. (3.1), the elastic properties can be slightly underestimated.

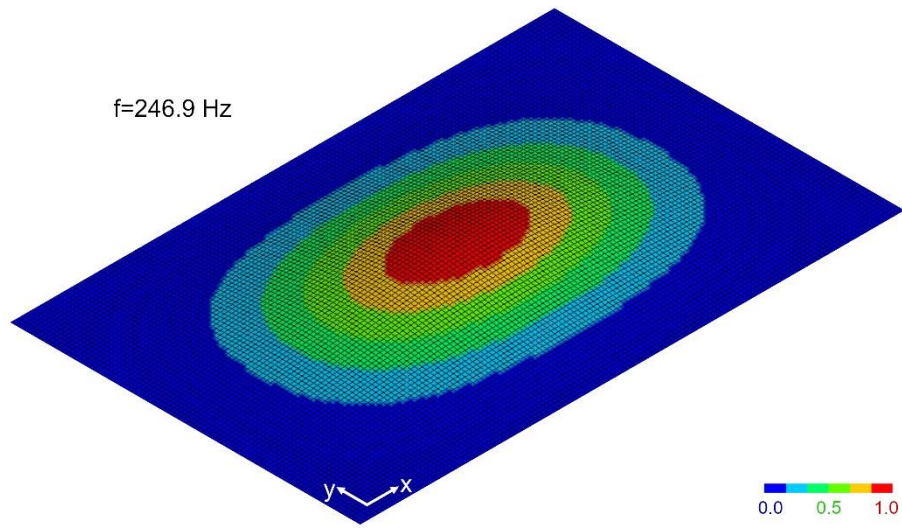
In Table 3.4, the measured resonant frequencies are compared to the corresponding numerical results, as obtained with the computed elastic estimates.

Orientation	Measured frequency [Hz]	Numerical frequency [Hz]	Percent error
0°	246	246.9	-0.4%
30°	252.7	257.4	1.8%
60°	341.4	351.5	-2.9%
90°	410.1	403.4	1.6%

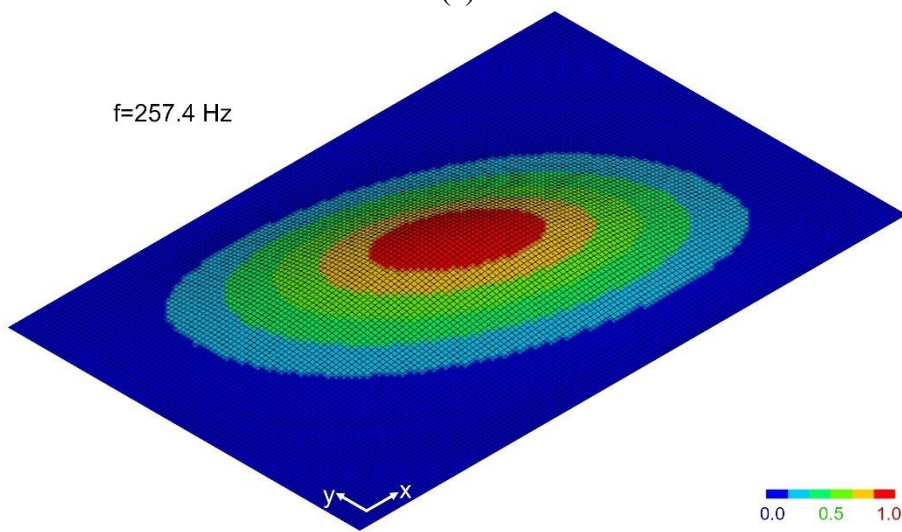
Table 3.4 Comparison of experimental and numerical resonant frequency.

The relative error between experimental and numerical frequency, namely the objective function of the optimization problem in Eq. (3.1), is reported for each orientation. As shown in Table 3.4, the most significant discrepancies between experimental and numerical frequencies are obtained at 30° and 60°. Indeed, uncertainty in frame positioning particularly affects these intermediate orientations. However, the differences are limited and smaller than 3%, thus proving the effectiveness of the proposed experimental methodology.

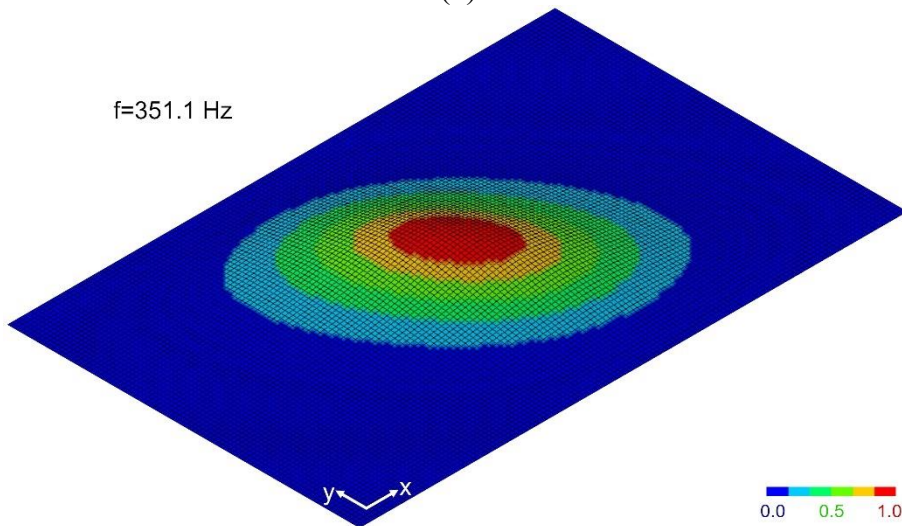
Fig. 3.8 shows the modal shape for each orientation as resulting from the numerical analysis. Isosurfaces of the first fundamental mode are also represented.



(a)



(b)



(c)

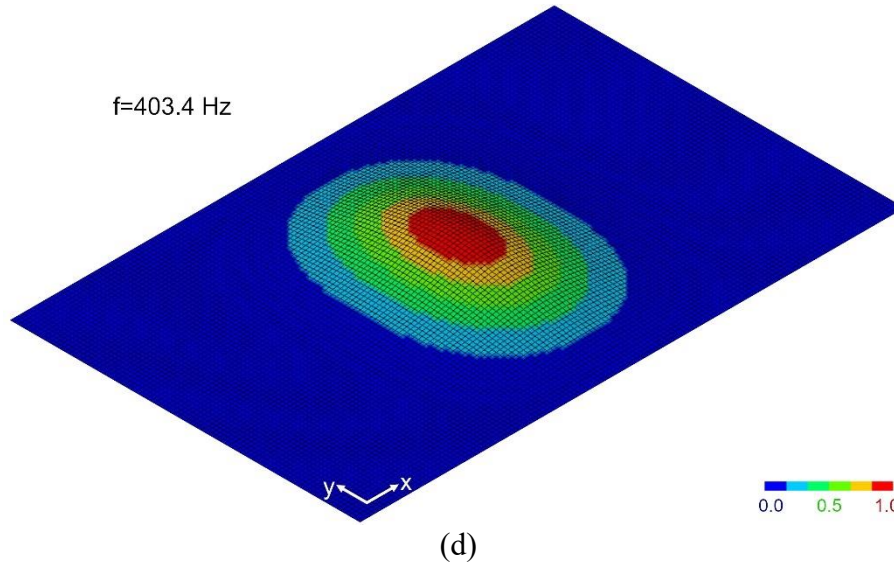


Figure 3.8 Mode shape with contour lines at different orientations: (a) 0° ; (b) 30° ; (c) 60° ; (d) 90° .

According to Fig. 3.8, the modal shape varies with the material orientation. In particular, the isosurfaces follow the fibre direction. As the orientation varies from 0° to 90° , the vibrating phenomenon involves lower amount of plate material, in accordance with the increasing values of the resonant frequencies.

3.6 Sensitivity Analysis

Three sensitivity analyses are performed to investigate the robustness of the methodology in assessing the material properties. In particular, the first concerns the effect of the thickness assumed uniform in the finite element model. The second investigates the effect of the design domain limits on the optimization problem of Eq. (3.1). Finally, in the third, the effect of the extension of the clamped region on the assessment of the elastic properties is analysed, when a local defect is present.

3.6.1 Effect of the thickness variation

The variability of the thickness along the plate consistently affects the measure of the resonant frequency. In particular, its value decreases as the plate becomes thinner. Given the inverse problem formulated in Eq. (3.1), which computes elastic properties from measured resonant frequencies, thickness variability influences in turn the estimation of material constants.

In order to show this effect, the optimization process in Eq. (3.1) is repeated considering both the maximum and minimum thickness in the plate, even though these two thicknesses do not belong to the isolated region in the plate. Local elastic properties are assessed assuming in the numerical model firstly the uniform value of 0.94 mm, i.e., the minimum thickness, and then the uniform value of 1.13 mm, i.e., the maximum thickness.

Table 3.5 shows the results of the sensitivity analysis, compared to the elastic properties obtained with the average thickness of the isolated region in the plate, equal to 1.08 mm.

Property	Local value t=1.08 mm	Local value t=1.13 mm	Local value t=0.94 mm	Nominal value
E_{11} [GPa]	126.0	112.1	186.0	131.1
E_{22} [GPa]	6.8	6.0	10.0	7.0
G_{12} [GPa]	3.8	3.0	5.6	3.93
ν_{12} [-]	0.34	0.31	0.35	0.35

Table 3.5 Effect of thickness scatter on local material properties.

The marked discrepancy highlights the sensitivity of the inverse problem formulated in Eq. (3.1) with the thickness of the plate. The sensitivity of the IET to the laminate thickness is a further evidence of the need for a local measure. Only in case of small isolated regions, the thickness variation is limited and it does not significantly affect the estimation of the material properties. The more the measure is localized, the more the variations of the thickness are limited and so the influence on the estimation of the elastic properties. Indeed, manufacturing defects, which include large thickness variations in the plate as well as local weaknesses in the laminate, can be effectively identified with the proposed approach.

3.6.2 Effect of the design domain limits

The effect of the design domain limits is also investigated in order to assess the accuracy of the proposed methodology. As the design domain of Eq. (3.1) increases, multiple solutions can be obtained which minimizes the stated problem. The measured frequencies can be thus obtained with multiple sets of elastic properties. This aspect will be detailed in the next chapter.

In particular, it is known that the first resonant frequency slightly depends on the shear modulus and on the Poisson's coefficient. Therefore, the effect of the limits assumed for these properties is firstly analysed. In particular, the optimization of Eq. (3.1) is performed without considering any limit for the shear modulus and on the Poisson's coefficient. Then, the optimization is also run without any limit on the design variables.

The resultant elastic properties and the relative discrepancy with respect to those obtained in Section 3.5 are reported in Table 3.6.

Property	Local value	Local value – no limits on G_{12} and ν_{12}	Local value - no limits
E_{11} [GPa]	126.0	127.0	127.0
E_{22} [GPa]	6.8	6.7	6.7
G_{12} [GPa]	3.8	3.7	3.7
ν_{12} [-]	0.34	0.29	0.29

Table 3.6 Effect of the design domain limits on local material properties.

As it can be seen, it is confirmed that in the retained region the properties are slightly lower than the nominal values. Further, the Young moduli in longitudinal and transverse directions and the shear modulus are almost the same as those previously calculated.

In regard to the Poisson's coefficient, a more significant discrepancy is obtained. This is due to the limited dependency of the first resonant frequency on this property. As a consequence, multiple values of the Poisson's coefficient can minimize the objective function of Eq. (3.1). In order to increase the robustness of the proposed methodology, further measures of the first resonant frequency can be obtained by considering other relative orientations of the plate with respect to the clamping system.

Furthermore, it should be noticed that, as multiple solutions are allowed for the inverse problem of Eq. (3.1), the optimal results can depend on the initial guess of the optimization process. Here, the initial point was assumed equal to the nominal properties in all the performed optimizations. This aspect has to be investigated especially if the methodology has to be adopted for the detection of local material variations.

In regard to the computational time, the computational effort was slightly influenced by the optimization formulation. In all cases, almost 100 iterations were necessary to reach the optimal result. Due to the zero order of the adopted algorithm, the starting point can play a key role in the computational time.

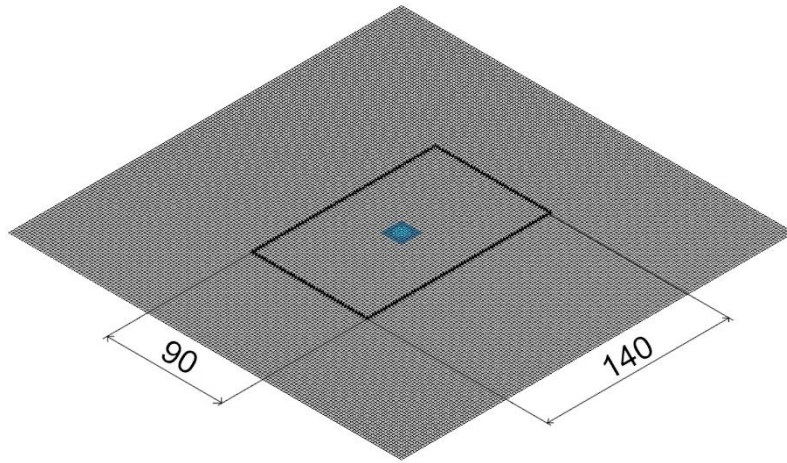
3.6.3 Effect of the clamped boundaries extension

The presented methodology aims at detecting local material variations due to the presence of local anomalies or defects. In this regard, the extension of the clamped region plays a significant role. Indeed, as the investigated domain increases, possible local material variations can be concealed by the surrounding undamaged material. Ideally, the boundaries size should be as small as possible, in order to create punctual measurements. The smaller is the clamped region, the more local are the assessed properties. However, the reduction of the investigated domain is counteracted by the necessity of realizing almost perfectly clamped boundaries in the experimental setup. From an experimental point of view, boundaries can be approximated as perfectly clamped if the displacement in their correspondence is consistently limited with respect to the maximum displacement, which is in the centre of the plate in the case of the first resonant mode of vibration. As the dimension of the clamped region decreases, due the noninfinite stiffness of the clamping system, the displacement in correspondence of the boundaries becomes ever more comparable to that at the centre of the domain, where the measure is acquired through the accelerometer.

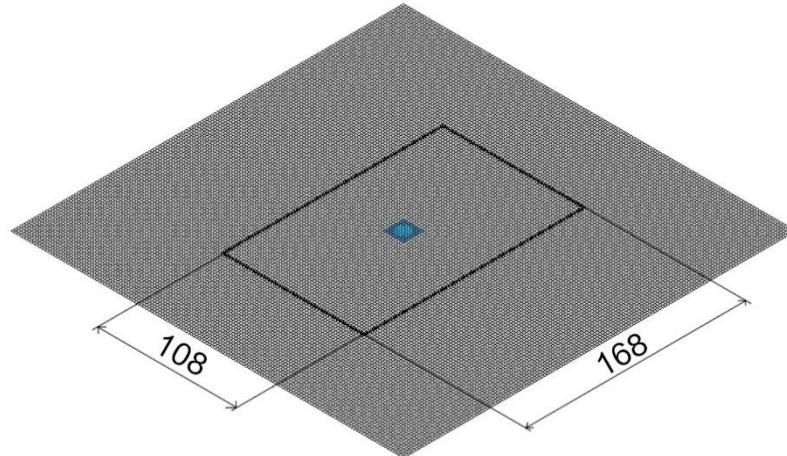
The sensitivity of the optimization problem is thus investigated with respect to the extension of the clamped boundaries. In particular, a local material variation is

considered in the model in order to simulate the presence of a local damage and the elastic properties are assessed by varying the clamped region size.

Fig. 3.9 shows the unidirectional plate with different highlighted paths of nodes. The highlighted nodes indicate the location of the clamped boundaries. Four different locations are considered. The first involves a size of the investigated domain equal to the presented experimental setup, i.e., $a_1 = 140$ mm and $b_1 = 90$ mm, (Fig. 3.9a). The other three locations are proportional to these dimensions with factors 1.2, 1.6 and 2.0, respectively. The selected factors allowed to investigate the sensitivity for a small increment of the domain, i.e., the 20% increment, for a medium increment, i.e., the 60%, and for a consistent increment, as in the case of the 2.0 factor. The resultant dimensions are therefore $a_2 = 168$ mm $b_2 = 108$ mm (Fig. 3.9b), $a_3 = 224$ mm $b_3 = 144$ mm (Fig. 3.9c) and $a_4 = 280$ mm and $b_4 = 180$ mm (Fig. 3.9d).



(a)



(b)

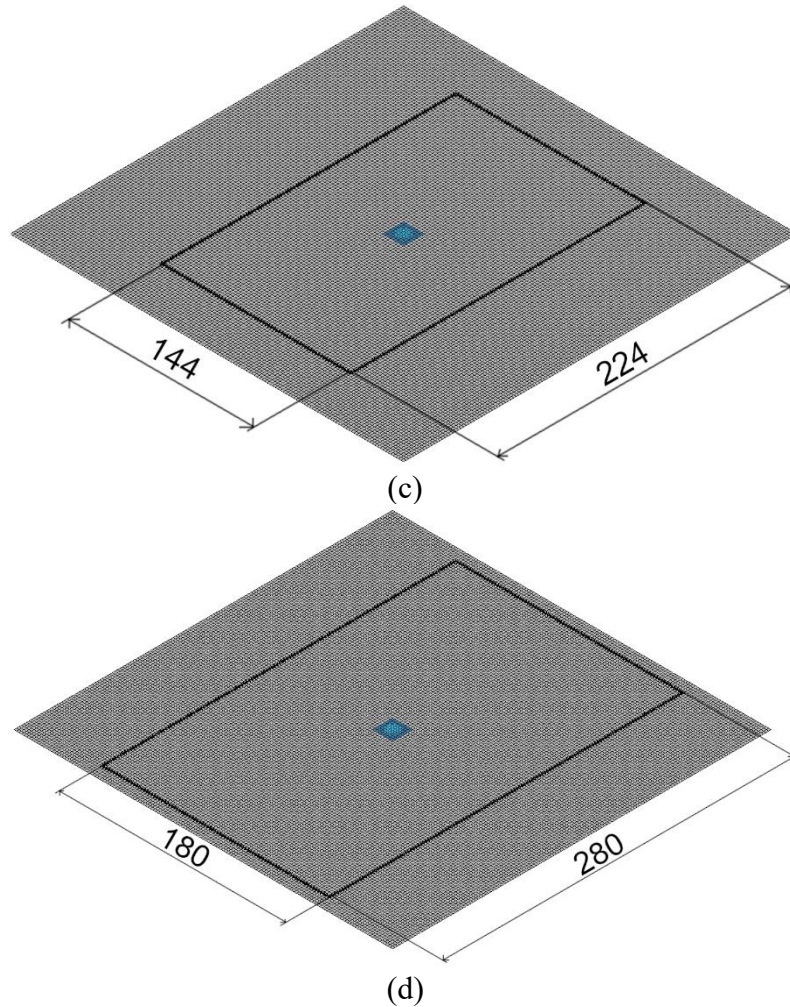


Figure 3.9 Different sizes of the clamped boundaries: (a) 140x90; (b) 108x168; (c) 144x244; (d) 280x180; blue region indicates a local material variation.

The nominal material properties of the analysed unidirectional laminate reported in Table 3.2 are considered for the plate. Further, a local material variation is assumed in the centre of the plate, as shown in Fig. 3.9 through the blue shells. This material variation intends to represent a local defect or damage. The material properties are reduced to the 75% of the nominal elastic constants of Table 3.2 in this defective or damaged region, while its dimensions are 15x15 mm. In particular, the size, the position with respect to the boundaries and the elastic properties of this defect are such that the first resonant frequencies for the different orientations of the clamped plate with dimensions $a = 140$ mm and $b = 90$ mm are those reported in Table 3.4. Therefore, the resultant material properties of the investigated region are those assessed in Subsection 3.5.2.

In order to evaluate the sensitivity of the proposed methodology to the extension of the clamped boundaries, finite element modal analyses are firstly performed with the described local material variation for the different orientations. The resultant first resonant frequencies are then assumed as the measured frequencies in the optimization problem of Eq. (3.1) and the elastic properties of the retained region are accordingly determined.

Results of the assessed elastic properties are reported in Table 3.7, according to the extension of the investigated region.

Property	$a_1 \cdot b_1$	$a_2 \cdot b_2$	$a_3 \cdot b_3$	$a_4 \cdot b_4$
E_{11} [GPa]	126.0	128.0	130.0	130.3
E_{22} [GPa]	6.8	6.87	6.93	6.96
G_{12} [GPa]	3.8	3.86	3.91	3.92
ν_{12} [-]	0.34	0.34	0.35	0.35

Table 3.7 Effect of the design domain limits on local material properties.

In particular, as the dimensions increase, the assessed elastic properties tend to the nominal values. Therefore, the presence of the local anomaly is increasingly concealed as much as the dimensions increase. This can be also observed by comparing the first resonant frequencies of the clamped plate with the local defect (f_{DAM}) with those obtained when no defects are present (f_{UNDAM}). As an example, the resultant frequencies for the 90° orientation are reported in Table 3.8.

Property	$a_1 \cdot b_1$	$a_2 \cdot b_2$	$a_3 \cdot b_3$	$a_4 \cdot b_4$
$f_{90^\circ_UNDAM}$ [Hz]	419	331.5	236.5	179.4
$f_{90^\circ_DAM}$ [Hz]	403	320	230.6	176
Percent variation	4.0%	3.6%	2.6%	1.9%

Table 3.8 Effect of the design domain limits on the first resonant frequency for 90° orientation.

As shown, as the dimensions increase, the first resonant frequency progressively tends to the value of the undamaged plate, with the discrepancy ever more comparable to the measurement uncertainty.

3.7 Limitations and possible criticalities of the methodology

An innovative experimental methodology for the nondestructive assessment of the elastic properties of anisotropic materials has been presented in the previous sections. The methodology is based on the Impulse Excitation Technique (IET) and the material elastic properties are locally determined, i.e., the assessment concerns an isolated region of the material. Differently from the literature, where standard IET tests are performed with freely-supported boundary conditions, thus involving the overall component in the vibrating phenomenon, here, a local region is isolated and analysed. In particular, a rather simple experimental setup is adopted, which clamps the extremities of the investigated zone, without damaging the material. Clamped conditions permit to isolate the zone where vibrational response is of interest, thus resulting in a modal response of the system which is function only of the analysed region characteristics.

With the IET, only the first resonant frequency of the investigated local region is measured. In order to take into account the anisotropy of composite plates, the measurement of the first resonant frequency is repeated by varying the angle

between the fibre direction and the main axis of the frame. The material anisotropy is thus exploited in order to obtain different measures of the resonant frequency. The material parameters are finally obtained through an optimization procedure based on finite element analysis, which aims at finding the elastic properties that minimize the differences between the experimental and the numerical resonant frequencies. The proposed procedure has been successfully validated on a unidirectional carbon fibre composite plate.

In this Section, limitations and possible criticalities will be discussed, some of which will be addressed in the next chapters. Firstly, it is worth noticing that the current experimental setup is only suitable for laboratory testing conditions of laminated flat plates. In particular, both sides of the test plate must be accessible for clamping. This is far from most practical situations in which only one side is accessible and arbitrary curved shapes occur. A nondestructive technique should require only one side access to investigate the component [75]. However, it is worthwhile noticing that the preliminary experimental setup allowed to investigate multiple aspects of the clamping system. For example, it has been established that the clamped boundaries do not require high clamping force. Rather, the clamping force has to be limited in order to avoid spurious in-plane stresses due to the deformation of the clamping system. Spurious in-plane stresses can significantly alter the measure of the first resonant frequency, as discussed in Section 3.2.

Furthermore, in the presented methodology, material anisotropy is exploited to obtain different measures of the first resonant frequency. This approach is thus only suitable for laminated composites, whose stacking sequence is known and whose stacked plies are made of the same material. The optimization problem formulated in Eq. (3.1) indeed is not able to deal with laminates made of multiple materials. It is also worth noting that, as discussed in the dedicated sensitivity analysis, design domain limits, i.e., limits to the space where the design variables can vary, were necessary to achieve the optimal solution for the elastic parameters. As the presented methodology intends to non-destructively inspect composite structures, limitations on the variability of the material properties can be inconvenient. In this regard, it is also important to notice that the optimization problem is based on finite element analyses, whose computational cost is not negligible, thus limiting the application in real-world components.

Finally, as shown in the sensitivity analysis, where the effect of the clamped boundaries size is investigated, in presence of local damage, the reduction of the elastic properties is not necessarily consistent. The sensitivity analysis showed that in presence of a local damage whose material properties are reduced to 75% of their original value, a decrease of only 4% is calculated for the local elastic properties. The current methodology is not able to assess the elastic properties of the damage zone, rather it estimates equivalent residual values for the investigated region. A different strategy is thus necessary in order to assess the elastic properties of the damaged zone.

In the next chapters, possible solutions to the discussed criticalities will be presented. In Ch. 4, an enhancement of the current methodology will be proposed, which particularly addresses the robustness and the rapidness of the optimization problem formulated in Eq. (3.1). In Ch. 5, the attention will be focused on the damage severity. A new strategy will be presented, which aims at assessing the residual elastic properties of the damaged zone.

IV

Enhancement of the methodology for increasing the optimization robustness

In the previous chapter, a new experimental methodology has been presented which allows to non-destructively assess local elastic properties of composite laminates. The methodology aims at:

- i) isolating a region of the component through a specific equipment, which clamps the extremities of the region without damaging the material;
- ii) adopting the Impulse Excitation Technique to measure the first resonant frequency of the retained region;
- iii) exploiting the material anisotropy to obtain at least four different measures of the first resonant frequency, by varying the relative orientation between the clamping system and the material;
- iv) assessing the elastic properties of the investigated region from the measured resonant frequencies through an optimization process.

The methodology adopts a testing machine to compress two rectangular frames on the plate and isolate the region to investigate.

In vibrational methods, an inverse problem is formulated in order to determine the elastic properties from the measured resonant frequencies. Material constants are calculated through an optimization process based on finite element models, Rayleigh-Ritz formulations or analytical formulas. For laminated composites, whose stacking sequence is known and whose stacked plies are made of the same material, four resonant frequencies are usually sufficient to obtain a reasonable set of elastic estimates [61].

The robustness of the assessed elastic properties is a critical aspect of vibrational methods. It might occur that the inverse problem can be undetermined, i.e., the measured frequencies can be obtained with multiple sets of elastic estimates. In order to avoid such indeterminacy, further information is usually considered within the inverse problem, such as the modal shape and/or further frequencies. However, multiple resonant frequencies can be difficult to recognize, while the investigation of the modal shape can require expensive equipment, developed for laboratory [62].

By specifically referring to the presented methodology, its accuracy can be enhanced by increasing the number of relative orientations of the clamping system with respect to the material. As discussed in the previous chapter, the use of higher mode frequencies is instead limited by the proximity of the clamped boundaries, whose noninfinite stiffness can consistently affect the result. Indeed, the higher modes increasingly involve the material in proximity of the clamped boundaries in the modal displacement. As a consequence, the effect of the noninfinite stiffness, which is negligible for the first mode, as shown in Ch. 3, increasingly affects the measurement of the higher resonant frequencies.

Further, in order to guarantee the robustness of the methodology, limits on the design domain of the elastic properties, i.e., E_{11} , E_{22} , G_{12} and ν_{12} , are to be considered, which is undesirable, especially when assessing damage level. The design domain identifies the space where the aforementioned material properties can vary, while the optimization problem minimizes the discrepancy between the measured and the numerical resonant frequencies. Indeed, if the methodology has to be adopted for detecting local material variations, limitations on the material properties can be particularly inconvenient.

In this chapter, a new approach is presented, which aims at enhancing the robustness of the inverse problem. In particular, the inverse problem is completed with information related to the modal shape. This is analysed only by considering the effect of a concentrated mass on the first resonant frequency. The effect on the first resonant frequency depends on its position on the plate in accordance with the modal shape. Only two measurements of the first resonant frequency, which correspond to two locations of the concentrated mass, are necessary to identify the modal shape.

The approach is validated only through numerical analyses, which considers laminated composites with different elastic constants and stacking sequences. In order to compute the first resonant frequency of the clamped plate loaded by a concentrated mass, a specific Rayleigh-Ritz method is formulated, which is based on the higher order shear deformation theory. The use of Rayleigh-Ritz formulation permits to consistently decrease the computational cost with respect to the finite element based optimization described in Ch. 3. The Rayleigh-Ritz formulation thus represents a further step towards the application of the proposed methodology to real-world composite structures.

In this chapter, the Rayleigh-Ritz formulation is firstly presented and validated on experimental data taken from the literature. The inverse problem is

formulated which considers the information related to the modal shape. For each retained material, the frequencies are calculated for the different material orientations and mass positions, in order to constitute the reference values. The elastic properties are then handled as the design variables of an optimization process, which minimizes the discrepancy between the resonant frequency calculated at each iteration and the corresponding reference value. Results show that with the proposed approach, the modal shape can be identified only through a concentrated mass positioned in two different spots, thus avoiding the need of costly equipment. In addition, by accounting for the modal response within the optimization process, the sensitivity of the inverse problem to the elastic properties is enhanced. Results of the present Chapter have been also published in [76].

4.1 Methods

This section firstly presents the Rayleigh-Ritz formulation here adopted to calculate the first resonant frequency of clamped laminates loaded by a concentrated mass. Then, the approach for retaining the modal shape through the added mass is detailed.

4.1.1 Rayleigh-Ritz formulation

A Rayleigh-Ritz formulation is here presented in order to calculate the first resonant frequency of clamped plates made of laminated composites and loaded by a concentrated mass. A rectangular plate of dimensions a and b and constituted by N orthotropic layers for a total thickness h is considered, as shown in Fig. 4.1.

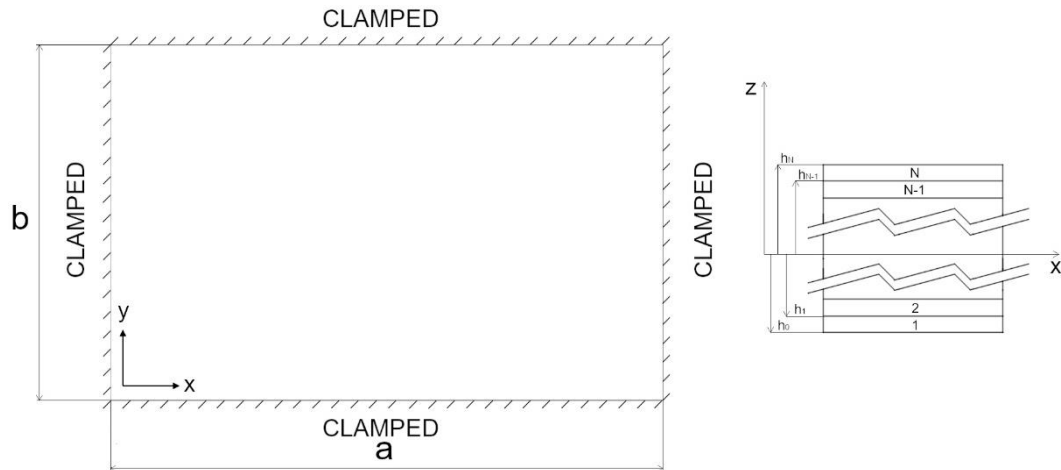


Figure 4.1 Scheme of the clamped plates made of laminated composites.

The displacements in x , y and z directions are denoted with u , v and w , respectively. The strain energy for the entire laminate is thus expressed as:

$$U = \frac{1}{2} \sum_{k=1}^N \int_{V_k} \underline{\varepsilon}_k^T \cdot \underline{\sigma}_k dV_k, \quad (4.1)$$

where subscript k refers to k -th lamina, N is the total number of layers, V_k the volume of each lamina, $\underline{\varepsilon}_k$ and $\underline{\sigma}_k$ are the strain and stress vectors at the lamina level.

Due to the presence of the concentrated mass, the kinetic energy is given by the following sum:

$$T = \frac{1}{2} \sum_{k=1}^N \int_{V_k} \rho_k \left[\left(\frac{\delta u}{\delta t} \right)^2 + \left(\frac{\delta v}{\delta t} \right)^2 + \left(\frac{\delta w}{\delta t} \right)^2 \right] dV_k + \frac{M}{2} \left[\left(\frac{\delta u_{lm}}{\delta t} \right)^2 + \left(\frac{\delta v_{lm}}{\delta t} \right)^2 + \left(\frac{\delta w_{lm}}{\delta t} \right)^2 \right], \quad (4.2)$$

where ρ_k is the mass density of the k -th lamina and M is the concentrated mass located at $x = l$ and $y = m$. Therefore, as an example, u_{lm} indicates the displacement in the x direction in correspondence of the mass location. Here, it is neglected the effect of the concentrated mass on rotary inertia and it is assumed for simplicity that the mass is located on the mid-plane, i.e. at $z = 0$.

The Rayleigh-Ritz formulation is based on the higher-order shear deformation theory for laminated composites proposed by Reddy [77,78]. According to the Reddy's theory, the displacements u , v and w of an arbitrary point of the plate are represented as

$$\begin{aligned} u(x, y, z, t) &= u_0(x, y, t) + z\varphi_x(x, y, t) - \frac{4z^3}{3h^2} \left(\varphi_x(x, y, t) - \frac{\delta w(x, y, t)}{\delta x} \right), \\ v(x, y, z, t) &= v_0(x, y, t) + z\varphi_y(x, y, t) - \frac{4z^3}{3h^2} \left(\varphi_y(x, y, t) - \frac{\delta w(x, y, t)}{\delta y} \right), \\ w(x, y, z, t) &= w_0(x, y, t), \end{aligned} \quad (4.3)$$

where u_0 , v_0 and w_0 are the displacements of the mid-plane and φ_x and φ_y are the rotations around the x and y axes, respectively. The stress and strain vectors of Eq.(4.1) are hence $\underline{\sigma}_k = [\sigma_x, \sigma_y, \sigma_{xz}, \sigma_{yz}, \sigma_{xy}]^T$ and $\underline{\varepsilon}_k = [\varepsilon_x, \varepsilon_y, \gamma_{xz}, \gamma_{yz}, \gamma_{xy}]^T$, respectively. The congruent equations for each lamina can be written as follows:

$$\underline{\varepsilon}_k = B \cdot \underline{u}, \quad (4.4)$$

where $\underline{u} = [u_0, v_0, w_0, \varphi_{0x}, \varphi_{0y}]$ and the matrix B is defined as

$$B = \begin{bmatrix} \frac{\delta}{\delta x} & 0 & -\frac{4z^3\delta^2}{3h^2\delta x^2} & \left(z - \frac{4z^3}{3h^2}\right) \frac{\delta}{\delta x} & 0 \\ 0 & \frac{\delta}{\delta y} & -\frac{4z^3\delta^2}{3h^2\delta y^2} & 0 & \left(z - \frac{4z^3}{3h^2}\right) \frac{\delta}{\delta y} \\ 0 & 0 & \left(1 - \frac{4z^2}{h^2}\right) \frac{\delta}{\delta y} & 0 & \left(1 - \frac{4z^2}{h^2}\right) \\ 0 & 0 & \left(1 - \frac{4z^2}{h^2}\right) \frac{\delta}{\delta x} & \left(1 - \frac{4z^2}{h^2}\right) & 0 \\ \frac{\delta}{\delta y} & \frac{\delta}{\delta x} & -\frac{8z^3\delta^2}{3h^2\delta x\delta y} & \left(z - \frac{4z^3}{3h^2}\right) \frac{\delta}{\delta y} & \left(z - \frac{4z^3}{3h^2}\right) \frac{\delta}{\delta x} \end{bmatrix}. \quad (4.5)$$

At the lamina level, the constitutive equations are as usual:

$$\underline{\sigma}_k = D_k \cdot \underline{\varepsilon}_k, \quad (4.6)$$

where D_k is related to the elastic constants through the rotation matrix, as follows

$$D_k = T_k \cdot Q \cdot T_k^T, \quad (4.7)$$

with

$$T_k = \begin{bmatrix} \cos^2 \theta_k & \sin^2 \theta_k & 0 & 0 & -2 \cdot \cos \theta_k \cdot \sin \theta_k \\ \sin^2 \theta_k & \cos^2 \theta_k & 0 & 0 & 2 \cdot \cos \theta_k \cdot \sin \theta_k \\ 0 & 0 & \cos \theta_k & \sin \theta_k & 0 \\ 0 & 0 & -\sin \theta_k & \cos \theta_k & 0 \\ \cos \theta_k \cdot \sin \theta_k & -\cos \theta_k \cdot \sin \theta_k & 0 & 0 & \cos^2 \theta_k - \sin^2 \theta_k \end{bmatrix}, \quad (4.8)$$

and

$$Q = \begin{bmatrix} \frac{E_{11}}{(1 - \nu_{12} \cdot \nu_{21})} & \frac{\nu_{12} \cdot E_{22}}{(1 - \nu_{12} \cdot \nu_{21})} & 0 & 0 & 0 \\ \frac{\nu_{12} \cdot E_{22}}{(1 - \nu_{12} \cdot \nu_{21})} & \frac{E_{22}}{(1 - \nu_{12} \cdot \nu_{21})} & 0 & 0 & 0 \\ 0 & 0 & G_{23} & 0 & 0 \\ 0 & 0 & 0 & G_{13} & 0 \\ 0 & 0 & 0 & 0 & G_{12} \end{bmatrix}, \quad (4.9)$$

where E_{11} is the Young modulus in the longitudinal direction, E_{22} is the Young modulus in the transverse direction, G_{12} , G_{13} and G_{23} are the shear moduli and ν_{12} is the Poisson's ratio. Here, the angle θ_k accounts for both the stacking angle of the lamina and the relative orientations between the clamped boundaries and the material. Further, it is assumed that $G_{13} = G_{23} = G_{12}$. The assumption, for which the three material properties are equal, is certainly coarse for some composite materials as well as it is exact for some others [72]. Further, it is worth noticing that the G_{23} material property cannot be assessed from the measurement of the first resonant frequency. Therefore, it is assumed here that the three properties are equal.

As clamped boundaries do not admit an exact solution, the displacements u , v and w are approximated through a set of admissible functions. The plate is firstly assumed to be in harmonic motion, which allows to write the displacement vector \underline{u} as

$$\begin{aligned} u_0 &= U(x, y) \sin \omega t, \\ v_0 &= V(x, y) \sin \omega t, \\ w_0 &= W(x, y) \sin \omega t, \\ \varphi_x &= \Phi_x(x, y) \sin \omega t, \end{aligned} \quad (4.10)$$

$$\varphi_y = \Phi_y(x, y) \sin \omega t,$$

where ω is the natural angular frequency. The displacements and rotations are then approximated with the following polynomial functions

$$\begin{aligned} U(x, y) &= \sum_{i=1}^{I_1} \sum_{j=1}^{J_1} c_{ij}^u \left(\frac{x}{a}\right)^i \left(\frac{y}{b}\right)^j \left(1 - \frac{x}{a}\right) \left(1 - \frac{y}{b}\right), \\ V(x, y) &= \sum_{i=1}^{I_2} \sum_{j=1}^{J_2} c_{ij}^v \left(\frac{x}{a}\right)^i \left(\frac{y}{b}\right)^j \left(1 - \frac{x}{a}\right) \left(1 - \frac{y}{b}\right), \\ W(x, y) &= \sum_{i=2}^{I_3} \sum_{j=2}^{J_3} c_{ij}^w \left(\frac{x}{a}\right)^i \left(\frac{y}{b}\right)^j \left(1 - \frac{x}{a}\right)^2 \left(1 - \frac{y}{b}\right)^2, \\ \Phi_x(x, y) &= \sum_{i=1}^{I_4} \sum_{j=1}^{J_4} c_{ij}^{\varphi_x} \left(\frac{x}{a}\right)^i \left(\frac{y}{b}\right)^j \left(1 - \frac{x}{a}\right) \left(1 - \frac{y}{b}\right), \\ \Phi_y(x, y) &= \sum_{i=1}^{I_5} \sum_{j=1}^{J_5} c_{ij}^{\varphi_y} \left(\frac{x}{a}\right)^i \left(\frac{y}{b}\right)^j \left(1 - \frac{x}{a}\right) \left(1 - \frac{y}{b}\right). \end{aligned} \quad (4.11)$$

Here the extremities of the summations are considered as $I_1 J_1 = I_2 J_2 = (I_3 - 1)(J_3 - 1) = I_4 J_4 = I_5 J_5$. These products define the number of terms n of the polynomials. In particular, parameters I and J represent the degrees of the polynomial functions, adopted to approximate the modal shape of the resonant frequencies. Finally, substituting Eqs. (4.11), (4.10), (4.6), (4.4) in Eqs. (4.1) and (4.2), the strain and kinetic energies can be written as

$$\begin{aligned} U &= \frac{1}{2} [C]^T [K] [C], \\ T &= \frac{1}{2} \omega^2 [C]^T [M] [C], \end{aligned} \quad (4.12)$$

where $[K]$ and $[M]$ are the stiffness and mass matrices of dimensions $R = I_1 J_1 + I_2 J_2 + (I_3 - 1)(J_3 - 1) + I_4 J_4 + I_5 J_5$ and are related to the functions of Eqs. (4.11) adopted to describe the displacements field. $[C]$ is the vector of coefficients:

$$[C]^T = [c_{11}^u, c_{12}^u, \dots, c_{I_1 J_1}^u, c_{11}^v, \dots, c_{I_2 J_2}^v, c_{11}^w, \dots, c_{I_3 J_3}^w, c_{11}^{\varphi_x}, \dots, c_{I_4 J_4}^{\varphi_x}, c_{11}^{\varphi_y}, \dots, c_{I_5 J_5}^{\varphi_y}]. \quad (4.13)$$

Finally, by equalling the strain and kinetic energy, as prescribed by the Rayleigh-Ritz method, the following eigenvalue problem can be written

$$([K] - \omega^2 [M])[C] = 0, \quad (4.14)$$

which allows to calculate the resonant frequencies, by zeroing the determinant of the matrix. For further details on the matrix elements, the reader can refer to Chen et al. [79].

4.1.2 Mode shape information through a concentrated mass

The approach is based on the experimental methodology presented in Ch. 3. As discussed, the inverse problem which intends to determine the elastic

properties from the measurements of the first resonant frequency, can be undetermined. In other words, the measured frequencies can be obtained with multiple sets of elastic estimates. In this regard, the inverse problem was firstly formulated by considering limits on the design domain of the elastic properties, as shown in Eq. (3.1). However, this is undesirable when the damage level has to be assessed. In this section, it is shown that information related to the modal shape can be considered within the optimization problem, in order to increase the accuracy of the methodology.

Modal shapes can be investigated through a concentrated mass. Low et al. [80] firstly proposed to move a concentrated mass on the plate and to measure the resultant resonant frequencies. As it is well known, due to the presence of an added mass, the resonant frequencies of the plate decrease. In particular, the reduction of a retained resonant frequency is function of the modal shape. According to the location of the concentrated mass, the higher is the modal displacement in correspondence of the mass position, the lower is the resultant resonant frequency. Therefore, by moving a mass on a clamped plate, the first modal shape can be investigated by considering the reduction of the first resonant frequency.

In the case of anisotropic materials, the modal shape is particularly dependent on the elastic parameters. For anisotropic material, the isolines of the modal shape are not necessarily parallel to the clamped boundaries. For instance, this is the case of an orthotropic material whose axes of orthotropy are not parallel to the boundaries. As shown in Fig. 4.2, which refers to the unidirectional fibre plate of Ch. 3 (Fig. 3.16-3.19), the first mode shape rotates in accordance with the orientation of the unidirectional reinforcement with respect to the main axis of the rectangular frames.

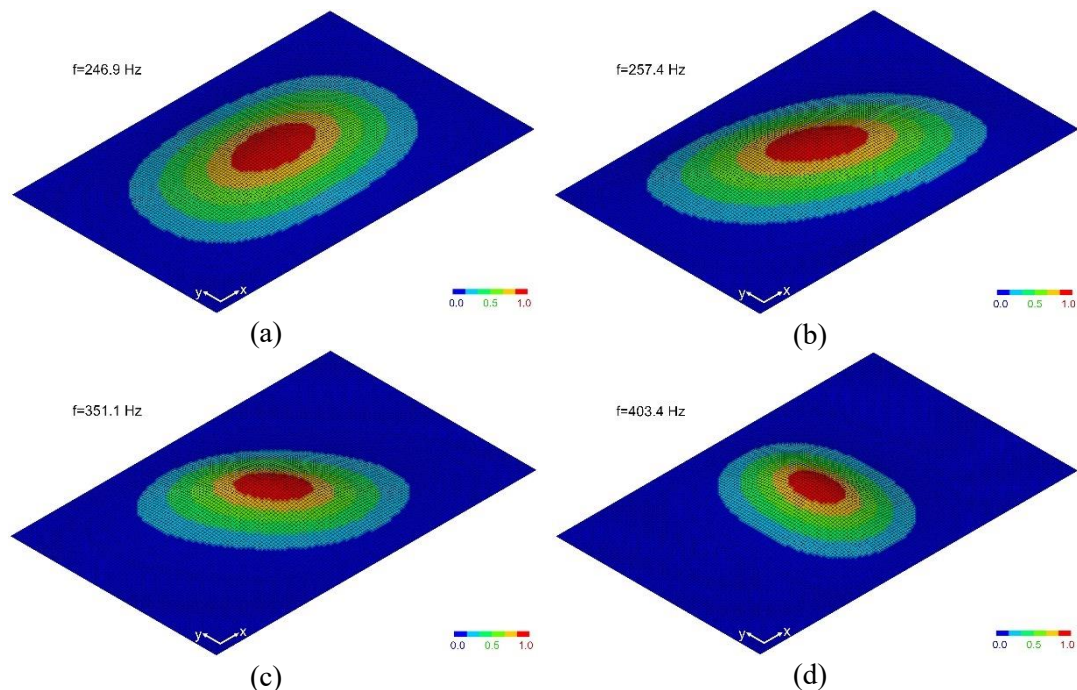


Figure 4.2 Mode shape with contour lines at different orientations of the unidirectional reinforcement with respect to the x axis: (a) 0°; (b) 30°; (c) 60°; (d) 90°.

In particular, for 0° and 90°, material axes of orthotropy are parallel to the boundaries and so the isolines of the modal shape. Instead, for 30° and 60°, whereas the material anisotropy is enhanced, the isolines are not parallel to the boundaries. This also shows that the modal shape strictly depends on the material properties and on its anisotropy. As the modal shape relates to the material anisotropy, information on the modal shape can be exploited to assess the elastic parameters with increased accuracy and robustness.

To this aim, a concentrated mass can be exploited. Two locations are sufficient to investigate the isolines of the first modal shape and hence the material anisotropy. In particular, the two positions are to be symmetric with respect to one of the axes of symmetry of the rectangle, while not lying on the other axis. For an example of mass locations, the reader can refer to Fig. 4.3.

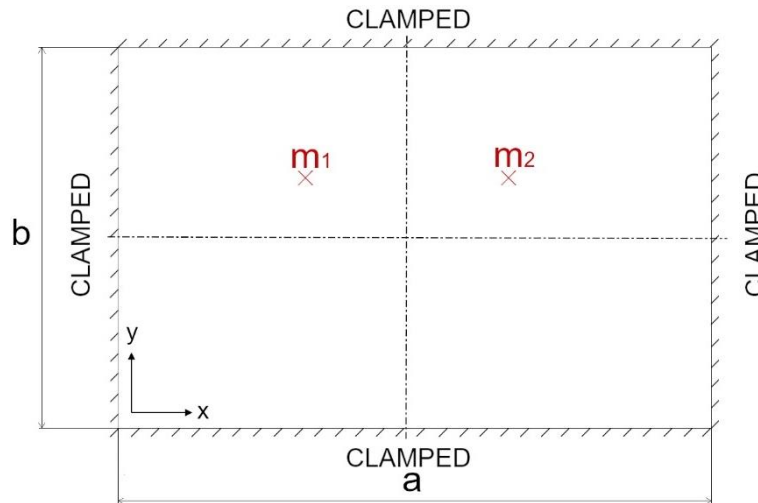


Figure 4.3 Example of mass spots symmetric with respect to one of the axes of the rectangular plate.

When the isolines are not parallel to the boundaries, the modal displacement is different in correspondence of the two mass locations. As a consequence, the reduction of the first resonant frequency is different. Instead, when the isolines are parallel to the clamped boundaries, the first resonant frequency equally decreases, as the two mass positions are symmetric with respect to one of the axes of the rectangular plate. The discrepancy between the reductions of the first resonant frequency due to the two mass locations thus represents a measure of the material anisotropy.

The methodology, previously presented in Ch. 3, is completed as follows:

- i) isolate a rectangular region of the component through a specific equipment, which clamps the extremities of the region without damaging the material;
- ii) measure the first resonant frequency of the retained region, $f_{ref,i}$, through the Impulse Excitation Technique;

- iii) measure the first resonant frequency for each location of the concentrated mass, $f_{ref,m1,i}$ and $f_{ref,m2,i}$;
- iv) repeat the frequency measurements after rotating the clamping system with respect to the material. It is worth noticing that there is not a prescribed value of rotation angle, even though 15° or 30° can represent a good choice according to the investigated laminate;
- v) assess the elastic properties of the investigated region from the measured resonant frequencies through an optimization process.

The information related to the modal shape is thus accounted within the inverse problem, which can be formulated as follows:

$$\min_{\underline{x}=[E_{11},E_{22},G_{12},\nu_{12}]} \sum_i \left| \frac{f_{ref,i}-f_i}{f_{ref,i}} \right| + \left| \frac{f_{ref,m1,i}-f_{m1,i}}{f_{ref,m1,i}} \right| + \left| \frac{f_{ref,m2,i}-f_{m2,i}}{f_{ref,m2,i}} \right|, \quad (4.15)$$

where $f_{ref,i}$, $f_{ref,m1,i}$ and $f_{ref,m2,i}$ constitute the reference frequencies for the i -th material orientation, while f_i , $f_{m1,i}$ and $f_{m2,i}$ are the values of the first resonant frequencies computed at each iteration of the optimization process.

A numerical validation of the approach is presented in the next section. The reference values $f_{ref,i}$, $f_{ref,m1,i}$ and $f_{ref,m2,i}$ are calculated with the Rayleigh-Ritz method for the considered materials. Further, according to the values assumed by the elastic constants at each iteration of the optimization process, the Rayleigh-Ritz method is also used to calculate the three frequencies f_i , $f_{m1,i}$ and $f_{m2,i}$ for each material orientation. The discrepancy between the reference values and the calculated frequencies is thus minimized by varying the material parameters \underline{x} . The elastic constants are hence assessed as the result of the optimization process. It is worth noticing that the formulation of the inverse problem Eq. (4.15) does not involve limits for the design variables.

4.2 Results

The Rayleigh-Ritz formulation is firstly validated on experimental data reported in the literature. Then the proposed approach is applied on four different laminated composites.

4.2.1 Validation of the Rayleigh-Ritz formulation

In order to validate the Rayleigh-Ritz described in Subsection 4.1.1, literature data [80–82] on clamped plates are considered. For convergence and validation studies, the comparison concerns six different laminates with unidirectional reinforcement plies. Further, the Rayleigh-Ritz formulation is validated on the experimental results of an isotropic aluminium plate loaded by a concentrated mass.

In regard to the laminated composites, data and results are taken from Chow et al. [81] and Lam and Chun [82]. In these works, the dimensions of the plates were $a = b = 1270$ mm with thickness $h = 25.4$ mm. The plate was hence relatively thin with the aspect ratio, i.e., the ratio between the in-plane dimension and the thickness is equal to 50. The laminated composites were clamped at the extremities and the first resonant frequency was acquired.

In their studies, the laminated composites were constituted by four layers with unidirectional reinforcement and presented symmetric stacking sequences ($[0^\circ, 0^\circ, 0^\circ, 0^\circ]$, $[15^\circ, -15^\circ, -15^\circ, 15^\circ]$, $[30^\circ, -30^\circ, -30^\circ, 30^\circ]$ and $[45^\circ, -45^\circ, -45^\circ, 45^\circ]$), an anti-symmetric stacking sequence ($[30^\circ, -30^\circ, 30^\circ, -30^\circ]$) and a non-symmetric sequence ($[0^\circ, 30^\circ, 60^\circ, 90^\circ]$). Material properties of the unidirectional plies are reported in Table 4.1 with reference to the axes of orthotropy.

Property	Value
Density	$1.61 \cdot 10^3$ kg/m ³
Young's modulus in longitudinal direction (E_{11})	131.69 GPa
Young's modulus in transverse direction (E_{22})	8.55 GPa
Shear modulus (G_{12})	6.76 GPa
Poisson's ratio (ν_{12})	0.3

Table 4.1 Material properties at ply level of the unidirectional layers.

Firstly, it is addressed the convergence study. Results of the convergence study are reported in Table 4.2 in terms of frequency parameter λ for different numbers of terms n of the polynomials in Eq. (4.11). Indeed, as the polynomial degree increases, i.e., the number of terms n increases, the exact solution is better approximated through the Rayleigh-Ritz method. Table 4.2 shows that the convergence is reached even for $n=36$. However, for a better approximation, a degree of the polynomial equal to 7 is assumed in the following calculations, with the number of terms n equal to 49.

Stacking Sequences	Present – 36 terms	Present – 49 terms	Present – 64 terms	Literature Result
$[0^\circ, 0^\circ, 0^\circ, 0^\circ]$	23.42	23.41	23.41	23.86 ¹
$[15^\circ, -15^\circ, -15^\circ, 15^\circ]$	22.89	22.89	22.89	23.29 ¹
$[30^\circ, -30^\circ, -30^\circ, 30^\circ]$	21.91	21.90	21.90	22.22 ^{1,2}
$[45^\circ, -45^\circ, -45^\circ, 45^\circ]$	21.44	21.42	21.42	21.75 ¹
$[30^\circ, -30^\circ, 30^\circ, -30^\circ]$	21.56	21.56	21.56	21.94 ²
$[0^\circ, 30^\circ, 60^\circ, 90^\circ]$	15.82	15.80	15.80	16.23 ²

Table 4.2 Convergence results of frequency parameter λ and comparison to the

experimental data presented in the literature - $\lambda = \left(\frac{\rho h \omega^2 a^4}{D_{11}} \right)^{\frac{1}{2}}$, $D_{11} = \frac{E_{11} h^3}{12(1-\nu_{12}\nu_{21})}$;

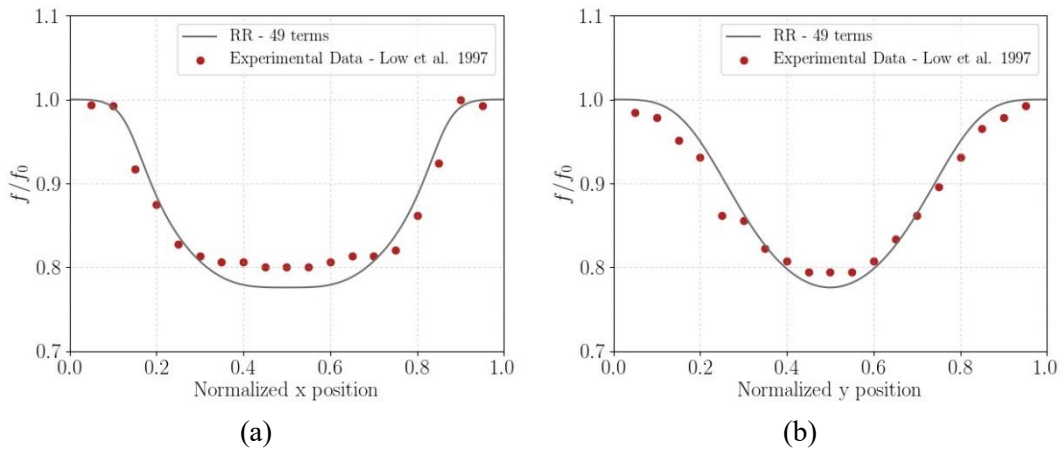
¹ Chow et al. [81]; ² Lam and Chun [82].

Table 4.2 also reports a comparison of the results obtained with the formulation proposed in Section 4.1.1 with those obtained by Chow et al. [81] and

Lam and Chun [82] in their works. The discrepancy is very limited. The frequency parameters λ calculated through the proposed formulation are always smaller than those calculated in the literature. This is mainly due to the different shear deformation theories. Indeed, the present Rayleigh-Ritz formulation is based on the higher-order shear deformation theory. Instead, the first order shear deformation theory was adopted in the considered works. The higher order of the presented formulation indeed considers additional degrees of freedom, which allows to better capture the mechanical deformation of the cross-section. The less rigid behaviour of the higher order shear deformation theory thus results in slightly lower values of the frequency parameter λ [79].

The Rayleigh-Ritz formulation is also validated with respect to the experimental results reported by Low et al. [80], who analysed the first resonant frequency of a clamped rectangular plate made of aluminium for different positions of a concentrated mass of 96 g. The mass was moved along the axes of symmetry of the rectangle and the first resonant frequency was measured. The clamped plate had dimensions $a = 600$ mm and $b = 300$ mm. Therefore, while moving the mass along the x direction, its y coordinate was equal to $\frac{b}{2} = 150$ mm. Instead, while moving the mass along the y direction, the x coordinate was $\frac{a}{2} = 300$ mm.

Even though the Rayleigh-Ritz formulation of Subsection 4.1.1 is specifically developed for angle-ply laminates, an isotropic material can be considered as a particular case. The longitudinal and transverse Young moduli are equal to 69 GPa, as the Young modulus of the aluminium plate, while the Poisson's coefficient is 0.3. Finally, the shear modulus can be related to the Young modulus and to the Poisson's coefficient as usual, $G = E/(2(1 + \nu^2))$.



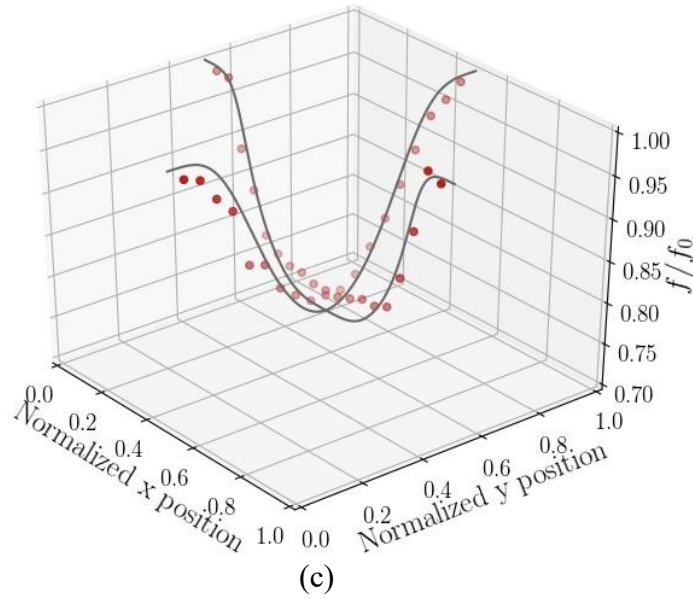


Figure 4.4 Comparison between experimental data obtained by Low et al. [80] and the presented Rayleigh-Ritz formulation: variation of the frequency for the mass positioned (a) along the x direction ($y = \frac{b}{2} = 150$ mm) and (b) along the y direction ($x = \frac{a}{2} = 300$ mm); (c) 3D view.

Fig. 4.4 shows the comparison of the experimental results with those obtained with the present formulation. Also the 3D view is reported in Fig. 4.4c. Results are reported in normalized form, where f_0 is the frequency obtained without the mass loading and the position x and y of the concentrated mass are normalized with respect to a and b , respectively. Results of the Rayleigh-Ritz formulation have been obtained by moving the concentrated mass along the plate axes of symmetry with a step of 2 mm and calculating the resultant first resonant frequency. An acceptable agreement is obtained, with the Rayleigh-Ritz formulation able to catch the global trend of the experimental results. Further, it can be appreciated that, by moving a mass on the plate and measuring the resultant resonant frequency, the modal shape can be obtained.

4.2.2 Calculation of the reference frequencies

Four different materials are here considered for the validation of the proposed methodology. In addition to the unidirectional ($[0^\circ, 0^\circ, 0^\circ, 0^\circ]$), the symmetric ($[30^\circ, -30^\circ, -30^\circ, 30^\circ]$) and the asymmetric materials ($[30^\circ, -30^\circ, 30^\circ, -30^\circ]$) already presented in Subsection 4.2.1, a woven fabric laminate is considered. The woven laminate is also constituted by four layers, with the material properties reported in Table 4.3 with reference to the axes of orthotropy. These materials have been chosen to show the applicability of the proposed approach to a rich selection of laminates.

Property	Value
Density	$1.43 \cdot 10^3 \text{ kg/m}^3$
Young's modulus in longitudinal direction (E_{11})	59.0 GPa
Young's modulus in transverse direction (E_{22})	59.0 GPa
Shear modulus (G_{12})	3.4 GPa
Poisson's ratio (ν_{12})	0.04

Table 4.3 Material properties at ply level of the woven fabric.

The reference frequencies are here calculated through the Rayleigh-Ritz formulation. Dimensions of the rectangular region are $a = 150 \text{ mm}$ and $b = 100 \text{ mm}$, as in the assumption of assessing local elastic properties, according to the methodology described in Subsection 4.1.2. The thicknesses of the four laminates are 1 mm for the unidirectional, 1.5 mm for both the symmetric and anti-symmetric laminates and 2.5 mm for the woven fabric. With respect to the reference axes shown in Fig. 4.1, the mass locations are $(x_1, y_1) = (50, 60)$ and $(x_2, y_2) = (100, 60)$, which are symmetric with respect to the y -axis of the rectangle. It is worth noting that, in order to obtain a measurable discrepancy in the reduction of the first resonant frequency, the two locations are not necessarily far from the centre of the plate. The mass is assumed equal to 1 g. In this regard, it is worth highlighting that the higher the mass, the higher the reduction of the frequency and so the discrepancy in the frequencies of the two mass locations.

For the unidirectional, the symmetric and anti-symmetric plates, the reference values are calculated considering the material orientated at 0° , 30° , 60° and 90° with respect to the clamped boundaries. For the woven fabric, the assumed rotations are 0° , 15° , 30° , 45° . Indeed, after 45° , the frequency values are repeated as the longitudinal and transverse Young moduli are equal. Results of the reference values of the first resonant frequencies are reported in Tables 4.4-4.7.

	0°	30°	60°	90°
f_{ref} [Hz]	505.1	535.5	773.1	948.3
$f_{ref,m1}$ [Hz]	472.3	507.8	720.8	855.2
$f_{ref,m2}$ [Hz]	472.3	494.0	705.9	855.2

Table 4.4 First resonant frequency values with and without the 1 g mass load of the unidirectional plate ($[0^\circ, 0^\circ, 0^\circ, 0^\circ]$) for different material orientations.

	0°	30°	60°	90°
f_{ref} [Hz]	850.2	1117.4	1361.7	1191.8
$f_{ref,m1}$ [Hz]	817.3	1070.3	1283.9	1126.8
$f_{ref,m2}$ [Hz]	808.1	1054.9	1283.2	1136.4

Table 4.5 First resonant frequency values with and without the 1 g mass load of the symmetric plate ($[30^\circ, -30^\circ, -30^\circ, 30^\circ]$) for different material orientations.

	0°	30°	60°	90°
f_{ref} [Hz]	843.6	931.8	1100.4	1151.4
$f_{ref,m1}$ [Hz]	806.6	894.6	1050.8	1095.5
$f_{ref,m2}$ [Hz]	806.6	885.4	1045.4	1095.5

Table 4.6 First resonant frequency values with and without the 1 g mass load of the anti-symmetric plate ($[30^\circ, -30^\circ, 30^\circ, -30^\circ]$) for different material orientations.

	0°	15°	30°	45°
f_{ref} [Hz]	1793.8	1757.9	1686.7	1650.5
$f_{ref,m1}$ [Hz]	1738.0	1702.0	1633.8	1600.5
$f_{ref,m2}$ [Hz]	1738.0	1705.2	1636.6	1600.5

Table 4.7 First resonant frequency values with and without the 1 g mass load of the woven fabric plate ($[0^\circ, 0^\circ, 0^\circ, 0^\circ]$) for different material orientations.

As expected, the presence of the concentrated mass reduces the value of the first resonant frequency. Further, when the isolines are parallel to the clamped boundaries, as in the case of the unidirectional laminate with fibres oriented at 0° or at 90° with respect to the clamped boundaries, the first resonant frequency equally decreases for the two mass locations. This is due to the modal shape combined with the choice of the mass positions which are symmetric with respect to one of the symmetry-axes of the rectangular plate. Instead, when the isolines are not parallel to the boundaries, the mass affects the first resonant frequency differently in the two locations. As a consequence, the discrepancy between the reductions of the first resonant frequency due to the two mass locations is a measure of the material anisotropy. Further, in regard to the resultant first frequency, it is important to notice that its value is higher for the mass disposed in the first position. Indeed, the modal shape follows the rotations of the material with respect to the clamped boundaries.

Furthermore, the discrepancy between the first resonant frequencies for the two mass positions is inversely proportional to the mass of the concentrated mass, while it is enhanced by the thickness of the laminate. An added mass reduces the resonant frequencies and higher values of concentrated mass lead to higher reduction of the resonances, thus flattening any discrepancy. On the contrary, the thickness plays a key role in the bending stiffness of the laminate, which in turn affects the resonant frequency. As the thickness increases, the first resonant frequencies for the two mass spots proportionally increase, and so the discrepancy. It is the case of the woven laminate, whose anisotropy is particularly limited but still recognizable, as shown in Table 4.7.

Finally, it can be argued that, as the resonant frequencies do not change after a rotation of 90° for the unidirectional reinforcement laminates or 45° in case of woven fabric, further information can be considered within the optimization process without the need of other replications of the first resonant frequency measure. In particular, in the case of unidirectional reinforced laminates, results obtained for 30° and 60° are respectively equal to those obtained for rotations

equal to 150° and 120°, respectively. However, the results obtained with the concentrated mass must be switched, as the modal shape follows the rotations of the material with respect to the clamped boundaries. The same can be applied to the woven fabric, thus extending the acquired information to the range 45°-90°. This provides further information to the optimization process which can further increase its robustness.

4.2.3 Optimization results

Material properties for the four considered materials are determined through Eq. (4.15). The Nelder-Mead zero order algorithm is again considered for the optimization process [71]. It was observed that the algorithm can fail in reaching the optimal solution. In particular, the algorithm got stuck into solution where the objective function was different from zero. The difficulty in reaching an optimal solution was mainly due to the limited dependency of the first resonance frequency on the Poisson's coefficient ν_{12} and on the shear modulus G_{12} . Indeed, the first resonant frequency of a clamped composite plate mainly depends on the longitudinal and transverse Young moduli. In this regard, it is worth highlighting that the rectangular shape of the analysed region enhances the sensitivity of the first resonant frequency on the elastic properties in the direction of the short edge of the rectangle, i.e., the transverse direction.

As the algorithm can fail in reaching the optimal solution, several repetitions of the optimizations are performed. In particular, the result of an optimization process is used as starting point for the next. Indeed, at the beginning of the optimization, the algorithm more extensively probes the design domain, which allows to avoid the stuck effect. After few iterations, the algorithm is able to reach the optimal solution. Table 4.8 reports the elastic constants calculated through Eq. (4.15) for each analysed material.

	E_{11} [GPa]	E_{22} [GPa]	G_{12} [GPa]	ν_{12} [-]
Unidirectional [0°, 0°, 0°, 0°]	131.72	8.56	6.74	0.29
Symmetric [30°, -30°, -30°, 30°]	131.7	8.55	6.75	0.29
Anti-symmetric [30°, -30°, 30°, -30°]	131.7	8.55	6.75	0.30
Woven fabric	59.0	59.0	3.4	0.04

Table 4.8 Optimized material properties at ply level for each material.

The dependency of the inverse problem on the shear modulus and on the Poisson's coefficient represents a critical aspect of the optimization algorithm, particularly when the elastic properties are calculated considering only the first resonant plate without disposing the mass load. In this case, limits on the design domain are necessary. Instead, by considering further information related to the modal shape, the optimization is able to catch all the four elastic constants without

the need of limiting the domain of the elastic properties. This is particularly useful when damage level, i.e., residual elastic properties, are to be assessed. If a formulation similar to that of Eq. (3.1) is adopted for detecting local material variations, the results of the optimization problem can be constrained by the limits of the design domain, i.e., the space where the aforementioned material properties can vary, and can be, in the end, wrong. Further, as shown in Table 4.8, even though the objective function of Eq. (4.15) is equal to zero, very limited discrepancies from the nominal values are obtained. Only the shear modulus and the Poisson's ratio are slightly different from the nominal values of Table 1 and 2, with discrepancies lower than 0.3% for the shear modulus and 3% for the Poisson's ratio.

The optimization is also performed without retaining the modal shape information for the symmetric and anti-symmetric stacked laminates. Results are reported in Table 4.9 with relative errors with respect to the elastic properties of Table 4.1.

	E_{11} [GPa] - ϵ_{rel}	E_{22} [GPa] - ϵ_{rel}	G_{12} [GPa] - ϵ_{rel}	ν_{12} [-] - ϵ_{rel}
Symmetric	132.0 –	8.55 –	7.586 –	0.129 –
[30°, -30°, -30°, 30°]	0.24%	0.0%	12.2%	57%
Anti-symmetric	132.5 –	8.85 –	7.2 –	0.073 –
[30°, -30°, 30°, -30°]	0.615%	3.51%	6.51%	76%

Table 4.9 Optimized material properties at ply level and relative errors for the symmetric and anti-symmetric laminates without considering the modal shape information.

It is worth noting that, even though the resultant first resonant frequencies without mass load for the different material orientations are those reported in the first line of Tables 4.5 and 4.6, respectively, the relative errors can be very high. This shows that the inverse problem can be undetermined, i.e., multiple solutions are feasible. In addition, it is evident the limited dependency of the first resonant frequency of a clamped plate on the shear modulus and on the Poisson's ratio. A decrease of the Poisson's ratio seems to be compensated by an increase of the shear modulus. Further, the errors on these properties can affect in turn the determination of the Young modulus in the transverse direction. Instead, the Young modulus in the longitudinal direction is assessed with very limited discrepancy.

By comparing the results reported in Table 4.8 and 4.9, it is clear that, by increasing the number of information retained within the optimization problem, the two low-influencing material parameters, i.e., G_{12} and ν_{12} , can be correctly assessed. The approach here described retains the modal shape within the optimization process. In particular, the modal shape is simply identified through the use of a concentrated mass, positioned in two different points. In accordance with the methodology described in Ch. 3, other possibilities to increase the

number of information retained in the optimization problem as well as its robustness, could consist of:

- i) increasing the number of relative orientations between the clamping system and the plate;
- ii) considering higher modes, with the limitations already discussed in the introduction of this chapter.

Finally, it is worth noting that, as shown in Table 4.8, even in the numerical analysis here pursued with the further information of the modal shape, the shear modulus and the Poisson's ratio can still present very limited discrepancies with respect to the nominal values. The sensitivity of the first resonant frequency on these parameters is low but not null. Therefore, by increasing the information retained within the optimization problem, the allowable solutions of the inverse problem accordingly decrease, thus allowing to also estimate the two low-influencing parameters with very limited discrepancy.

4.3 Conclusions and possible limitations of the approach

In this chapter, a new approach for the nondestructive determination of the elastic properties of composite laminates is presented. The approach represents an enhancement of the experimental methodology presented in Ch. 3. The illustrated approach intends to increase the number of the retained information and therefore the accuracy of the methodology by identifying the modal shape of the clamped plate. In particular, a concentrated mass is exploited, whose effect on the first resonant frequency depends on its position in the plate in accordance with the modal shape. According to the location of the concentrated mass, the higher is the modal displacement in correspondence of the mass position, the lower is the resultant resonant frequency. Only two mass positions, i.e. two additional measures of the first resonant frequency, are sufficient to investigate the modal shape, as the reduction of the first resonant frequency is different for the two mass spots. Mass locations have to be symmetric with respect to one of the axes of symmetry of the rectangle, while not lying on the other axis. The modal shape is in turn a function of the material properties, which allows to increase the accuracy and the robustness of the optimization problem.

As the approach is an enhancement of the experimental methodology introduced in Ch. 3, it shares most of the limitations previously discussed. In particular, the methodology is suitable only for laminated composites characterized by material anisotropy. The stacking sequence must be known, and the stacked plies must be of the same material. Further, the methodology is still only applicable in laboratory conditions, where both sides of the composite plate are addressable. It is also worth to note that, in this chapter, only a numerical validation of the approach has been performed. An experimental validation, which

confirms the limited influence of the dislocated mass on the boundaries, is still required.

However, a Rayleigh-Ritz formulation based on higher order shear deformation theory has been implemented to compute the first resonant frequency of the clamped plate loaded by a concentrated mass. It is worth noticing that the use of the Rayleigh-Ritz formulation allows to consistently decrease the computational cost with respect to the finite element-based optimization adopted in Ch. 3. To give an order of magnitude, the optimization based on finite element method required from $3.6 \cdot 10^3$ s to $14.4 \cdot 10^3$ s on a desktop computer with Intel Core i7-8700 (3.2 GHz) and 32 GB of RAM. Instead, the optimization based on the Rayleigh-Ritz method took at most 60 s to achieve the result. The Rayleigh-Ritz formulation thus represents a further step towards the application of the proposed methodology to real-world composite structures.

Finally, the validation on the four laminated composites, namely a unidirectional, a symmetric angle-ply, an anti-symmetric angle-ply and a woven fabric, shows that by increasing the number of information, i.e., by retaining the modal shape, the accuracy in the assessment of the four elastic properties is increased. In particular, results show that even in the numerical analysis here pursued with the further information of the modal shape, the shear modulus and the Poisson's ratio can still present very limited discrepancies with respect to the nominal values. These are 0.3% for the shear modulus and 3% for the Poisson's ratio. Instead, when the information related to the modal shape is not accounted, the discrepancies reach the values of 12% for the shear modulus and 76% for the Poisson's ratio. This confirms that the sensitivity of the first resonant frequency on these parameters is low but not null. Therefore, by increasing the information retained within the optimization problem, the feasible solutions of the inverse problem accordingly decrease, thus allowing to also estimate the two low-influencing parameters with very limited discrepancy. The optimization is thus able to catch all the four elastic constants for all the considered materials without the need of limiting the domain of the elastic properties, as presented in Ch.3.

V

Determination of damage severity through local IET

In Ch. 1, it has been highlighted the importance of assessing damage severity in composites. Differently from metals, where residual strength expressed as a function of the most “critical” crack is sufficient to estimate the damage tolerance, composites generally present a highly rich and complex collection of cracks, whose evolution is hardly predictable through energy-based criteria and crack-front stress fields as provided by fracture mechanics. As a consequence, for composites, residual strength degradation does not represent a suitable metric of the material damage tolerance. In composites, damage severity needs to be determined also in terms of residual elastic properties, rather than only in terms of extension of the cracked area, as in current nondestructive practices.

In Ch. 3 a new methodology has been introduced which allows to assess local elastic properties in laminated composites where the stacked plies are made of the same material. The sensitivity of the methodology to the extension of the inspected region has been also analysed. The sensitivity analysis showed that the methodology is not able to assess the elastic properties of the damaged zone, i.e., of the area where cracks are confined. The technique rather estimates equivalent material constants for the whole inspected region, whose value greatly depends on its extension.

Furthermore, the practical constraint to assess impact damage severity by in-field inspection is that any observations and measurements are restricted to the exposed surface [14]. The methodology described in Ch. 3 and enhanced in Ch. 4 is thus suitable only for laboratory testing conditions, as it requires the access to both sides of the plate.

In this chapter, a new technique is presented which intends to:

1. specifically assess the elastic properties of the damaged zone;
2. limit the investigations to only one surface of the component.

To this aim, a proper device is proposed and designed. The technique also involves a new analytical approach for the determination of the elastic properties from the measured resonant frequencies. In particular, a formula for the residual material constants of the damaged zone is derived. The analytical approach allows to further increase the robustness of the inverse problem, with a negligible computational cost.

Experimental validation is performed on two glass fibre woven fabric composites. The laminates are damaged by impact at an incident energy of 1.8 J. The determined material properties of the damaged zone are compared to the results of tensile tests performed on specimens cut from the impacted plates. The specimens are equipped with optic fibre in order to punctually measure the longitudinal strain and so the elastic parameters. The chapter is concluded with a discussion of the possible limitations of the technique.

5.1 Materials

Experimental tests are performed on two laminated composite plates realized in the laboratory of Politecnico di Torino. The first composite laminate consists of six layers of glass fibre fabric impregnated with epoxy resin. The same constituents are used for the second plate which is made of 8 layers. The glass fabric is a twill 2x2 with slightly different fibre concentrations in the two perpendicular directions. In particular, the yarn densities are 11.5 and 12 in the warp and weft directions, respectively. In order to realize the plates, the glass fabric plies are stacked in parallel and vacuum bagged. The resin is then infused through vacuum and the plates are cured in oven at 100°C for 3 hours without providing any adding pressure. Fig. 5.1 shows the resin infusion process to manufacture the plates.





Figure 5.1 Vacuum bag infusion process.

The stacking sequence is $[0]_6$ for the 6-layers plate and $[0]_8$ for the 8-layers plate. The plates are manually cut with dimensions of 300 mm x 250 mm.

In regard to the thickness, the 6-layers plate is 1.31 mm thick, while the 8-layers plate 1.24 mm. A larger amount of resin is thus present in the 6-layers plate. The resulting elastic properties are reported in Table 5.1 for the two plates. Tensile tests were performed on specimens cut from the plates at 0° , 45° and 90° .

	Property	Value
6-layers	Density	$1.50 \cdot 10^3 \text{ kg/m}^3$
	Young's modulus in longitudinal direction (E_{11})	17.5 GPa
	Young's modulus in transverse direction (E_{22})	16.7 GPa
	Shear modulus (G_{12})	3.1 GPa
	Poisson's ratio (ν_{12})	0.13
8-layers	Density	$1.66 \cdot 10^3 \text{ kg/m}^3$
	Young's modulus in longitudinal direction (E_{11})	21.5 GPa
	Young's modulus in transverse direction (E_{22})	19.5 GPa
	Shear modulus (G_{12})	3.7 GPa
	Poisson's ratio (ν_{12})	0.17

Table 5.1 Material properties of the 6- and 8-layer plates.

A servo-hydraulic testing machine (Instron 8801) was adopted which has a cell load of 100 kN. Strains were measured through two strain gauges mounted at 0° and 90° . The crosshead speed was set equal to 2 mm/min, in accordance with the recommendations of the ASTM standard D3039 [83]. Fig. 5.2 shows the experimental setup. The extensometer was also mounted to confirm the results.



Figure 5.2 Experimental setup of the tensile tests.

From the applied load, the elastic properties were calculated. The difference in the elastic constants of the two plates is mainly due to the different amounts of resin.

5.2 Methods

In this Section, the methodology will be described. Firstly, the experimental setup which clamps the boundaries from only one side will be presented. Then, the numerical calculations for the assessment of the residual elastic properties of the damaged zone will be detailed.

5.2.1 Experimental setup

The nondestructive inspection must be restricted to one surface of the test plate. It is rather unlikely that both sides are accessible for clamping in real-world components. In order to realize clamped boundaries from only one side, vacuum technique is adopted. Fig. 5.3 shows the experimental setup.

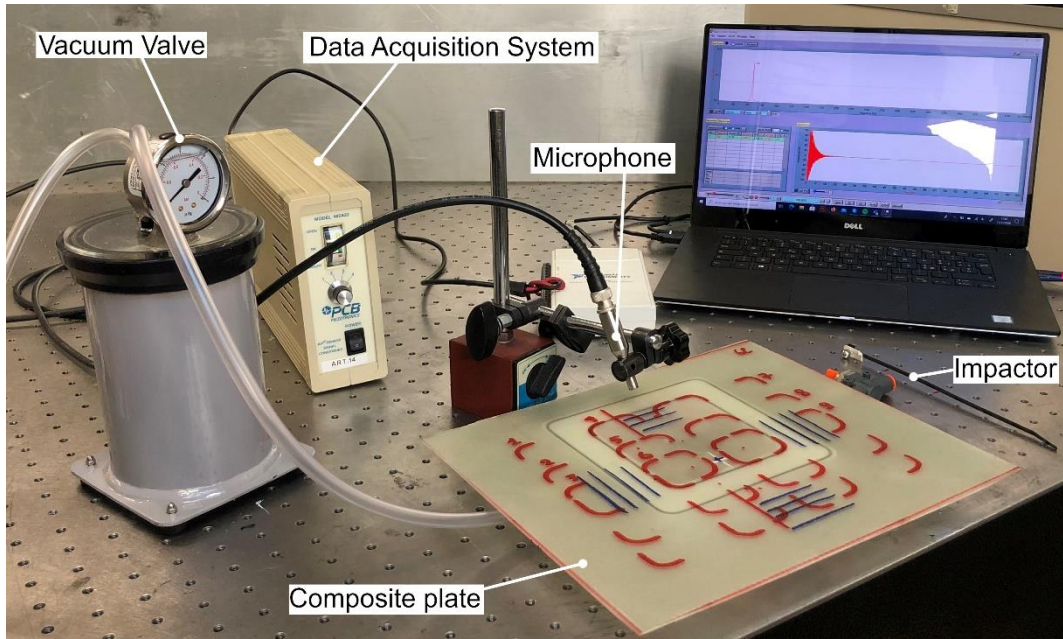


Figure 5.3 Experimental setup.

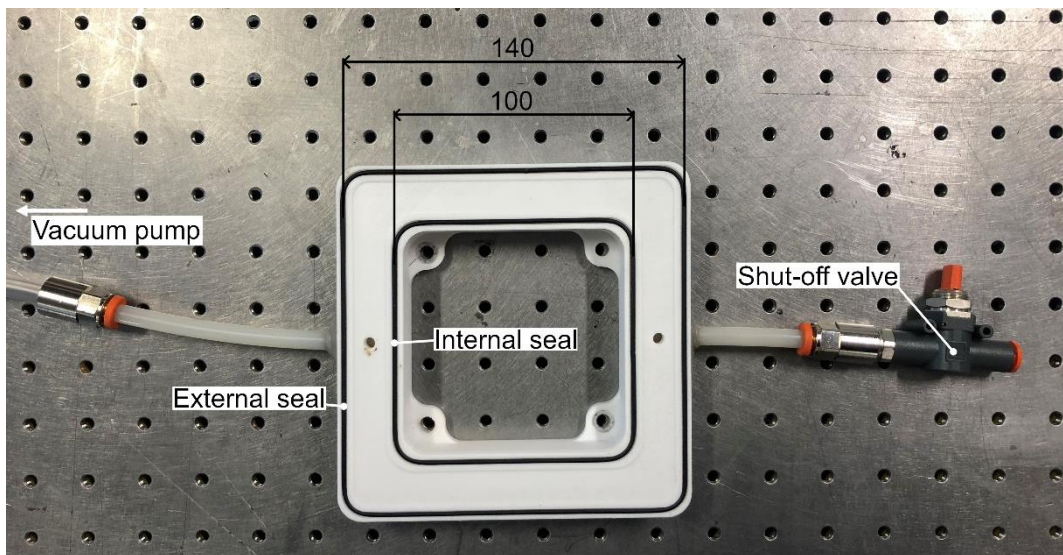


Figure 5.4 Clamping device: dimensions and details of the vacuum system.

A proper device is used to perform the local investigations. The device is 3D printed and is made of polyethylene terephthalate (PET). As shown in Fig. 5.4, the device has a frame shape and the vacuum is realized in the thin chamber comprised between the external and internal seals by means of a vacuum pump. A shut-off valve is also adopted in order to facilitate the entrance of the air once the measurement is performed. The region under investigation is thus limited by the internal seal, which has square shape of dimension $a = 100$ mm.

Thanks to their flexibility under the applied pressure load, the rubber seals compensate for thickness variations along the composite plates. Their presence also affects the stiffness of the boundaries, which is consequently noninfinite. As a major consequence, the resultant resonant frequency of the non-perfectly clamped plate is smaller than the resonance of the fully clamped. However, for the local investigations, it is required that the vibrational response must be mostly

related to the inspected region, with limited influence of the excluded surrounding material. This aspect will be further discussed in the next Section.

The methodology is based on the IET. An impulser is used to excite the plate and the resulting mechanical vibrations are measured through a microphone. The data acquisition system is the same adopted in Ch. 3. The acquisition system (National Instruments NI USB-6210) receives the signal, and the analyser (Buzz-o-sonic[®]) provides the fundamental resonant frequency through a Fast Fourier Transform of the signal. The data acquisition system has a sample rate of 25 kHz and the signal is analogic-to-digital converted with a resolution of 16 bits. The analyser performs the Fast Fourier Transform of the signal with a resolution smaller than 1 Hz.

As shown in Fig. 5.4, the device is fixed to a working table, in order to avoid vibrations of the whole system, i.e., device and composite plate. Therefore, both sides of the plate are utilized in this preliminary test setup. However, it is worthwhile noticing that the experimental setup can be easily converted in order to limit the nondestructive investigations to only one side of the plate.

5.2.2 Damage characterization

The presence of a damage within the region inspected through the device results in a reduction of the first resonant frequency. Such reduction is function of the participation of the damage to the modal displacement. The higher the modal displacement in correspondence of the damaged zone, the higher the reduction of the first resonant frequency. This can be shown through a finite element model, where a local material variation is assumed in order to simulate the presence of the local damage. The 8-layers plate is considered. Similarly to the discussion of Subsection 3.6.3, the material properties are reduced to the 50% of the nominal elastic constants of Table 5.1 in this defective region, while its dimensions are 20x20 mm. Two locations of the damage are considered: the first assumes the damage in the correspondence of the boundaries, while in the second the damage is in the centre. The first resonant frequency is calculated through a modal analysis. Fig. 5.5 shows the finite element models.

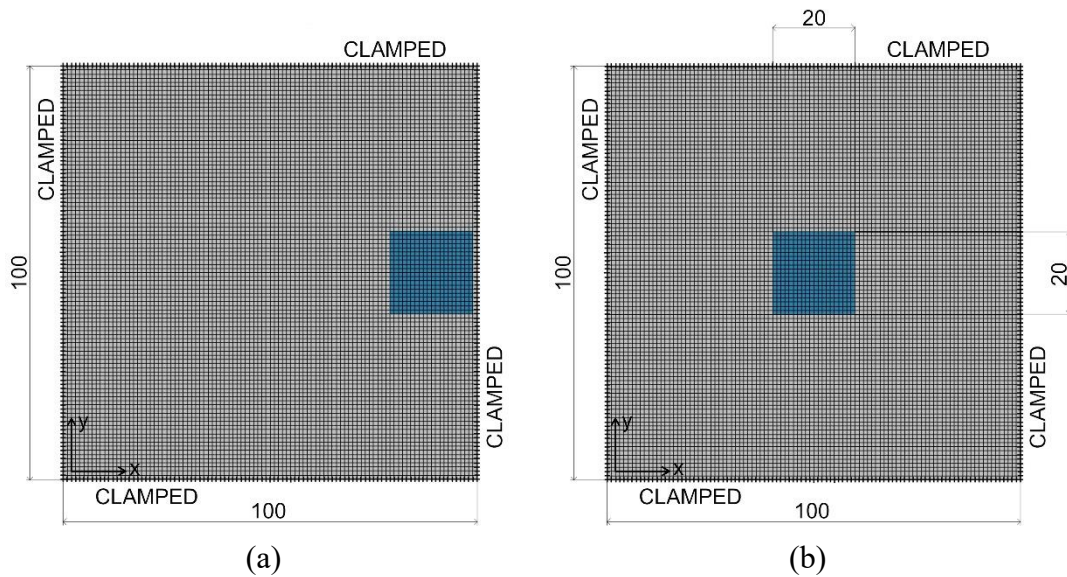


Figure 5.5 Numerical model with local material variation: a) damage in proximity of the boundary; b) damage in the centre.

The original value of the first resonant frequency of the clamped plate is 665 Hz. For the damage in proximity of the boundaries, its value decreases to 653 Hz, while when the damage is in the centre, the first resonant frequency has the minimum value of 640 Hz. Given the symmetry of the problem, same results are obtained in proximity to the other boundaries.

In order to characterize the damage in terms of residual elastic properties, the first resonant frequency is measured at different locations on the plate. The mapping procedure intends to identify the position of the damage and to measure the minimum value of the first resonant frequency. Here, the frequency is mapped in the x direction, as shown in Fig. 5.6, which refers to the longitudinal direction of the material.

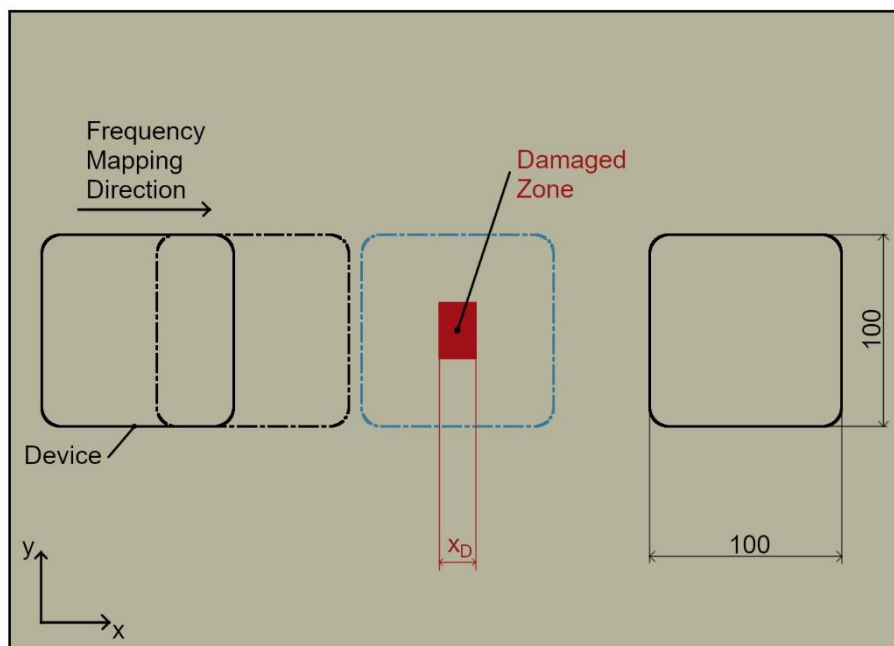


Figure 5.6 Frequency mapping procedure.

It is worthwhile to notice that through the mapping procedure is theoretically possible to identify also the dimensions of the damaged zone x_D , as shown in Fig. 5.6. Indeed, when the damage firstly enters in the region inspected by the device, a first reduction of the first resonant frequency occurs. Instead, when the damage finally exits from the investigated region, the first resonant frequency returns to its original value.

However, it should be also noted that in correspondence of the boundaries the effect of the damage is limited as well as the modal displacement. In addition, scattering in the measurement of the first resonant frequency might be present. Therefore, the identification of the damage extension is not straightforward from the reduction of the first resonant frequency. In this regard, other well-known techniques can be adopted to assess the damage extension. Here, the dimensions of the defective zone will be established through the optic fibre LUNA system [84], which will be also used to validate the results.

Once the extension is known, the residual elastic properties can be determined following Warburton [85], who showed that the first resonant frequency of an isotropic plate can be expressed as:

$$f = \frac{\lambda}{2\pi} \cdot \sqrt{\frac{D}{\rho \cdot h}} \cdot \sqrt{\frac{1}{a^4} + \frac{1}{b^4} + \frac{0.605}{a^2 b^2}} \quad (5.1)$$

where a and b are the dimensions of the plate, h the thickness, ρ the material density and λ numerical parameter which depends on the boundary conditions. For instance, for simply supported boundaries, λ is equal to 1, while for fully clamped boundaries, its value is 4.73². Finally, D is the flexural stiffness and is expressed as:

$$D = \frac{E \cdot h^3}{12(1 - \nu^2)} \quad (5.2)$$

where E is the Young modulus and ν the Poisson's coefficient.

In an intact plate, the frequency is proportional to the undamaged material properties (E_0 and ν_0) as:

$$f_0 \sim \sqrt{D_0} \quad (5.3)$$

Instead, in presence of a damage, the first resonant frequency is proportional to the residual elastic properties as:

$$f_d \sim \sqrt{D_d} \quad (5.4)$$

From Eqs. (5.3) and (5.4), the residual elastic properties can be expressed as a function of the undamaged material parameters as:

$$D_d = D_0 \left(\frac{f_d}{f_0} \right)^2, \quad (5.5)$$

which finally leads to

$$\frac{E_d}{(1 - \nu_d^2)} = \frac{E_0}{(1 - \nu_0^2)} \left(\frac{f_d}{f_0} \right)^2 \quad (5.6)$$

It is worthwhile to notice that, by considering the ratio between the first resonant frequencies of the damaged and undamaged state, the λ parameter which represents the dependency of the resonant frequency on the boundary conditions is reduced. By expressing E_d and ν_d as function of the undamaged material properties, i.e., $E_d = k_E \cdot E_0$ and $\nu_d = k_\nu \cdot \nu_0$, Eq. (5.6) results in

$$k_E = \frac{1 - k_\nu^2 \cdot \nu_0^2}{1 - \nu_0^2} \left(\frac{f_d}{f_0} \right)^2 \quad (5.7)$$

k_E and k_ν are the damage parameters of the Young modulus and of the Poisson's coefficient, respectively. Infinite combination of k_E and k_ν can satisfy Eq. (5.7). Here, it is assumed that k_ν is equal to 1 and, consequently, k_E is equal to $\left(\frac{f_d}{f_0} \right)^2$ as the damage is totally attributed to the Young modulus. It is worth noticing that, according to Eq. (5.7), k_E is a parabolic function of k_ν , as shown in Fig. 5.7. In particular, k_E increases as k_ν decreases.

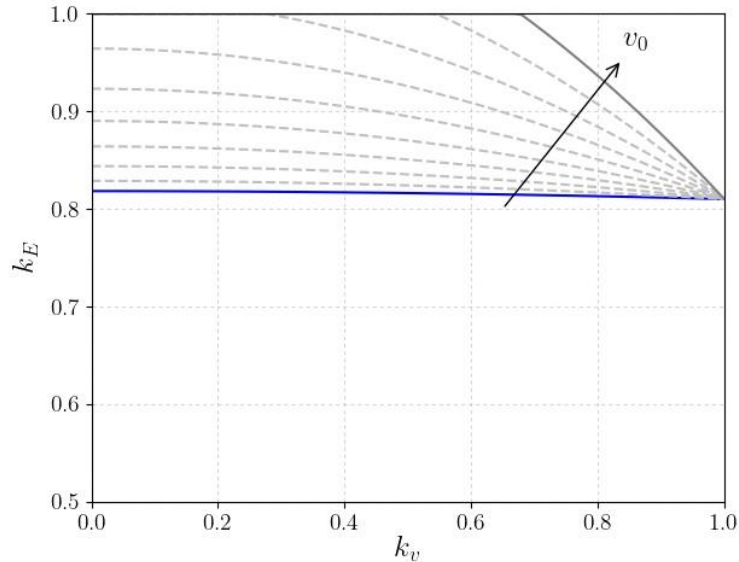


Figure 5.7 Damage parameter k_E as function of k_ν .

The assumption for which k_ν is equal to 1, is thus conservative for the most predominant property in the mechanical behaviour of structures.

Hearmon [86] extended the formula of Eq. (5.1) proposed by Warburton to orthotropic materials as follows:

$$f = \frac{\lambda}{2\pi} \cdot \sqrt{\frac{1}{\rho \cdot h}} \cdot \sqrt{\frac{D_{11}}{a^4} + \frac{D_{22}}{b^4} + \frac{0.605 \cdot H}{a^2 b^2}}, \quad (5.8)$$

where

$$\begin{aligned} D_{11} &= \frac{E_{11} \cdot h^3}{12(1 - \nu_{12} \cdot \nu_{21})} \\ D_{22} &= \frac{E_{22} \cdot h^3}{12(1 - \nu_{12} \cdot \nu_{21})} \\ H &= \nu_{12} \cdot D_{22} + \frac{G_{12} \cdot h^3}{6} \end{aligned} \quad (5.9)$$

With similar considerations to the isotropic case, the following equation can be written as:

$$\frac{D_{11,d}}{a^4} + \frac{D_{22,d}}{b^4} + \frac{0.605 \cdot H_d}{a^2 b^2} = \left(\frac{D_{11,0}}{a^4} + \frac{D_{22,0}}{b^4} + \frac{0.605 \cdot H_0}{a^2 b^2} \right) \left(\frac{f_d}{f_0} \right)^2, \quad (5.10)$$

where subscripts d and 0 refer to the damaged and undamaged properties, respectively.

Among the infinite solutions of Eq. (5.10), it is assumed that:

$$\begin{aligned} D_{11,d} &= D_{11,0} \left(\frac{f_d}{f_0} \right)^2 \\ D_{22,d} &= D_{22,0} \left(\frac{f_d}{f_0} \right)^2 \\ H_d &= H_0 \left(\frac{f_d}{f_0} \right)^2 \end{aligned} \quad (5.11)$$

Again, by expressing the residual elastic properties as function of the undamaged constants through some damage parameters, i.e., $E_{11,d} = k_{E_{11}} \cdot E_{11,0}$, $E_{22,d} = k_{E_{22}} \cdot E_{22,0}$, $G_{12,d} = k_{G_{12}} \cdot G_{12,0}$ and $\nu_{12,d} = k_{\nu_{12}} \cdot \nu_{12,0}$, similar expressions to Eq. (5.7) can be written for each elastic constant:

$$\begin{aligned} k_{E_{11}} &= \frac{1 - k_{\nu_{12}}^2 \cdot \nu_{12} \nu_{21}}{1 - \nu_{12} \nu_{21}} \left(\frac{f_d}{f_0} \right)^2 \\ k_{E_{22}} &= \frac{1 - k_{\nu_{12}}^2 \cdot \nu_{12} \nu_{21}}{1 - \nu_{12} \nu_{21}} \left(\frac{f_d}{f_0} \right)^2 \\ k_{G_{12}} &= \left(\frac{f_d}{f_0} \right)^2 \end{aligned} \quad (5.12)$$

Again, it is conservatively assumed that the damage is totally attributed to the Young moduli and to the shear modulus, while it does not affect the Poisson's coefficient. It should be noticed that in composites the product between the Poisson's coefficients, $\nu_{12}\nu_{21}$, is usually very small. Therefore, the variation of the damage parameters as function of $k_{\nu_{12}}$ approximates the blue curve of Fig. 5.7. The assumption for which the damage is attributed to the elastic moduli is thus suitable for composites. The residual elastic properties are given as:

$$\begin{aligned} E_{11,d} &= E_{11,0} \left(\frac{f_d}{f_0} \right)^2 \\ E_{22,d} &= E_{22,0} \left(\frac{f_d}{f_0} \right)^2 \\ G_{12,d} &= G_{12,0} \left(\frac{f_d}{f_0} \right)^2 \\ \nu_{12,d} &= \nu_{12,0} \end{aligned} \tag{5.13}$$

In regard to the device described in Subsection 5.2.1, when the damage is comprised within the investigated region, the measurement of the first resonant frequency f_d is the result of the contribution of both the damaged zone, i.e., the area where cracks are confined, and the surrounding intact material. Therefore, Eq. (5.13) allows to obtain some equivalent elastic properties which account for both the defective and intact material. For the device, Eq. (5.13) is thus rewritten as:

$$\begin{aligned} E_{11,eq} &= E_{11,0} \left(\frac{f_d}{f_0} \right)^2 \\ E_{22,eq} &= E_{22,0} \left(\frac{f_d}{f_0} \right)^2 \\ G_{12,eq} &= G_{12,0} \left(\frac{f_d}{f_0} \right)^2 \\ \nu_{12,eq} &= \nu_{12,0} \end{aligned} \tag{5.14}$$

In order to establish the residual elastic properties of the damaged zone, it is useful to recall that the reduction of the first resonant frequency depends on the participation of the damage to the modal shape. The higher is the modal displacement in correspondence of the damage, the lower is the resultant resonant frequency. For the first resonance, the higher reduction is obtained when the damage is in the centre of the device. Through the mapping procedure of Fig. 5.6, the minimum value of the frequency is established.

As the reduction depends on the participation of the damage to the modal displacement, each equivalent elastic property of Eq. (5.14) can be seen as the average of the corresponding elastic properties of the damaged and undamaged

material, weighted on the modal displacement. In first instance, the modal displacement w of the first resonant frequency can be approximated as:

$$w = \left(\frac{1}{2} + \frac{x}{a}\right)^2 \cdot \left(\frac{1}{2} - \frac{x}{a}\right)^2 \quad (5.15)$$

where x is the longitudinal direction and a is the longitudinal dimension of the device (here 100 mm). It is worthwhile to note that Eq. (5.15) describes the one-dimensional displacement, even though the investigated region has a bidimensional domain. Fig. 5.8 graphically represents the modal displacement, where the red arrows refer to the damaged zone, while the black arrows to the intact material.

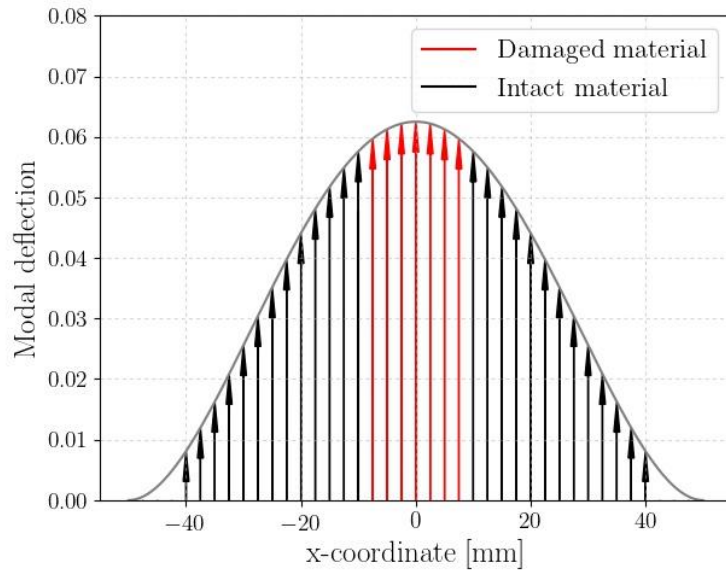


Figure 5.8 Modal contribution of the damaged and intact zones.

By referring to the longitudinal direction, the average Young modulus weighted on the modal displacement can be expressed as:

$$E_{11,d} \left(\int_{-\frac{x_D}{2}}^{\frac{x_D}{2}} w dx \right) + E_{11,0} \left(\int_{-\frac{a}{2}}^{\frac{a}{2}} w dx - \int_{-\frac{x_D}{2}}^{\frac{x_D}{2}} w dx \right) = E_{11,eq} \left(\int_{-\frac{a}{2}}^{\frac{a}{2}} w dx \right) \quad (5.16)$$

where $E_{11,d}$ is the longitudinal Young modulus of the damaged zone. Eq. (5.16) thus assumes a constant value for the residual elastic properties of the defective area. From Eq. (5.16), the longitudinal Young modulus of the damaged zone can be calculated as:

$$E_{11,d} = E_{11,0} - (E_{11,0} - E_{11,eq}) \left(\frac{\int_{-\frac{a}{2}}^{\frac{a}{2}} w dx}{\int_{-\frac{x_D}{2}}^{\frac{x_D}{2}} w dx} \right) \quad (5.17)$$

or, by considering Eq. (5.14)

$$E_{11,d} = E_{11,0} \left[1 - \left(1 - \left(\frac{f_d}{f_0} \right)^2 \right) \left(\frac{\int_{-\frac{a}{2}}^{\frac{a}{2}} w dx}{\int_{-\frac{x_D}{2}}^{\frac{x_D}{2}} w dx} \right) \right] \quad (5.18)$$

It is worthwhile to note that the ratio between the integrals of the displacement w over the entire domain and over the damaged zone is only a function of the extension of the device (a) and of the extension of the damaged area (x_D). Fig. 5.9 reports the variation of the integral ratio, according to the damage and device extensions.

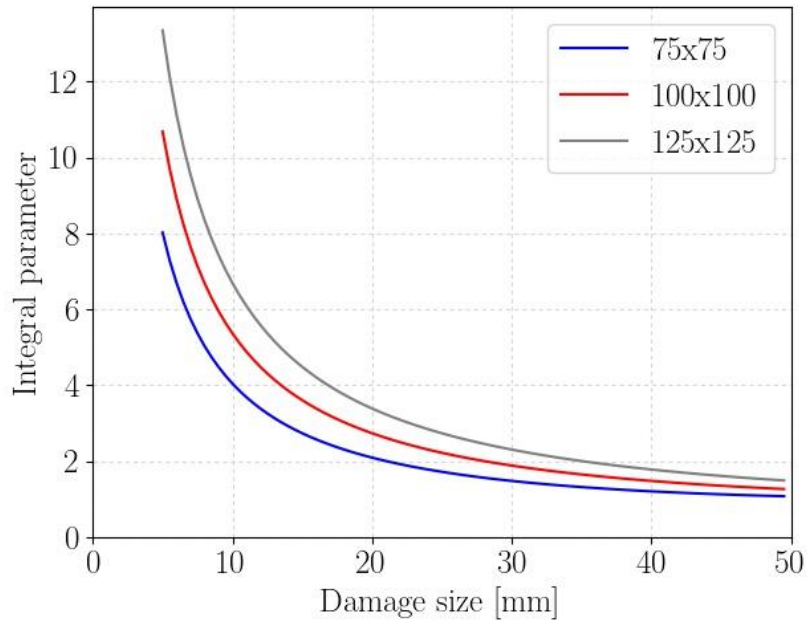


Figure 5.9 Integral parameter as function of the device domain and defect size.

Eq. (5.18) thus permits to assess the residual elastic properties of the damaged zone, once its extension is known. In order to validate Eq. (5.18), tensile tests are performed on specimens cut from the impacted plates around the damaged area. Fig. 5.10 shows the tensile test setup.



Figure 5.10 Tensile test of specimens equipped with optic fibre.

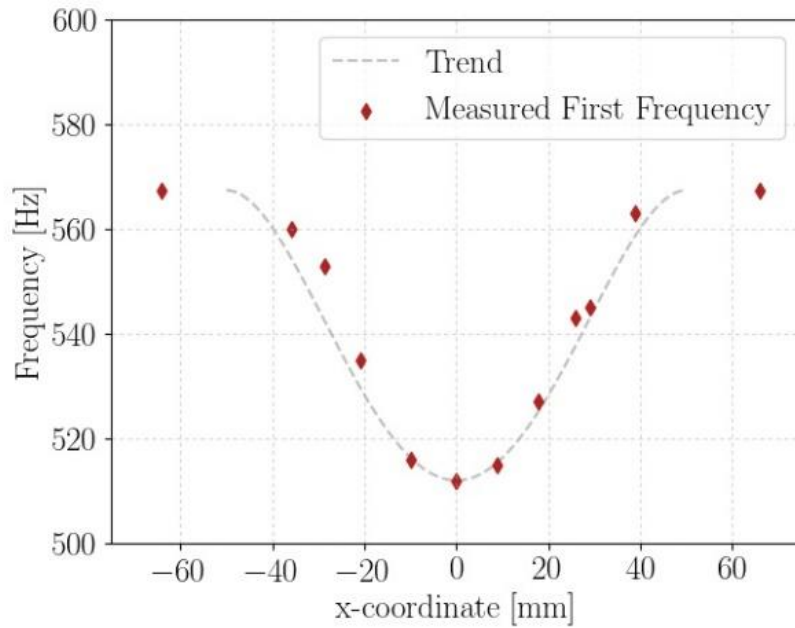
Specimens are equipped with optic fibre in order to obtain a punctual measure of the strain. The optic fibre is managed through the LUNA control system and its strain gauge is set to 0.65 mm. The tensile tests are performed on a servohydraulic machine (Instron 8801) equipped with a cell load of 100 kN. Tests are performed in the elastic regime. Therefore, from the measurement of the applied load and of the induced deformation, the longitudinal Young modulus is punctually assessed.

5.3 Results

As Eq. (5.14) requires the first resonant frequency of the undamaged material condition f_0 , a mapping procedure was performed before impacting the plate. In particular, the frequency was measured at nine different locations on the plate. The mean value was then assumed for f_0 , which is 567.4 Hz and 594.3 Hz for the 6- and 8-layers plates, respectively.

The first resonant frequency is mapped according to the procedure described in Subsection 5.2.2. Measurements are taken by moving the device in the x direction, with steps of about 10 mm. Fig. 5.11a and 5.11b report the variation of

the first resonance for the 6-layers plate and for the 8-layers plate, respectively. The measured frequencies are plotted according to the position of the central crack of the damaged area with respect to the centre of the device.



(a)

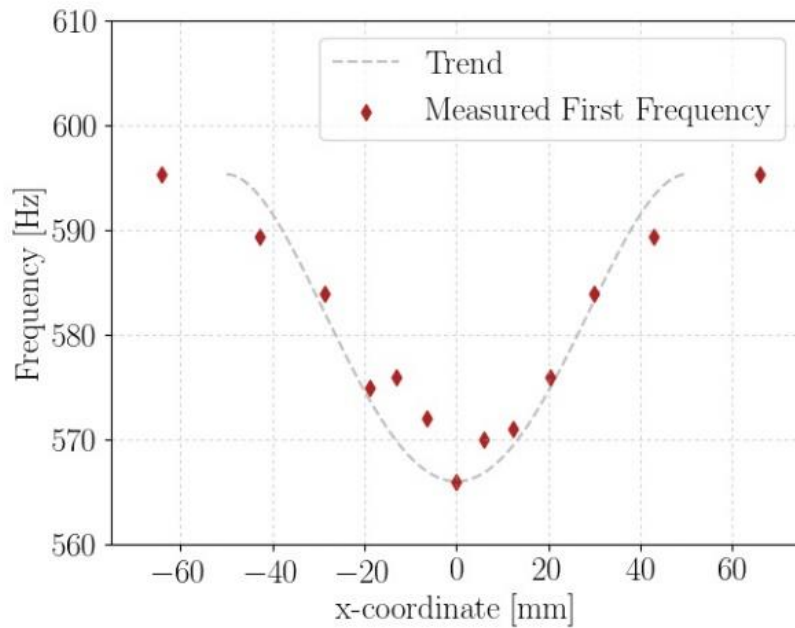


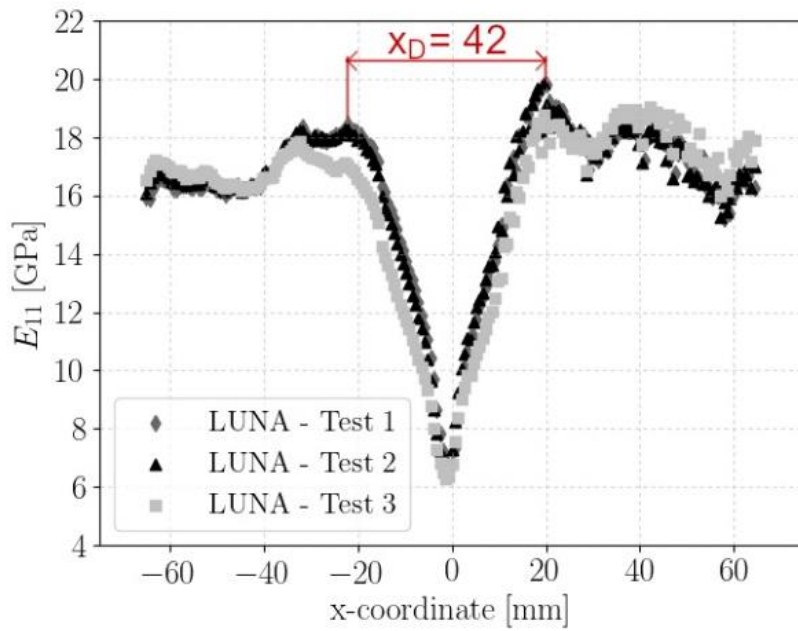
Figure 5.11 Frequency trend as function of the damage position with respect to the device: (a) 6-layers plate; (b) 8-layers plate.

As shown in Fig. 5.11, the first resonant frequency changes in accordance with the position of the damaged zone with respect to the device boundaries. When the impacted area is external to the system boundaries, no changes occur in the first resonant frequency. By moving the device with respect to the plate, the damage enters the inspected region. At this point the frequency starts decreasing and by further moving the device, the minimum value is reached when the

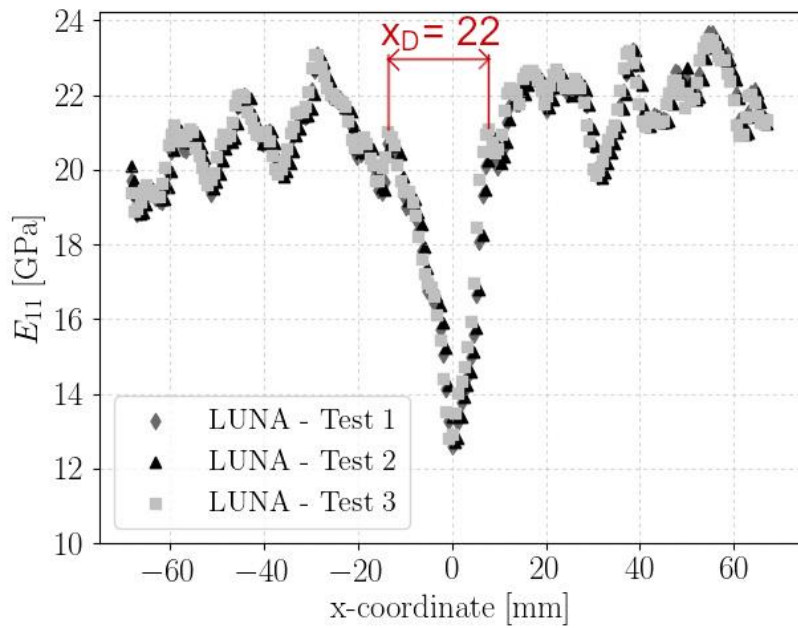
damaged zone is exactly in the centre. The minimum values are 512 Hz for the 6-layers plate and 566 Hz for the 8-layers plate. The reduction of the first resonant frequency is well interpolated through the modal displacement equation (Eq. (5.15)), as shown with trendline in the figures. This confirms that the participation of the damage to the first mode displacement governs the reduction of the first resonant frequency, as observed with the finite element analysis of Fig. 5.5. Therefore, when the damaged zone is in correspondence of the boundaries, where the displacement is null, no reduction occurs in the first frequency. When the damage is in the centre of the inspected region, its participation to the modal displacement is maximum and so the first resonant frequency falls to the minimum value.

It is also worth noticing that for fully clamped boundaries, the expected first resonant frequency of the 8-layers plate is equal to 665 Hz, as shown with a modal analysis in Subsection 5.2.2. The lower value of the mean frequency f_0 is due to the limited stiffness of the seals of the clamping system. This can be also shown through the parameter λ , which is equal to 1 for simply supported boundaries and to 4.73^2 for clamped conditions. For the 6-layers plate, λ is equal to 4.44^2 , while for the 8-layers it is equal to 4.39^2 . For both the plates the parameter λ is slightly lower than the value reported by Hearmon for fully clamped boundaries [87]. The difference between the λ s of the two plates might be interpreted as a material dependency of the clamping system effectiveness. Indeed, vibrations of a lower material stiffness are more easily limited. However, it should be noticed that for the correct calculation of the λ parameter, flexural elastic properties should be considered. In composites, flexural properties can be significantly different from those assessed through standard tensile tests [88]. This might also justify the limited difference between the λ s of the two plates. Further, it is worth reminding that flexural response of a composite-based component is significantly affected by the material quality, such as resin rich areas, fibre alignment and thickness variations. Although the nonperfect clamping system, results of Fig. 5.11 show that the vibrational response is only related to the inspected region. Indeed, when the damage is not comprised within the device, the first resonant frequency returns to the undamaged value.

Tensile tests are performed on specimens cut from the impacted plates around the damaged area. Fig. 5.12a and 5.12b report the variation of the longitudinal Young modulus E_{11} along the specimen axis for the 6- and 8-layers composites, respectively.



(a)



(b)

Figure 5.12 Young's modulus variation along the specimen axis as measured through the fibre optic: (a) 6-layers composite; (b) 8-layers composite.

Repeatability of results is confirmed through three test repetitions. Both in the 6- and 8-layer plates, in correspondence of the damaged area, the Young modulus progressively decreases to a minimum value. The size of the damaged zone is accordingly identified from the variation of the Young modulus, as shown in Fig. 5.10. As expected, the size of the damage in the 6-layers is larger than that in the 8-layers, as the impact energy was the same for both the plates.

Table 5.2 reports a comparison of the results obtained with the optic fibre system and with the local vibrational analysis for the 6- and 8-layers composites.

Material	Method	E_{eq} [GPa]	E_d [GPa]
6-layers	Optic Fibre	15.0	12.5
	Local Vibrational analysis	13.7	12.4
8-layers	Optic Fibre	20.2	16.6
	Local Vibrational analysis	19.3	16.4

Table 5.2 Comparison of the residual elastic properties for the 6- and 8-layers plate.

In order to consistently compare the results, as Eq. (5.18) assumes a constant value for the residual elastic properties of the damaged area, a mean value for the damaged zone is also calculated from the tensile test results. The discrepancy between the residual Young moduli E_d is equal to 1% for both the plates, thus validating Eq. (5.18).

Table 5.3 also reports a comparison between the equivalent Young moduli E_{eq} , as defined in Eq. (5.14). For the optic fibre, its value has been calculated by considering in series stiffnesses. In particular, the range between -50 mm and 50 mm is considered. The discrepancy is mainly due to the oscillations of the Young modulus along the specimen axis, as shown in Fig. 5.12, which in turn affect the calculation of the E_{eq} from the tensile test. These oscillations are due to local material variations as well as thickness variations. Further, it is worth to recall that Eq. (5.14) conservatively attributes the damage to the Young and shear moduli.

The accuracy of the determined Young modulus of the damaged region, i.e., E_d , can be also proved by comparing the equivalent Young modulus E_{eq} as calculated from Eq. (5.16) and from Eq. (5.14) for the different locations of the damage with respect to the device. Indeed, the equivalent Young modulus E_{eq} is the Young modulus of the whole inspected region for a given position of the damage. Eq. (5.14) assess the equivalent Young modulus from the square ratio of the frequencies, i.e., $\left(\frac{f_d}{f_0}\right)^2$. Instead, Eq. (5.16) calculates E_{eq} from the residual Young moduli E_d , reported in Table 5.2. Table 5.3 reports the relative errors between the equivalent Young moduli calculated through Eq. (5.16) and Eq. (5.14) for the 6- and 8-layer plates for the first four locations of the damage (Fig. 5.11).

	x -coordinate [mm]	E_{eq} [GPa] – Eq. (5.16)	E_{eq} [GPa] – Eq. (5.14)	ε_{rel} [%]
6-layers	-35.8	15.7	16.3	3.7%
	-29.0	15.2	15.9	4.3%
	-21.1	14.6	14.9	2.2%
	-9.8	13.9	13.9	0.1%
	-42.8	21.0	20.9	0.4%
8-layers	-28.8	20.4	20.5	0.8%
	-18.8	19.8	19.9	0.5%
	-13.1	19.6	20.0	2.1%
	-6.5	19.2	19.7	2.4%

Table 5.3 Comparison of the equivalent Young moduli for the 6- and 8-layer plates.

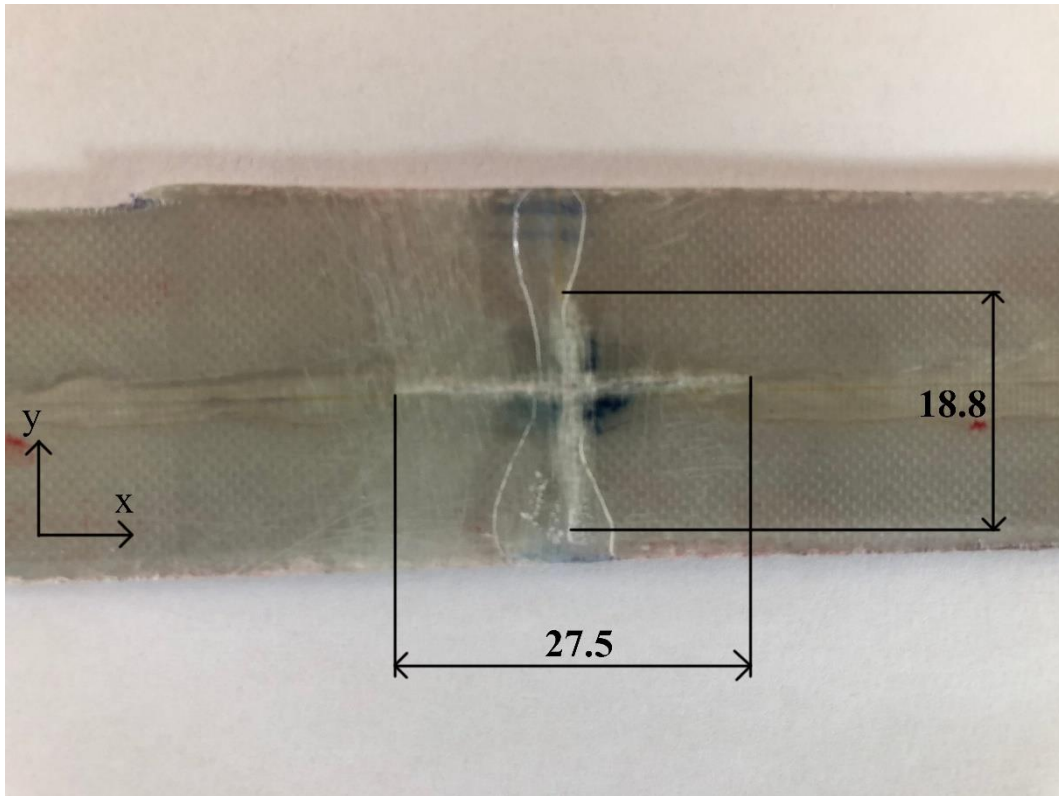
The relative error is very small in each location for both plates, thus validating the assessed residual Young moduli for the damaged area E_d and therefore the use of Eq. (5.18). Graphically, the relative error can be seen as the distance between the measured resonant frequencies and the trend line in Fig. 5.11.

For the 6-layers plate, major errors are obtained in proximity of the extremities of the device. Here the effect of the nonperfect boundaries can influence the measurement of the first resonant frequency. Further, in Eq. (5.18) the modal displacement is approximated (see Eq. (5.15)). In proximity of the boundaries, the accuracy of the mode shape function is coarse. For the 8-layers plate, major errors are instead obtained in proximity of the centre. This seems mainly due to measurement scatter, as shown in Fig. 5.11b.

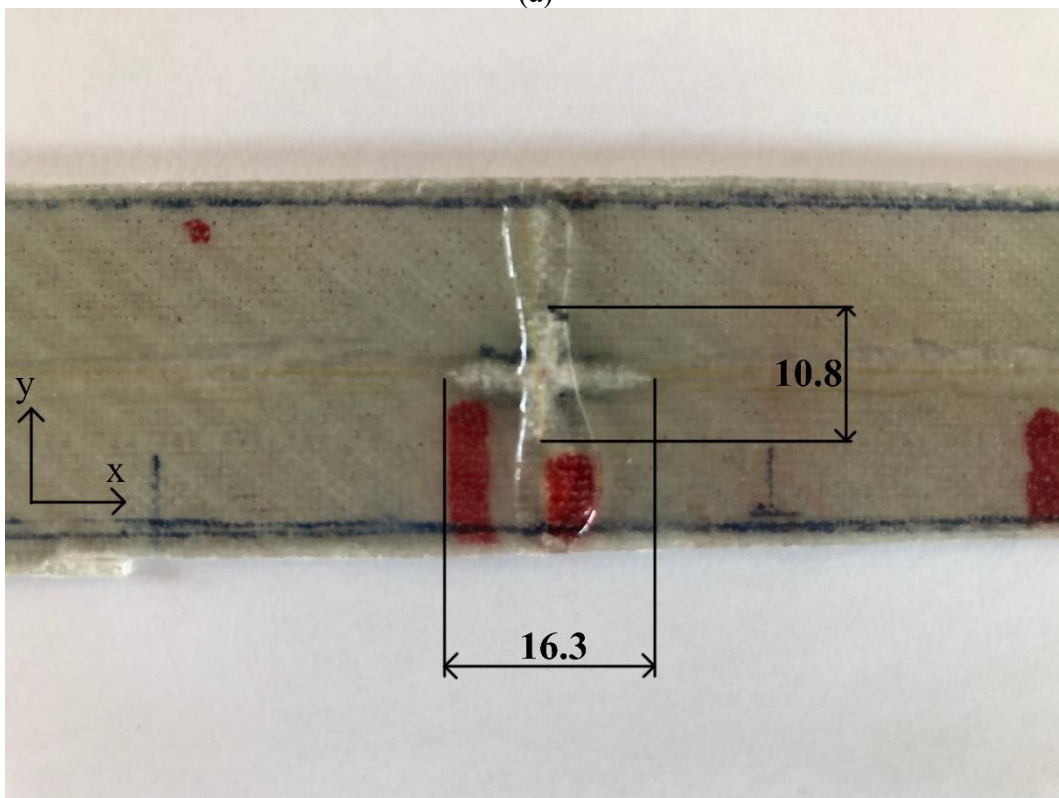
5.4 Discussion on the damage size

In the current analysis, the damage extension was set equal to that estimated by the fibre optic measurements. However, as discussed, its estimation can be theoretically determined through the vibration technique and represents a possible future development. Indeed, when the damage firstly enters in the region inspected by the device, a first reduction of the first resonant frequency occurs. Instead, when the damage finally exits from the investigated region, the first resonant frequency returns to its original value. The limited effect of the damage in proximity of the boundaries combined with the inevitable measurement scatter however challenges such approach.

In addition, as the plates are made of glass fibre, a comparison between the damage extension as estimated by the optic fibre and that measured by simple visual inspection is allowed. In particular, from the visual inspection, it is observed that two main cracks developed from the impact and were perpendicular to each other. Fig. 5.13 shows a magnification of the cracked area in the two plates.



(a)



(b)

Figure 5.13 Dimensions in mm of the main cracks in (a) 6-layers plate and (b) 8-layers plate.

The crossed cracks have dimensions of 27.5x18.8 mm and 16.3x10.8 mm for the 6-layers and the 8-layers plates, respectively, as shown in the figure. In both

plates, the longest crack developed along the first principal direction of the material, i.e., the longitudinal x -direction, while the shortest crack was perpendicular to it.

In the optic fibre tests, the fibre punctually measured the strains in the longitudinal direction of the material. In Fig. 5.12, the graphical representation of residual elastic properties with respect to the longitudinal x -direction has shown that the size of the damaged region is equal to 42 mm and to 22 mm for the 6-layers and for the 8-layers plate, respectively. These results are not in accordance with those estimated by simple visual inspection and deserve further investigations.

In both cases, the size estimated by the optic fibre is bigger than that visually observed. For example, the 42 mm size measured for the 6-layers plate by the optic fibre is much higher than the 27.5 mm observed in the same direction by visual inspection.

This difference can be explained by the fact that the visual inspection is limited to the cracked area. However, other damage mechanisms can occur, such as some local plasticization of the matrix, which in turn cannot be assessed by simple visual inspection.

In addition, it is worth noticing that the size estimated by the optic fibre is also, if not mainly, related to the crack transverse to the applied tensile load, i.e., the 18.8 mm crack and the 10.8 mm crack for the 6-layers and 8-layers plate, respectively. The size of the damaged area, estimated by the optic fibre, thus corresponds to the portion of material affected by the presence of the transverse crack, i.e., the portion of material which is unloaded because of the presence of the transverse crack. Indeed, the presence of a damage region affects the material response not only in correspondence of the damaged area, but also in the neighbouring part. According to the well-known Westergaard equations (which were developed for isotropic materials), the portion of material unloaded because of the presence of a transverse crack extends infinitely from the crack. From the optic fibre measurements, it seems that this region is instead confined. However, such conclusion needs further investigations, for example by realizing laminates with defects of known dimension and assessing the material response in presence of such defects.

Generally speaking, the definition of the damaged area is crucial for the proposed technique, as the material response in presence of damage, i.e., the goal of the proposed the technique, also depends on its extension. It is worth noticing that, if the size of the material influenced by the presence of the damage is assumed equal to the extension of the damage, as determined by visual inspection or other more sophisticated technique, the residual material response, i.e., the residual elastic properties, would result lower. For example, in the case of the layers plate, if the damage is assumed equal to 27.5 mm, i.e., the extension of the crack in the longitudinal direction, the resulting residual Young modulus would be equal to 10.5 GPa.

In conclusion, a severe distinction is observed between the size of the damaged area, i.e., that determined by visual inspection, and the portion of material, whose response is affected by the damage, which we can briefly call as “damage influence size”. Future activity will be indeed focused on addressing this topic. The definition of a “damage influence size” needs particular attention.

5.5 Conclusions and possible limitations

In this chapter, an innovative methodology for the local and nondestructive assessment of the residual elastic properties in damaged composites has been presented. The methodology is based on the Impulse Excitation Technique (IET). An innovative experimental setup has been proposed which allows to isolate the vibrational response of a region of the material by clamping its extremities. In addition to the setup presented in Ch. 3, as in real-world components it is rather unlikely that both surfaces are accessible for clamping, a proper device has been designed which is able to clamp the boundaries of the investigated region from only one side. The nondestructive inspections are restricted to the exposed surface, thus extending the approach proposed in Ch. 3.

The device, which is here 3D printed and made of polyethylene terephthalate (PET), adopts the vacuum technique. The inspected region is framed by a vacuum chamber whose air is aspirated through a vacuum pump. The frame chamber is delimited by internal and external rubber seals, which prevent any air escape.

The assessment of the residual elastic properties is nondestructive and local, i.e., it specifically concerns the damaged zone. The presence of a damage within the region inspected through the device results in a reduction of the first resonant frequency. Such reduction is function of the participation of the damage to the modal displacement. The higher the modal displacement in correspondence of the damaged zone, the higher the reduction of the first resonant frequency.

The first resonant frequency is mapped in order to identify the position of the damage and to measure the minimum value of the first resonant frequency. As the square of the frequency is proportional to the stiffness, an equivalent set of elastic properties can be calculated for the investigated region from the ratio between the minimum frequency and its value for intact material. Once the extension of the damaged zone is known, the residual elastic properties can be determined by accounting for the participation of the damage to the mode shape. An analytical formula for the residual elastic properties of the damaged area has been proposed. It is worthwhile to notice that, as the damage is equivalently attributed to all the plies of the laminate, the technique is suitable also for composites made of laminae of different materials. Nevertheless, the combination of the presented method with other nondestructive techniques might increase the accuracy in damage assessment, thus particularly identifying through-the-thickness damage location.

Validation has been performed on two glass fibre woven fabric laminates. Firstly, the two plates have been impacted at the energy of 1.8 J. Thereafter, the

first resonant frequency has been mapped according to the prescribed procedure, in order to calculate the residual elastic properties of the damaged zone.

In order to prove the effectiveness of the methodology, tensile tests have been performed on specimens cut from the impacted plates around the damaged area. Specimens have been cut along the longitudinal material direction and equipped with optic fibre managed through LUNA control system. The optic fibre permits to obtain punctual measure of the strain and hence of the longitudinal Young modulus.

Results show that the proposed formula is able to assess the damage severity, as the discrepancy between the Young modulus determined through the proposed technique and that calculated from fibre optic measurements is smaller than 1% for both plates. Thanks to the proposed technique, the health state of damaged components can be quantitatively assessed and decisions on maintenance can be made with enhanced confidence, once limits on the acceptable damage level are defined.

The encouraging results of this preliminary testing campaign demand for further investigations. Firstly, the proposed analytical formula for the nondestructive assessment of the damage severity has been here validated only for the longitudinal Young modulus. It is necessary to prove its effectiveness also for the other elastic properties, in particular for the shear modulus, whose effect on the first resonant frequency is limited, as also discussed in Ch. 4.

In regard to the analytical formulation here derived, it is worthwhile noticing that the expression of the first resonant frequency is valid only for orthotropic materials [86]. In particular, it is necessary that the isolines of the mode shape are parallel to boundaries of the inspected region [89]. Therefore, the proposed technique still needs to be validated on anisotropic materials. In this regard, finite element analyses can be performed to firstly investigate its accuracy. In particular, it is necessary to verify that, in presence of a damage, equivalent material properties at lamina level are proportional to the intact values through the squared ratio of the frequencies, as proposed in Eq. (5.14). Preliminary analyses have been performed on the symmetric laminate considered in Ch. 4, which is made of unidirectional plies stacked as $[30^\circ, -30^\circ, -30^\circ, 30^\circ]$. This is an anisotropic material whose isolines are not parallel to the boundaries of the domain. The first resonant frequency for clamped boundaries of size $a = 100$ mm is equal to 914 Hz. A local material variation is then considered as also described in Subsection 5.2.2 and shown in Fig. 5.5b, i.e., with the damaged region in the centre. A 50% reduction of all the elastic constants is assumed specifically for the region of dimensions 20×20 . The resulting first resonant frequency decreases to 898.3 Hz. A modal analysis is finally performed with the equivalent elastic properties determined through Eq. (5.14) for each lamina. The resulting resonant frequency is 898.3 Hz, which preliminary confirms the accuracy of Eq. (5.14).

In addition, the effect of the dimensions of the device on the assessed residual elastic properties needs to be determined. As the size increases, the existence of the damage is increasingly concealed by the surrounding intact material, as also

discussed in Subsection 3.6.3. In this regard, Hatiegan et al. [90] have shown that in clamped rectangular plates, the reduction of the first resonant frequency due to the presence of a damage can be very limited when the size of the plate is large with respect to the damage extension. However, it should be noticed that as the dimensions of the device decrease, the noninfinite stiffness of the boundaries increasingly affects the result. For very small sizes, the insulation of the inspected region might be challenged.

In this regard, it is worth to note that results discussed in this chapter concern two thin glass fibre laminates. The limited stiffness of the retained materials might play an important role in the correct functioning of the device, as it permits to isolate more easily the vibrational response of the inspected region. Further investigations are thus required for highly stiff materials. The thickness of the laminate might also play a key role in this regard.

Finally, it is worthwhile noticing that the proposed methodology, as well as that introduced in Ch. 3, is currently limited to planar regions of the component. Its extension to more complex shape typical of real-world structures needs to be addressed.

VI

Conclusions

In this chapter, a discussion of the damage tolerance approaches currently adopted is firstly addressed in comparison with the approach proposed in this dissertation. Then, a summary of the findings is given. Finally, an outlook on the possible implications and development is presented.

6.1 Damage tolerance approaches

The understanding of damage in composites is still far from being fulfilled. Damage tolerance and criteria for design in presence of damage are among the most important challenges for the widespread diffusion of composites in structural applications.

Damage tolerance criteria have been proposed for composites, pursuing the approach adopted for metals. For metals, damage tolerance was established in terms of sufficient strength in presence of cracks. In particular, this strength, also known as residual strength, was function of the most critical crack. Similarly, the assessment of a residual strength was proposed for composite materials.

With particular reference to the impact damage, which is usually characterized by a large collection of cracks as it involves multiple failure mechanisms in the composite, Cantwell and Morton [36] have firstly studied the residual tensile strength of impacted specimens. They modelled the region of fibre fracture as a sharp crack with equivalent transverse dimensions and analysed the residual tensile strength of damaged carbon fibre laminates. A notch insensitive behaviour was observed for the $[\pm 45^\circ]_s$ laminates, while a notch sensitive behaviour was observed in the $[0^\circ, \pm 45^\circ]_s$ laminates. The proposed model based on equivalent transverse crack permitted to determine a lower bound on the residual strength.

However, the use of tensile test to assess the damage tolerance is not suitable as a metric of the damage tolerance. Indeed, as shown by Abrate [91], the presence of delamination cracks, which is typical of impact damage, does not

significantly affect the tensile strength. Therefore, the tensile residual strength cannot be assumed as a critical indicator of the consequence of impact damage.

Compression test was thus proposed as an alternative, leading to the commonly used Compression After Impact (CAI) testing. CAI as a measure of the damage tolerance is still debated in the scientific community. When global buckling instability is prevented, the CAI failure process is governed by local buckling failures, which occur in the delaminated plies, and by the crack growth resistance at the lamina/lamina interfaces. Indeed, under compression, the delaminated plies tend to buckle out. The buckling instability is likely to occur if the delaminated ply has a free surface on one side, while is restrained by the other laminae, when the ply is internal to the laminate. The buckling of the ply then results in a further delamination. The CAI failure is thus governed by the interplays of the structural instabilities and material toughness which depend on the position and extent of the interlaminar cracks. Results of CAI tests thus depend on the testing conditions, which limits the interpretation of the measured ultimate load carrying capacity.

In aerospace industry, indentation depth is currently adopted to establish the damage severity in barely visible impact damage [7]. In particular, it is claimed that the indentation depth is the entire result of ply cracks and delaminations produced by lateral impact, which is not straightforward. Even though correlations between the residual strength and dent depth are known in the literature (e.g. [92,93]), the dent depth as indicator of damage is uncertain.

Generally speaking, in composite materials it is well-known that the definition of strength cannot be done by simply identifying a unique level stress which causes failure. Composites are inherently anisotropic and heterogeneous materials and so the strength is also anisotropic and spatially nonuniform. In addition, due to their nature, even the stress applied in one direction at the global level results in a complex stress state at the local level internal to the material. As discussed in Ch. 1, the large variety of failure mechanisms cannot be accounted through a single parameter of strength. With analogous considerations, we can conclude that the assessment of a residual strength is not suitable to fully characterize the damage severity.

Furthermore, it must be accounted that the damage state is usually represented by a multitude of cracks and its evolution depends on the mutual interactions of these cracks. Given the complex crack scenario of composites, it is not a priori known which failure mechanism will dominate. In presence of damage, the mode of failure depends not only on the internal stress state and on the material state, in accordance with their evolution in time as function of applied environments such as temperature, chemical agents etc. [94], but also on the interaction between cracks, in accordance with the operating conditions. The prediction of the failure mechanism thus depends on boundary conditions, whose complete description is unfeasible to address. The nondestructive inspection of the damage state in terms of location, typology and extension is thus not sufficient as indicator of the damage severity.

In this dissertation, a metric based on the residual elastic properties has been adopted to evaluate the damage severity. At nanoscale level, material properties are the result of the interaction between atoms. The elastic properties, i.e., the Young moduli and the Poisson's ratio, are the result of the repulsive and attractive forces interchanged between atoms. The presence of defects, such as cracks, voids etc., locally affect atomic interactions and, at the macroscopic material level, can be highlighted as local variation of the elastic properties. Reduction of local elastic properties can be thus adopted as metric of the damage severity. Such metric is only function of the actual multiple crack scenario, while it is not influenced by the dimensions of the damaged zone or by boundaries conditions, such as supports and attachments.

6.2 Summary of findings

In this dissertation, an innovative experimental methodology has been proposed and validated for the local and nondestructive assessment of the elastic properties in composite material components. Starting from the Detecting Damage Index (DI_d) technique, which was previously introduced in the realm of the nondestructive techniques and whose accuracy was demonstrated also in combination with the finite element method, the methodology aims at overcoming the main disadvantages of the DI_d , while benefiting of the main findings.

In particular, the methodology intends to isolate the vibrational response of a region of the component by clamping its extremities. The resulting mechanical vibrations induced by impulse are thus function of only the elastic characteristics of the inspected region. In particular, the first resonant frequency is measured by adopting the Impulse Excitation Technique which is usually predominant and more easily recognizable.

Firstly, the assessment of the local elastic properties in undamaged composite laminates has been addressed by designing a preliminary clamping system which consisted of two rectangular frames disposed above and below the plate and compressed through a testing machine equipped with compression blocks. A unidirectional carbon fibre laminate was considered for validation. In order to take into account the material anisotropy, values of the first resonant frequency were measured after rotating the clamping system with respect to the composite plate. For the orientations of 0° , 30° , 60° and 90° , the resulting resonant frequencies were 247 Hz, 253 Hz, 341 Hz and 410 Hz, respectively. The material constants were finally obtained from the measured frequencies through an optimization problem based on Finite Element (FE) analysis.

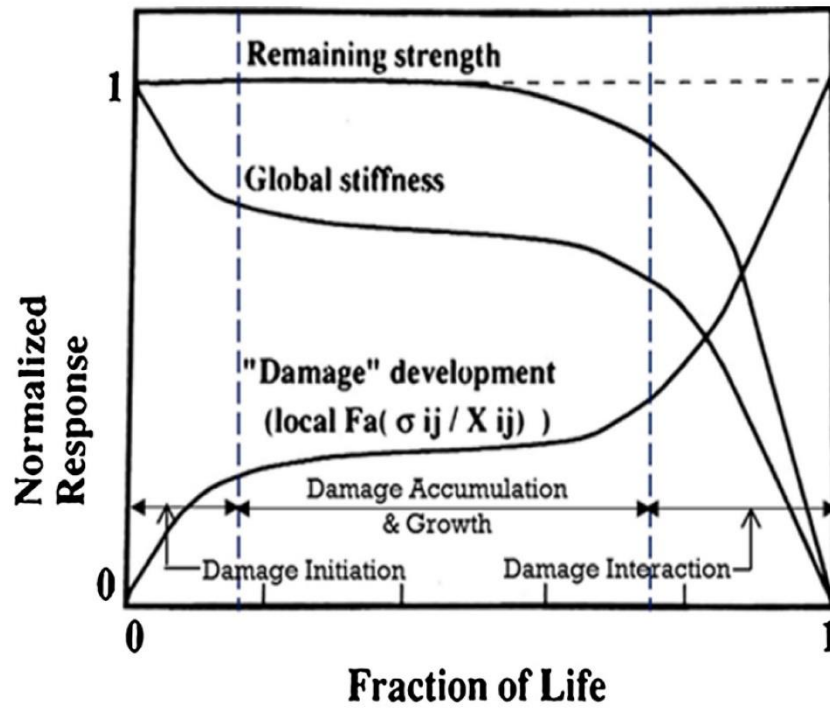
In order to increase the robustness of the inverse problem, which determines the elastic properties from the measured resonant frequencies, information related to the modal shape was then retained. In particular, the effect of an additional concentrated mass on the first resonant frequency was exploited. According to the location of the concentrated mass, the higher the modal displacement in correspondence of the mass position, the lower is the resultant resonant frequency.

Only two mass positions, i.e., two measures of the first resonant frequency, were necessary to investigate the modal shape. A Rayleigh-Ritz formulation based on higher order shear deformation theory was also implemented, which permitted to consistently decrease the computational effort with respect to the FE-based optimization. The numerical calculations show that even the shear modulus and the Poisson's ratio, whose influence on the first resonant frequency is limited, can be accurately predicted when the information related to the modal shape is retained. Instead, when the information related to the modal shape is not accounted, consistent discrepancies can be obtained, up to the values of 12% for the shear modulus and 76% for the Poisson's ratio for the considered materials.

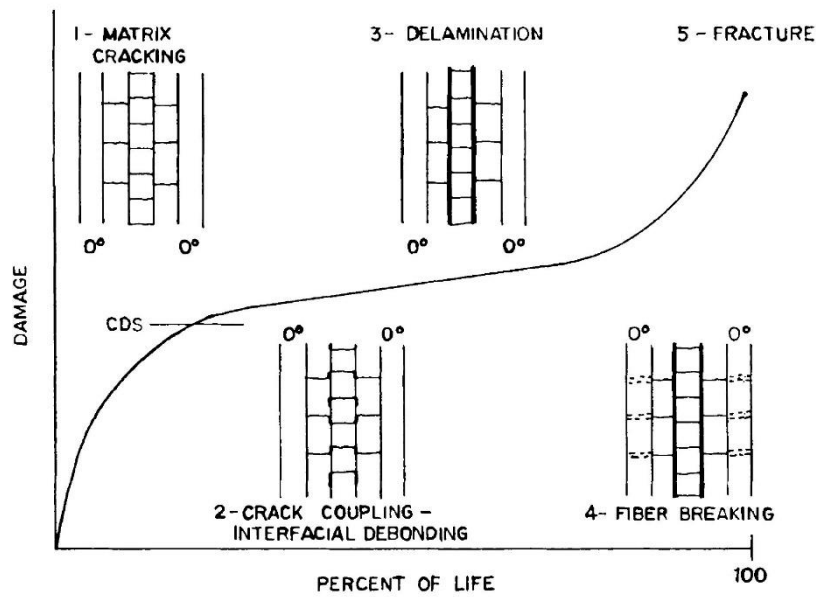
Finally, the assessment of the residual elastic properties in damaged composites has been addressed. As in nondestructive inspections, any observations or measurements are restricted to the exposed surface, an innovative clamping system was designed. The system exploited the vacuum technique in order to clamp the boundaries of the inspected region and isolate the vibrational response. Residual elastic properties of impacted glass fibre laminates were assessed for the damaged area through a new analytical approach. A formula for the residual elastic properties was derived and validated. In particular, the determined material constants were compared to the results of tensile tests performed on specimens cut from the impacted plates. The excellent agreement, with discrepancies between the proposed approach and the fibre optic measurements lower than 1%, proved the effectiveness of the technique. It is also worth noticing that the proposed technique is characterized by easiness of testing and low-cost testing setups, especially if compared to other nondestructive methods. Furthermore, it should be noted that the presented technique investigates the material health state through the first flexural resonant frequency. The use of flexural modes is particularly suitable for composites, as the presence of cracks between plies, i.e., delamination, also affects the vibrational response of these modes [95]. On the contrary, the use of in-plane loading conditions, such as thermal loads adopted in shearography techniques, might conceal the presence of delaminated areas [96].

6.3 Outlook

Damage tolerance is the remaining strength after some period of service, while prognosis concerns the durability of the structure. In order to characterize and monitor the rate of strength change in composites, stiffness degradation is sometimes adopted to that purpose. Fig. 6.1a, taken from [46], shows the evolution of strength and stiffness in unidirectional composites during fatigue. Such trends are also typical of cross-ply laminates subjected to static tensile load [97]. Fig. 6.1b, taken from [97], shows the corresponding failure modes.



(a)



(b)

Figure 6.1 Damage evolution in cross-ply laminates: (a) strength and stiffness degradation [46]; (b) corresponding failure modes [97].

The strength remains almost constant until the end, whereas the stiffness shows an initial drop caused by the primary matrix cracking, i.e., the matrix cracks in plies perpendicular to the applied load. Subsequently, interlaminar cracks are generated, which still do not affect the global strength of the composite. Finally, these secondary cracks interact with those developed in the initial phase, leading to the sudden drop in the strength and to the final failure. By monitoring the stiffness reduction, it is possible to assess the damage tolerance, i.e., the residual strength, and the remaining life of the component. However, such

approach is not generally appropriate and requires additional information when other loading conditions or environments, such as creep, are applied [98].

The general definition of a prognosis law and of design criteria for damage tolerance for composites mainly depends on the physical description of the failure mechanisms, which particularly demands for a fracture mechanics methodology. As failure mechanisms initiate at the microscale (fibre failure, matrix cracking, fibre-matrix debonding etc.) and local stress fields evolve with the progression of the damage, multiscale approaches are necessary, where the failure process is defined firstly at the microstructural level and conditions of failure are subsequently passed to the macroscales (from lamina to laminate level, from laminate to global component level etc.) [15].

Even though the physical modelling of failure in composites has still challenges to address, the current capability of assessing local material degradation allows to outline a roadmap to a prognosis law and to design criteria for damage tolerance. Such roadmap firstly requires the characterization of the microstructure of the composite as it results from the manufacturing process or from the application of the in-service loading history. This step can be pursued with the presented technique in combination with other nondestructive inspection approaches. The goal is to calibrate a model (analytical or numerical) of the inspected region, which will include the appropriate manufacturing defects/in-service damage and will account for changes of the deformational response in accordance with the assessed degradation of the elastic properties. Also, as defects can be concentrated within only some plies, or damage severity can be nonuniformly distributed within the laminate, the combination of the present technique with other nondestructive techniques, able to determine the extension of the damaged area and to attribute damage extension to each specific lamina, would allow a more accurate description of the material state. For example, the combination of the present technique with a micro-computed tomography might allow the proper assessment of the residual elastic properties at the lamina level.

Finally, according to applied stress state, the failure analysis will define the conditions, i.e., the criteria, for each failure mode. The failure conditions at the lamina level can be then adopted in the failure analysis at the laminate level, in order to establish the final failure of the component.

The multiscale description of failure in composites thus lies on a proper fracture mechanics methodology. In this regard, several authors have proposed phenomenological models to describe the stiffness reduction in composite laminates while damage proceeds. As an example, matrix cracking typically affects off-axis plies in initial phases of load application. Although this subcritical damage does not cause ultimate failure, matrix cracking leads to loss of load-bearing capacity and causes nucleation of more severe damage mechanisms, such as delamination and fibre cracking [99]. Therefore, great effort has been pursued in the literature for the correct modelling of such damage mechanism. This, in combination with a proper nondestructive technique, would lead to safer and more cost-effective designs. Numerical models are thus focused on the stiffness

reduction due to transverse cracks, i.e., matrix cracks in the off-axis plies. Highsmith and Reifsnider [100] measured the crack density in cross-ply laminates under tensile load and proposed to account for stiffness reduction by discounting in the calculation of the laminate stiffness the ply where matrix cracks have saturated. Thereafter, Talreja [97,101] modelled the degradation of the elastic properties in cross-ply laminates subjected to tensile load, from crack initiation to crack saturation. A damage variable was introduced to define the variation of the elastic parameters as function of the crack density. The author showed a good agreement of the model with the experimental results reported by Highsmith and Reifsnider. The model has been then extended to fatigue loading conditions [102] and more recently to the description of the interaction between cracked plies through computational micromechanical analysis, which they called synergistic damage mechanics [103]. Montesano et al. [104] have further developed this model, by extending the multiscale analysis to multiaxial strains. As a further step, the authors have proposed models for predicting the evolution of this sub-critical matrix crack damage [105–107].

The use of such models in combination with the characterization of the damage state, i.e., the current local microstructure, will permit to track local changes in the stiffness properties. Their extension to failure conditions through proper fracture mechanics models will allow to describe the interaction between cracks in different plies so to determine the most likely failure mechanism at the global level. In last instance, provisions on the residual life of the component can be made on the basis of the actual material state.

Therefore, future work should be focused on assessing the sensitivity of the proposed technique to each failure mechanism of composites. The effect of delaminated areas, which is supposed to affect the flexural behaviour, without modifying the in-plane stiffness, should be quantitatively assessed. In addition, in order to extend the validity of the technique, nonlocal damage mechanisms should be addressed, such as the subcritical matrix cracking damage, which is generally rather extended in the off-axis plies of a laminate. This damage mode is usually non catastrophic for the material, but might evolve in more severe damage and finally in the global failure. Therefore, it is of interest to characterize the sensitivity of the technique to this subcritical damage. More in detail, the technique should be proved effective on more anisotropic materials, such as laminates with off-axis plies, i.e., laminates made of unidirectional plies with symmetric and anti-symmetric stacking sequences, as those analysed in Ch. 4 of the present dissertation. Indeed, the formula provided by Hearmon is valid only for orthotropic materials which represent a limited set of composites.

Also, the effect of vacuum on the measurement of the first resonant frequency can be further investigated. Indeed, the vacuum application can induce in-plane spurious stresses which might affect the measurement of the first resonant frequency [108]. In this regard, it is worthwhile noticing that the proposed analytical approach involves the squared ratio between the frequency in presence

of damage f_d and that in absence of damage f_0 , i.e., $\left(\frac{f_d}{f_0}\right)^2$, which might involve some compensation of the vacuum effect.

By addressing these future challenges, the methodology could be definitely established in the realm of the nondestructive techniques with the peculiar characteristic of identifying the current material state. The proper assessment of damage severity thus could help the design engineer in defining the criteria for the damage tolerance.

References

1. Reynolds, N.; Ramamohan, A.B. High-volume thermoplastic composite for automotive structures. In *Advanced composite materials for automotive applications: Structural integrity and crashworthiness*; Elmarakbi, A., Ed.; John Wiley & Sons, Ltd., 2013; pp. 225–246 ISBN 9780784471531.
2. Sohn, H.; Farrar, C.R.; Hemez, F.M.; Shunk, D.D.; Stinemas, D.W.; Nadler, B.R.; Czarnecki, J.J. A Review of Structural Health Monitoring Literature 1996 – 2001 2003, 1–303.
3. Talreja, R. Manufacturing defects in composites and their effects on performance. In *Polymer Composites in the Aerospace Industry*; Elsevier, 2019; pp. 83–97 ISBN 9780081026793.
4. Schulte, K.; Marissen, R. Influence of artificial pre-stressing during curing of CFRP laminates on interfibre transverse cracking. *Compos. Sci. Technol.* **1992**, *44*, 361–367, doi:10.1016/0266-3538(92)90072-B.
5. Schoeppner, G.A.; Abrate, S. Delamination threshold loads for low velocity impact on composite laminates. *Compos. Part A Appl. Sci. Manuf.* **2000**, *31*, 903–915, doi:10.1016/S1359-835X(00)00061-0.
6. Belingardi, G.; Cavatorta, M.P.; Paolino, D.S. On the rate of growth and extent of the steady damage accumulation phase in repeated impact tests. *Compos. Sci. Technol.* **2009**, *69*, 1693–1698, doi:10.1016/j.compscitech.2008.10.023.
7. U.S. Department of Transportation. Federal Aviation Administration Composite aircraft structure. *Advis. Circ. AC No20-107B Chang. 1* 2010.
8. Fuwa, M.; Bunsell, A.R.; Harris, B. Tensile failure mechanisms in carbon fibre reinforced plastics. *J. Mater. Sci.* **1975**, *10*, 2062–2070, doi:10.1007/BF00557484.
9. Wilhelmsson, D.; Talreja, R.; Gutkin, R.; Asp, L.E. Compressive strength assessment of fibre composites based on a defect severity model. *Compos. Sci. Technol.* **2019**, *181*, 107685, doi:10.1016/j.compscitech.2019.107685.
10. Hsiao, H.M.; Daniel, I.M. Elastic properties of composites with fiber waviness. *Compos. Part A Appl. Sci. Manuf.* **1996**, *27*, 931–941, doi:10.1016/1359-835X(96)00034-6.
11. Hsiao, H.M.; Daniel, I.M. Effect of fiber waviness on stiffness and strength reduction of unidirectional composites under compressive loading. *Compos. Sci. Technol.* **1996**, *56*, 581–593, doi:10.1016/0266-3538(96)00045-0.
12. Asp, L.E.; Berglund, L.A.; Talreja, R. Prediction of matrix-initiated transverse failure in polymer composites. *Compos. Sci. Technol.* **1996**, *56*, 1089–1097, doi:10.1016/0266-3538(96)00074-7.
13. Hashin, Z. Failure criteria for unidirectional fiber composites. *J. Appl. Mech.* **1980**, *47*, 329–334, doi:https://doi.org/10.1115/1.3153664.
14. Talreja, R.; Phan, N. Assessment of damage tolerance approaches for composite aircraft with focus on barely visible impact damage. *Compos. Struct.* **2019**, *219*, 1–7, doi:10.1016/j.compstruct.2019.03.052.
15. Talreja, R. Physical modelling of failure in composites. *Philos. Trans. R. Soc. A Math. Phys. Eng. Sci.* **2016**, *374*, doi:10.1098/rsta.2015.0280.

16. Matthews, F.L. Damage in fibre-reinforced plastics; its nature, consequences and detection. In Proceedings of the Proceedings of the 3rd International Conference on Damage Assessment of Structures (DAMAS 99); Dublin, 1999; Vol. 168, pp. 1–16.
17. Aymerich, F.; Meili, S. Ultrasonic evaluation of matrix damage in impacted composite laminates. *Compos. Part B Eng.* **2000**, *31*, 1–6, doi:10.1016/S1359-8368(99)00067-0.
18. Garnier, C.; Pastor, M.L.; Eyma, F.; Lorrain, B. The detection of aeronautical defects in situ on composite structures using non destructive testing. *Compos. Struct.* **2011**, *93*, 1328–1336, doi:10.1016/j.compstruct.2010.10.017.
19. Vary, A. The acousto-ultrasonic approach. In *Duke J.C. (eds) Acousto-Ultrasonics*; Springer: Boston, 1988.
20. Pillarisetti, L.S.S.; Talreja, R. On quantifying damage severity in composite materials by an ultrasonic method. *Compos. Struct.* **2019**, *216*, 213–221, doi:10.1016/j.compstruct.2019.02.087.
21. Talreja, R. Application of Acousto-Ultrasonics to Quality Control and Damage Assessment of Composites. In *Acousto-Ultrasonics: theory and application*; JC, D., Ed.; 1988; pp. 177–190.
22. Arhamnamazi, S.A.; Arab, N.B.M.; Oskouei, A.R.; Aymerich, F. Accuracy assessment of ultrasonic C-scan and X-ray radiography methods for impact damage detection in glass fiber reinforced polyester composites. *J. Appl. Comput. Mech.* **2018**, *5*, 258–268, doi:10.22055/JACM.2018.26297.1318.
23. Khomenko, A.; Karpenko, O.; Koricho, E.; Haq, M.; Cloud, G.L.; Udpa, L. Theory and validation of optical transmission scanning for quantitative NDE of impact damage in GFRP composites. *Compos. Part B Eng.* **2016**, *107*, 182–191, doi:10.1016/j.compositesb.2016.09.081.
24. Montesano, J.; Fawaz, Z.; Bougherara, H. Use of infrared thermography to investigate the fatigue behavior of a carbon fiber reinforced polymer composite. *Compos. Struct.* **2013**, *97*, 76–83, doi:10.1016/j.compstruct.2012.09.046.
25. Montesano, J.; Bougherara, H.; Fawaz, Z. Application of infrared thermography for the characterization of damage in braided carbon fiber reinforced polymer matrix composites. *Compos. Part B* **2014**, *60*, 137–143, doi:10.1016/j.compositesb.2013.12.053.
26. Montesano, J.; Fawaz, Z.; Bougherara, H. Non-destructive assessment of the fatigue strength and damage progression of satin woven fiber reinforced polymer matrix composites. *Compos. Part B* **2015**, *71*, 122–130, doi:10.1016/j.compositesb.2014.11.005.
27. Ambu, R.; Aymerich, F.; Ginesu, F.; Priolo, P. Assessment of NDT interferometric techniques for impact damage detection in composite laminates. *Compos. Sci. Technol.* **2006**, *66*, 199–205, doi:10.1016/j.compscitech.2005.04.027.
28. Montalvão, D.; Maia, N.M.M.; Ribeiro, A.M.R. A review of vibration-based structural health monitoring with special emphasis on composite materials. *Shock Vib. Dig.* **2006**, *38*, 295–324, doi:10.1177/0583102406065898.
29. Caldersmith, G.W. Vibrations of Orthotropic Rectangular Plates. *Acustica* **1984**, *56*, 144–152.
30. Fällström, K. -E; Jonsson, M. A nondestructive method to determine

- material properties in anisotropic plates. *Polym. Compos.* **1991**, *12*, 293–305, doi:10.1002/pc.750120502.
31. Larsson, D. Using modal analysis for estimation of anisotropic material constants. *J. Eng. Mech.* **1997**, *123*, 222–229, doi:10.1061/(asce)0733-9399(1997)123:3(222).
 32. Tada, H.; Paris, P.C.; Irwin, G.R. *The stress analysis of cracks handbook*; Third Edit.; ASME Press: New York, 2000;
 33. Fualdes, C. Composites @ Airbus damage tolerance methodology. *FAA Work. Compos. damage Toler. maintance* **2006**, 40.
 34. Chisholm, S.A.; Rufin, A.C.; Chapman, B.D.; Benson, Q.J. Forty Years of Structural Durability and Damage Tolerance at Boeing Commercial Airplanes. *Boeing Tech. J.* **2016**.
 35. Ashforth, C.; Ilcewicz, L. Certification and compliance considerations for aircraft products with composite materials. In *Comprehensive Composite Materials II*; Elsevier Ltd., 2017; Vol. 3, pp. 1–25 ISBN 9780081005330.
 36. Cantwell, W.J.; Morton, J. An assessment of the residual strength of an impact-damaged carbon fibre reinforced epoxy. *Compos. Struct.* **1990**, *14*, 303–317, doi:10.1016/0263-8223(90)90012-4.
 37. Lifshitz, J.M.; Rotem, A. Determination of reinforcement unbonding of composites by a vibration technique. *J. Compos. Mater.* **1969**, *3*, 412–423, doi:10.1177/002199836900300305.
 38. Zak, A.; Krawczuk, M.; Ostachowicz, W. Numerical and experimental investigation of free vibration of multilayer delaminated composite beams and plates. *Comput. Mech.* **2000**, *26*, 309–315, doi:10.1007/s004660000178.
 39. Cawley, P.; Adams, R.D. The location of defects in structures from measurements of natural frequencies. *J. Strain Anal.* **1979**, *14*, 49–57, doi:https://doi.org/10.1243/03093247V142049.
 40. Hu, H.; Wang, J. Damage detection of a woven fabric composite laminate using a modal strain energy method. *Eng. Struct.* **2009**, *31*, 1042–1055, doi:10.1016/j.engstruct.2008.12.015.
 41. Paolino, D.S.; Geng, H.; Scattina, A.; Tridello, A.; Cavatorta, M.P.; Belingardi, G. Damaged composite laminates: Assessment of residual Young's modulus through the Impulse Excitation Technique. *Compos. Part B Eng.* **2017**, *128*, 76–82, doi:10.1016/j.compositesb.2017.07.008.
 42. Vary, A.; Bowles, K.J. An ultrasonic-acoustic technique for nondestructive evaluation of fiber composite quality. *Polym. Eng. Sci.* **1979**, *19*, 373–376, doi:10.1002/pen.760190509.
 43. Vary, A.; Lark, R.F. Correlation of fiber composite tensile strength with the ultrasonic stress wave factor. *J. Test. Eval.* **1979**, *7*, 185–191, doi:10.1520/jte11379j.
 44. Russell-Floyd, R.; Phillips, M.G. A critical assessment of acousto-ultrasonics as a method of nondestructive examination for carbon-fibre-reinforced thermoplastic laminates. *NDT Int.* **1988**, *21*, 247–257.
 45. Seo, D.C.; Lee, J.J. Damage detection of CFRP laminates using electrical resistance measurement and neural network. *Compos. Struct.* **1999**, *47*, 525–530, doi:10.1016/S0263-8223(00)00016-7.
 46. Vadlamudi, V.; Shaik, R.; Raihan, R.; Reifsnider, K.; Iarve, E. Identification of current material state in composites using a dielectric state variable. *Compos. Part A Appl. Sci. Manuf.* **2019**, *124*, 105494,

- doi:10.1016/j.compositesa.2019.105494.
47. Fazzino, P.D.; Reifsnider, K.L.; Majumdar, P. Impedance spectroscopy for progressive damage analysis in woven composites. *Compos. Sci. Technol.* **2009**, *69*, 2008–2014, doi:10.1016/j.compscitech.2009.05.007.
 48. Raihan, R.; Adkins, J.M.; Baker, J.; Rabbi, F.; Reifsnider, K. Relationship of dielectric property change to composite material state degradation. *Compos. Sci. Technol.* **2014**, *105*, 160–165, doi:10.1016/j.compscitech.2014.09.017.
 49. Tridello, A.; D’Andrea, A.; Paolino, D.S.; Belingardi, G. A novel methodology for the assessment of the residual elastic properties in damaged composite components. *Compos. Struct.* **2017**, *161*, 435–440, doi:10.1016/j.compstruct.2016.11.028.
 50. Cantwell, W.J.; Morton, J. The impact resistance of composite materials - a review. *Composites* **1991**, *22*, 347–362.
 51. Quaresimin, M.; Ricotta, M.; Martello, L.; Mian, S. Energy absorption in composite laminates under impact loading. *Compos. Part B Eng.* **2013**, *44*, 133–140, doi:10.1016/j.compositesb.2012.06.020.
 52. Belingardi, G.; Grasso, F.; Vadori, R. Energy absorption and damage degree in impact testing of composite materials. In Proceedings of the Proceedings of ICEM XI - International Conference on Experimental Mechanics; 1998; pp. 279–285.
 53. Belingardi, G.; Cavatorta, M.P.; Paolino, D.S. A new damage index to monitor the range of the penetration process in thick laminates. *Compos. Sci. Technol.* **2008**, *68*, 2646–2652, doi:10.1016/j.compscitech.2008.04.029.
 54. Belingardi, G.; Cavatorta, M.P.; Paolino, D.S. Repeated impact response of hand lay-up and vacuum infusion thick glass reinforced laminates. *Int. J. Impact Eng.* **2008**, *35*, 609–619, doi:10.1016/j.ijimpeng.2007.02.005.
 55. Boursier Niuitta, C.; Tridello, A.; Ciardiello, R.; Belingardi, G.; Paolino, D.S. Assessment of residual elastic properties of a damaged composite plate with combined damage index and finite element methods. *Appl. Sci.* **2019**, *9*, 1–14, doi:10.3390/app9122579.
 56. *ASTM Standard Test Method for Flexural Properties of Unreinforced and Reinforced Plastics and Electrical Insulating Materials by Four-Point Bending*; 2017;
 57. *ASTM Standard Test Method for Impact Resistance of Flat, Rigid Plastic Specimens by Means of a Falling Dart (Tup or Falling Mass)*; 2018;
 58. *LSTC LS-DYNA Keyword User’s Manual Volume II*; 2017; ISBN 978-3-540-23882-9.
 59. *LSTC LS-DYNA Theory Manual*; 2019; ISBN 9254492507.
 60. Hauert, A.; Rossoll, A.; Mortensen, A. Young’s modulus of ceramic particle reinforced aluminium: Measurement by the Impulse Excitation Technique and confrontation with analytical models. *Compos. Part A Appl. Sci. Manuf.* **2009**, *40*, 524–529, doi:10.1016/j.compositesa.2009.02.001.
 61. Ayorinde, E.O.; Gibson, R.F. Elastic constants of orthotropic composite materials using plate resonance frequencies, classical lamination theory and an optimized three-mode Rayleigh formulation. *Compos. Eng.* **1993**, *3*, 395–407, doi:https://doi.org/10.1016/0961-9526(93)90077-W.
 62. Fällström, K. -E Determining material properties in anisotropic plates using Rayleigh’s method. *Polym. Compos.* **1991**, *12*, 306–314,

- doi:10.1002/pc.750120503.
63. Hwang, S.F.; Chang, C.S. Determination of elastic constants of materials by vibration testing. *Compos. Struct.* **2000**, *49*, 183–190, doi:10.1016/S0263-8223(99)00132-4.
 64. Maletta, C.; Pagnotta, L. On the determination of mechanical properties of composite laminates using genetic algorithms. *Int. J. Mech. Mater. Des.* **2004**, *1*, 199–211, doi:10.1007/s10999-004-1731-5.
 65. ASTM *Standard Test Method for Dynamic Young's Modulus, Shear Modulus, and Poisson's ratio by Impulse Excitation of Vibration*; 2015;
 66. Tognana, S.; Salgueiro, W.; Somoza, A.; Marzocca, A. Measurement of the Young's modulus in particulate epoxy composites using the impulse excitation technique. *Mater. Sci. Eng. A* **2010**, *527*, 4619–4623, doi:10.1016/j.msea.2010.04.083.
 67. Maciel, M.M.Á.D.; Shiino, M.Y.; Voorwald, H.J.C.; Cioffi, M.O.H. Residual modulus degradation model for woven fabric composite determined by impulse excitation technique. *Int. J. Fatigue* **2020**, *133*, doi:10.1016/j.ijfatigue.2019.105456.
 68. Boursier Niutta, C.; Tridello, A.; Belingardi, G.; Paolino, D.S. Nondestructive determination of local material properties of laminated composites with the impulse excitation technique. *Compos. Struct.* **2021**, *262*, doi:10.1016/j.compstruct.2021.113607.
 69. Chakraborty, S.; Mukhopadhyay, M.; Mohanty, A.R. Free vibrational responses of FRP composite plates: experimental and numerical studies. *J. Reinf. Plast. Compos.* **2000**, *19*, 535–551, doi:https://doi.org/10.1177/073168440001900702.
 70. Kung, G.C.; Pao, Y.H. Nonlinear flexural vibrations of a clamped circular plate. *J. Appl. Mech.* **1972**, *39*, 1050–1054, doi:https://doi.org/10.1115/1.3422827.
 71. Nelder, J.A.; Mead, R. A Simplex Method for Function Minimization. *Comput. J.* **1965**, *7*, 308–313, doi:10.1093/comjnl/7.4.308.
 72. Reddy, J.N. *Mechanics of Laminated Composite Plates and Shells Theory and Analysis*; CRC Press LLC, 2003; ISBN 0849315921.
 73. Dong, C.; Davies, I.J. Flexural and tensile moduli of unidirectional hybrid epoxy composites reinforced by S-2 glass and T700S carbon fibres. *Mater. Des.* **2014**, *54*, 893–899, doi:10.1016/j.matdes.2013.08.086.
 74. Anderson, T.J.; Nayfeh, A.H. Natural frequencies and mode shapes of laminated composite plates: Experiments and FEA. *J. Vib. Control* **1996**, *2*, 381–414, doi:10.1177/107754639600200402.
 75. Tam, J.H.; Ong, Z.C.; Ismail, Z.; Ang, B.C.; Khoo, S.Y. Identification of material properties of composite materials using nondestructive vibrational evaluation approaches: A review. *Mech. Adv. Mater. Struct.* **2017**, *24*, 971–986, doi:10.1080/15376494.2016.1196798.
 76. Boursier Niutta, C. Enhancement of a new methodology based on the impulse excitation technique for the nondestructive determination of local material properties in composite laminates. *Appl. Sci.* **2021**, *11*, 1–17, doi:10.3390/app11010101.
 77. Reddy, J.N.; Phan, N.D. Stability and vibration of isotropic, orthotropic and laminated plates according to a higher-order shear deformation theory. *J. Sound Vib.* **1985**, *98*, 157–170, doi:10.1016/0022-460X(85)90383-9.
 78. Reddy, J.N. A simple higher-order theory for laminated composite plates.

- J. Appl. Mech.* **1984**, *51*, 745–752, doi:10.1115/1.3167719.
79. Chen, C.C.; Liew, K.M.; Lim, C.W.; Kitipornchai, S. Vibration analysis of symmetrically laminated thick rectangular plates using the higher-order theory and p-Ritz method. *J. Acoust. Soc. Am.* **1997**, *102*, 1600–1611, doi:10.1121/1.420072.
 80. Low, K.H.; Chai, G.B.; Tan, G.S. A comparative study of vibrating loaded plates between Rayleigh-Ritz and experimental methods. *J. Sound Vib.* **1997**, *199*, 285–297, doi:https://doi.org/10.1006/jsvi.1996.0633.
 81. Chow, S.T.; Liew, K.M.; Lam, K.Y. Transverse vibration of symmetrically laminated rectangular composite plates. *Compos. Struct.* **1992**, *20*, 213–226, doi:10.1016/0263-8223(92)90027-A.
 82. Lam, K.Y.; Chun, L. Analysis of clamped laminated plates subjected to conventional blast. *Compos. Struct.* **1994**, *29*, 311–321, doi:10.1016/0263-8223(94)90027-2.
 83. *ASTM Standard Test Method for Tensile Properties of Polymer Matrix Composite Materials*; 2017;
 84. Luna Innovations <https://lunainc.com/>.
 85. Warburton, G.B. The Vibration of Rectangular Plates. *Proc. Inst. Mech. Eng.* **1954**, *168*, 371–384, doi:10.1243/pime_proc_1954_168_040_02.
 86. Hearmon, R.F.S. The frequency of flexural vibration of rectangular orthotropic plates with clamped or supported edges. *J. Appl. Mech.* **1959**, *26*, 537–540.
 87. Hearmon, R.F.S. The fundamental frequency of vibration of rectangular wood and plywood plates. *Proc. Phys. Soc. London* **1946**, *58*, 78–92, doi:10.1088/0959-5309/58/4/319.
 88. Thomason, J.L.; Vlug, M.A. Influence of fibre length and concentration on the properties of glass fibre-reinforced polypropylene: 1. Tensile and flexural modulus. *Compos. Part A Appl. Sci. Manuf.* **1996**, *27*, 477–484, doi:10.1016/1359-835X(96)00066-8.
 89. Biancolini, M.E.; Brutti, C.; Reccia, L. Approximate solution for free vibrations of thin orthotropic rectangular plates. *J. Sound Vib.* **2005**, *288*, 321–344, doi:10.1016/j.jsv.2005.01.005.
 90. Hatiegan, L.; Hatiegan, C.; Gillich, G.R.; Hamat, C.O.; Vasile, O.; Stroia, M.D. Natural frequencies of thin rectangular plates clamped on contour using the Finite Element Method. In *Proceedings of the IOP Conference Series: Materials Science and Engineering* 294; 2018.
 91. Abrate, S. Impact on laminated composites: Recent advances. *Appl. Mech. Rev.* **1994**, *47*, 517–544, doi:10.1115/1.3111065.
 92. Caprino, G.; Lopresto, V. The significance of indentation in the inspection of carbon fibre-reinforced plastic panels damaged by low-velocity impact. *Compos. Sci. Technol.* **2000**, *60*, 1003–1012, doi:10.1016/S0266-3538(99)00196-7.
 93. Caprino, G.; Langella, A.; Lopresto, V. Indentation and penetration of carbon fibre reinforced plastic laminates. *Compos. Part B Eng.* **2003**, *34*, 319–325, doi:10.1016/S1359-8368(03)00002-7.
 94. Reifsnider, K.; Case, S.; Duthoit, J. The mechanics of composite strength evolution. *Compos. Sci. Technol.* **2000**, *60*, 2539–2546, doi:https://doi.org/10.1016/S0266-3538(00)00047-6.

95. Klepka, A.; Pieczonka, L.; Staszewski, W.J.; Aymerich, F. Impact damage detection in laminated composites by non-linear vibro-acoustic wave modulations. *Compos. Part B Eng.* **2014**, *65*, 99–108, doi:10.1016/j.compositesb.2013.11.003.
96. Abrate, S. *Impact on Composite Structures*; Cambridge University Press, 1998; ISBN 9780521473897.
97. Talreja, R. Damage Characterization. In *Fatigue of Composite Materials*; Reifsnider, K.L., Ed.; Elsevier Science Publishers B.V., 1990; pp. 79–103.
98. Reifsnider, K.L. Durability and Damage tolerance of fibrous composite systems. In *Handbook of Composites*; Peters, S.T., Ed.; Springer, 1998; pp. 794–809.
99. Singh, C. V. A multiscale synergistic damage mechanics approach for modeling progressive failure in composite laminates. In *Structural Integrity and Durability of Advanced Composites*; Beaumont, P.W.R., Soutis, C., Hodzic, A., Eds.; Elsevier Ltd, 2015; pp. 73–103 ISBN 9780081001370.
100. Highsmith, A.; Reifsnider, K. Stiffness-Reduction Mechanisms in Composite Laminates. In *Damage in Composite Materials, ASTM STP 775*; American Society for Testing and Materials, 1982; pp. 103–117.
101. Talreja, R. Transverse Cracking and Stiffness Reduction in Composite Laminates. *J. Compos. Mater.* **1985**, *19*, 355–375, doi:10.1177/002199838501900404.
102. Akshantala, N. V.; Talreja, R. A micromechanics based model for predicting fatigue life of composite laminates. *Mater. Sci. Eng. A* **2000**, *285*, 303–313, doi:10.1016/S0921-5093(00)00679-1.
103. Singh, C.V.; Talreja, R. A synergistic damage mechanics approach for composite laminates with matrix cracks in multiple orientations. *Mech. Mater.* **2009**, *41*, 954–968, doi:10.1016/j.mechmat.2009.02.008.
104. Montesano, J.; Singh, C.V. A synergistic damage mechanics based multiscale model for composite laminates subjected to multiaxial strains. *Mech. Mater.* **2015**, *83*, 72–89, doi:10.1016/j.mechmat.2015.01.005.
105. Singh, C.V.; Talreja, R. Evolution of ply cracks in multidirectional composite laminates. *Int. J. Solids Struct.* **2010**, *47*, 1338–1349, doi:10.1016/j.ijsolstr.2010.01.016.
106. Montesano, J.; Singh, C.V. Predicting evolution of ply cracks in composite laminates subjected to biaxial loading. *Compos. Part B* **2015**, *75*, 264–273, doi:10.1016/j.compositesb.2015.01.039.
107. Montesano, J.; Mccleave, B.; Veer, C. Prediction of ply crack evolution and stiffness degradation in multidirectional symmetric laminates under multiaxial stress states. *Compos. Part B* **2018**, *133*, 53–67, doi:10.1016/j.compositesb.2017.09.016.
108. Dickinson, S.M. The buckling and frequency of flexural vibration of rectangular isotropic and orthotropic plates using Rayleigh's method. *J. Sound Vib.* **1978**, *61*, 1–8, doi:10.1016/0022-460X(78)90036-6.